Computer calculations of the MgO-SiO2-AlO1.5 ternary and higher order phase diagrams through thermodynamic analysis of phase equilibria

by Matthew James Scanlon

A thesis submitted in partial fulfillment of the requirements for the degree of Doctor of Philosophy in Chemistry

Montana State University

Abstract:
Published data on the MgO-Sio2-A101.5 ternary system, along with the binaries and single component phases, are analysed in order to develop a computer model for the ternary system. In doing this a very useful relationship between the bulk modulus and coefficient of thermal expansion using the Murnaghan logarithmic equation of state is derived, thus allowing dK/dT to be calculated from thermal expansion measurements. Also, the alpha-beta transition in quartz was analysed using Pippard's theory of second order phase transitions, accurate X-ray data and the pressure dependence of the transition temperature.

Full equations of state for quartz are given up to 1900 K and 4000 MPa. The phase diagram is also calculated.

From analysis of the phase equilibria in the MgO-SiO2 system and the enthalpy of vitrification of MgSi03, the enthalpies of fusion of enstatite and forsterite were refined. The final best values for the heats of fusion were 48.8 ± 4 kJ/mole and 92.9 ± 12 kJ/mole respectively.

Also phase diagrams are calculated at 0.1 and 1000 MPa using Redlich-Kister coefficients.

Methods of dealing with three, four, and five component systems are developed using Redlich-Kister equations. Portions of the phase diagrams for the MgO-SiO2 A101.5 ternary and the FeO-Feo1.5-Cao-Sio1.5 system are calculated.

COMPUTER CALCULATIONS OF THE MgO-SiO_2-$AlO_{1.5}$ TERNARY AND HIGHER ORDER PHASE DIAGRAMS THROUGH THERMODYNAMIC ANALYSIS OF PHASE EQUILIBRIA

by

Matthew James Scanlon

A thesis submitted in partial fulfillment
of the requirements for the degree

of

Doctor of Philosophy

in

Chemistry

MONTANA STATE UNIVERSITY
Bozeman, Montana

March 1988

APPROVAL

of a thesis submitted by

Matthew James Scanlon

This thesis has been read by each member of the thesis committee and has been found to be satisfactory regarding content, English usage, format, citations, bibliographic style, and consistency, and is ready for submission to the College of Graduate Studies.

3/21/88
Date

Reed Howald
Chairperson, Graduate Committee

Approved for the Major Department

3/13/88
Date

Bradford Philip Mundy
Head, Major Department

Approved for the College of Graduate Studies

3-22-88
Date

Michael Malone
Graduate Dean

STATEMENT OF PERMISSION TO USE

In presenting this thesis in partial fulfillment of the requirements for a doctoral degree at Montana State University, I agree that the Library shall make it available to borrowers under rules of the Library. I further agree that copying of this thesis is allowable only for scholarly purposes, consistent with "fair use" as prescribed in the U. S. Copyright Law. Requests for extensive copying or reproduction of this thesis should be referred to University Microfilms International, 300 North Zeeb Road, Ann Arbor, Michigan 48106, to whom I have granted "the exclusive right to reproduce and distribute copies of the dissertation in and from microfilm and the right to reproduce and distribute by abstract in any format."

Signature Matthew J. Sommer

Date 3/16/88

ACKNOWLEDGMENT

My gratitude and thanks to all the people who helped and supported me through thick and thin during the course of this work. Reed Howald gave a tremendous amount of support and encouragement during the work and the writing, and Elaine Howald helped in the proof reading. A special thank you to Pat and Gayle Callis for their support and their friendship.

TABLE OF CONTENTS

LIST OF TABLES

LIST OF FIGURES

Figure Page

Figure Page

Figure Page

ABSTRACT

Published data on the MgO-SiO_2-$AlO_{1.5}$ ternary system, along with the binaries and single component phases, are analysed in order to develop a computer model for the ternary system. In doing this a very useful relationship between the bulk modulus and coefficient of thermal expansion using the Murnaghan logarithmic equation of state is derived, thus allowing dK/dT to be calculated from thermal expansion measurements. Also, the alpha-beta transition in quartz was analysed using Pippard's theory of second order phase transitions, accurate X-ray data and the pressure dependence of the transition temperature. Full equations of state for quartz are given up to 1900 K and 4000 MPa. The phase diagram is also calculated.

From analysis of the phase equilibria in the MgO-SiO_2 system and the enthalpy of vitrification of $MgSiO_3$, the enthalpies of fusion of enstatite and forsterite were refined. The final best values for the heats of fusion were 48.8 ± 4 kJ/mole and 92.9 ± 12 kJ/mole respectively. Also phase diagrams are calculated at 0.1 and 1000 MPa using Redlich-Kister coefficients.

Methods of dealing with three, four, and five component systems are developed using Redlich-Kister equations. Portions of the phase diagrams for the MgO-SiO_2-$AlO_{1.5}$ ternary and the FeO-$FeO_{1.5}$-CaO-SiO_2-$AlO_{1.5}$ system are calculated.

INTRODUCTION

In order to calculate a multicomponent phase diagram, one must to be able to calculate equilibrium constants for all the reactions between the various phases present. For the MgO-SiO_2-Al_2O_3 ternary system the one component systems are pure MgO, SiO_2 and $AlO_{1.5}$. The additional pure stoichiometric solids Mg_2SiO_4, $MgSiO_3$, $MgAl_2O_4$ and $Al_6Si_2O_{13}$ are also formed in this phase diagram.

In a one component phase diagram, volume, temperature and pressure can be modelled by fitting the volume data to a power series in both temperature and pressure. The computer program we are using can handle up to thirty-five of these terms, so that the calculated volumes are accurate over a wide range of temperatures and pressures. Once the coefficients for these polynomial terms are calculated the volume contour lines for the individual species can be determined. The representation of volume as a function of temperature and pressure is known as the equation of state for a pure material.

The heat capacity, C_P, at constant pressure can be fit to a power series of the form

$$C_P = A + B(T - T_o) + C(T - T_o)^2 + D(T - T_o)^3 + \ldots \quad (1)$$

where A, B, C and D are constants, T is the temperature and T_o is a standard temperature of 1000 K or 298.15 K. The derivative of the heat capacity with respect to pressure is

$$(dC_P/dP)_T = VT(d\ /dT)_p - T\alpha^2V$$
$$= -T(d^2V/dT^2)_P \qquad (2)$$

where α the thermal expansion coefficient is $1/V(dV/dT)_p$. Therefore, the heat capacity can be calculated at various pressures from the volume polynomials described earlier.

The temperature and pressure dependence of the enthalpy of a substance is related to the heat capacity and the volume through the equation

$$dH = (dH/dT)_p dT + (dH/dP)_T dP \qquad (3)$$

which becomes

$$dH = C_p dT + (V - T\alpha V)dP \qquad (4)$$

respectively. Thus, with a value for the enthalpy at a particular temperature and pressure referenced from the heats of formation from the elements at 298.15 K and the volume polynomial one can calculate the enthalpy at any temperature and pressure. We have choosen 1000 K and .1 MPa. as our standard temperature and pressure.

The equilibrium constant is related to the standard Gibbs free energies of the components involved in the equilibria through the equation

$$\Delta G°_T = -RT\ln(K_T). \qquad (5)$$

Since $\Delta G = \Delta H - T\Delta S$, the equilibrium constant can also be expressed by the equation

$$K_T = \exp(-\Delta G°/RT) = \exp(-\Delta H°/RT)\ \exp(\Delta S°/R) \quad (6)$$

or converting to base 10 and using J/mole yields

$$K_T = 10^{(-\Delta H°/19.14464\ T)}\ 10^{(\Delta S°/19.14464)}. \quad (7)$$

However in the literature, free energy is often tabulated in the form of Planck's function, Y. Planck's function includes the temperature dependence of both the enthalpy and the entropy and is defined as

$$Y_T = (G°_T - H°_{298.15})/T. \quad (8)$$

The pressure dependence of Plancks function is determined from the heat capacities pressure dependence. Thus the equation for the equilibrium constant can be written

$$K_T = 10^{(-\Delta H°298.15/19.14464T)}\ 10^{(\Delta Y_T/19.14464)}. \quad (9)$$

With the information described above gathered and incorporated into the computer, the properties of any compound at any temperature and pressure for which the equations are accurate can be calculated.

The Redlich-Kister Equations

In order to describe a two component phase diagram, one must model the thermodynamic properties as a function of mole fraction (x). There are a variety of methods of modelling phase diagrams in terms of chemical equilibria using known equilibrium constants.[1,2,3] Also sublattice

models have been proposed and used sucessfully for spinels.[4,5,6,7] However, it is difficult to do calculations of phase equilibria when various types of equations are being used. Therefore it is an advantage to use power series of a standard form, which are able to fit the most complex systems.

The quantities that have to be modelled in a two component system are the partial molal quantities of both components and the excess quantity. The partial molal quantity and the excess quantity are defined through the following equations

$$\overline{Q}_1 = (dQ/dn_1)_{n_2,T,P} \tag{10}$$

$$Q = n_1Q_1^\circ + n_2Q_2^\circ + (n_1 + n_2)Q^e \tag{11}$$

where $\overline{Q}_1$ is the partial molal quantity of component 1, Q is the thermodynamic quantity, Q° is the thermodynamic quantity of the pure substance, and Q^e is the excess molal quantity. Any power series representation of a two component system must satisfy certain conditions. As the mole fraction of a particular component, X_i, approaches 1 the partial molal quantity, $\overline{Q}_i$, approaches the value of the molal quantity of the pure substance Q°. Also, the excess quantity, Q^e, must approach zero.

The earliest proposed set of power series equations is that proposed by Margules[8] in 1895. The Margules equations are

$$\bar{Q}_1 - Q_1^\circ = (1 - x_1)^2(A_1 + B_1x_1 + C_1x_1^2 + D_1x_1^3 + \ldots)$$

$$\bar{Q}_2 - Q_2^\circ = x_1^2(A_2 + B_2x_1 + C_2x_1^2 + D_2x_1^3 + \ldots) \quad (12)$$

$$Q^e = x_1x_2(A_e + B_ex_1 + C_ex_1^2 + D_ex_1^3 + \ldots).$$

These equations satisfy the above conditions, however, each equation has a different set of coefficients, and the mole fraction terms within an equation are not orthogonal. Two terms are orthoganol if the integral of the product of the terms over all space is zero. If the mole fraction terms are orthogonal, then the four term series would have the same first three coefficients as the coefficients in a three term series.

Bale and Pelton[9,10] have proposed the following set of equations to model the thermodynamic quantities

$$\bar{Q}_1 - Q_1^\circ = (1-x_1)^2 \sum_{i=0}^{n} a_iP_i(x_i)$$

$$\bar{Q}_2 - Q_2^\circ = x_1^2 \sum_{i=0}^{n} b_iP_i(x_i) \quad (13)$$

$$Q^e = x_1x_2 \sum_{i=0}^{n} q_iP_i(x_i)$$

where $P_i(x_i)$ are the standard Legendre polynomials. These polynomials are completely orthogonal; however, they still have different coefficients for the mole fraction terms in each equation.

O. Redlich and A. T. Kister[11,12] in 1948 proposed the following set of power series equations

$$\bar{Q}_1 - Q_1^\circ = x_2^2[A + B(4x_1 - 1) + C(6x_1 - 1)(2x_1 - 1) + D(8x_1 - 1)(2x_1 - 1)^2 + \ldots] \quad (14)$$

$$\bar{Q}_2 - Q_2^\circ = x_1^2[A + B(4x_1 - 1) + C(6x_1 - 5)(2x_1 - 1) + D(8x_1 - 7)(2x_1 - 1)^2 + \ldots] \quad (15)$$

$$Q^e = x_1x_2[A + B(2x_1 - 1) + C(2x_1 - 1)^2 + D(2x_1 - 1)^3 + \ldots]. \quad (16)$$

These equations are not completely orthogonal, however, the same coefficients A, B, and C appear in all three equations.

The reason the coefficients are the same is that the mole fraction terms for $\bar{Q}_1 - Q_1^\circ$ and $\bar{Q}_2 - Q_2^\circ$ are derived from the excess partial molal quantity Q^e. From the definition of the partial molal quantity and the expression for the thermodynamic quantity given in equations 10 and 11 the following relationship can be found

$$\bar{Q}_1 = Q_1^\circ + Q^e + (n_1 + n_2)(dQ^e/dn_1)_{n_2,T,P}. \quad (17)$$

Since

$$(dQ^e/dn_1)_{n_2} = (dQ^e/dx_1)_{n_2}(dx_1/dn_1)_{n_2} \quad (18)$$

and

$$dx_1/dn_1 = x_2/(n_1 + n_2) \quad (19)$$

the equation

$$\bar{Q}_1 - Q_1^\circ = Q^e + x_2 dQ^e/dx_1 \quad (20)$$

can be written. Therefore, the derivative of the excess quantity with respect to x_1, multiplied by x_2, plus the

excess quantity for each Redlich-Kister term yields the Redlich-Kister equation for the partial molal quantity. For example, the excess quantity for the D term is

$$Q_D^e = x_1(1 - x_1)D(2x_1 - 1)^3 \qquad (21)$$

so that

$$Q_D^e + x_2(dQ^e/dx_1) = Dx_2[(1 - 2x_1)(2x_1 - 1)^3 + 3(2x_1 - 1)^2 2(x_1 - x_1^2)] \qquad (22)$$

and

$$Q_D^e + x_2(dQ^e/dx_1) = Dx_2[(1 - 2x_1)(2x_1 - 1)^3 + 6(2x_1 - 1)^2(x_1 - x_1^2)] + D[(x_1 - x_1^2)(2x_1 - 1)^3] \qquad (23)$$

This simplifies to

$$Q_D^e + x_2(dQ^e/dx_1) = D(2x_1 - 1)^2[3x_1^2 - 2x_1^3 - x_1 + 10x_1x_2 - 10x_1^2x_2 - x_2] \qquad (24)$$

Then using the relation $x_1 + x_2 = 1$, the equation can be rearranged to give

$$Q_D^e + x_2(dQ^e/dx_1) = x_2^2D(8x_1 - 1)(2x_1 - 1)^2. \qquad (25)$$

The Two Component Phase Diagram

To calculate a two component phase diagram one must be able to calculate the activity at any composition over the temperature range of interest. Redlich-Kister coefficients for the logarithm of the activity coefficient, $\log\gamma$, can provide information about the activity's dependence on composition through the equation

$$a = \gamma x \tag{26}$$

where a is the activity and γ is the activity coefficient. At other temperatures the logarithm of the activity coefficient can be calculated from the equation

$$d\log\gamma/d(1/T) = (\overline{H}_1 - H_1^\circ)/19.14464. \tag{27}$$

This equation is derived from the Gibbs-Helmholtz relationship. Therefore, if accurate enthalpy and heat capacity data as a function of temperature and composition are available, the Redlich-Kister coefficients for $\log\gamma$ can easily be calculated.

The phase diagram lines represent the point at which different species are in equilibrium. Therefore, if thermodynamic data are available for each of the species involved in a particular equilibrium, the equilibrium constant can be calculated for that reaction. The equilibrium constant can also be calculated from the activities of each species involved in the equilibria raised to the appropriate stochiometric power. Thus, the mole fraction at which equilibrium exists can be calculated for a particular temperature.

For example, suppose one is calculating the equilibrium curve for the melting of a solid into two liquid species. The equation for this reaction might be

$$Y_2Z_{(s)} = 2Y_{(l)} + Z_{(l)}. \tag{28}$$

The equilibrium constant for this reaction can easily be

calculated from $\Delta H°$ at 298.15 K and the Planck function for each of the species at the temperature of interest using the following equation:

$$K_{eq} = 10^{(-\Delta H°/19.14464T)}\ 10^{(\Delta Y_T/19.14464)}. \quad (29)$$

The equilibrium constant can also be calculated from the activities of each species by the equation:

$$K_{eq} = (a_Y^2 a_Z)/(a_{Y_2Z}). \quad (30)$$

However, the activity of the solid is normally equal to one so that this equation becomes

$$K_{eq} = a_Y^2 a_Z. \quad (31)$$

Substitution of the Redlich-Kister coefficients for log into this equation, we get

$$K_{eq} = x_Y{}^2 x_Z\ 10^{(2\log \gamma_Y)}\ 10^{(\log \gamma_Z)} \quad (32)$$

which becomes

$$K_{eq} = x_Y{}^2\ 10^{2(x_Z)^2[A + B(4x_Y - 1) + \ldots]}\ x_Z\ 10^{(x_Y)^2[A + B(4x_Y - 3) + \ldots]}. \quad (33)$$

With this equation the mole fraction at which the equilibrium point lies for a particular temperature can be calculated by a minimization process. By repeating this calculation at various temperatures the equilibrium curve can eventually be drawn.

Extended Redlich-Kister Notation

In describing phase diagrams of three or more components, R. A. Howald and I. Eliezer[13,14,15]

developed an extended Redlich-Kister notation which describes the mole fraction term for a particular coefficient. The coefficients through the seventh power, F, are shown in Table 1 for a three component system.

Table 1. The Redlich-Kister coefficients for a three component system through seventh power in mole fraction.

A_{12}	A_{13}	A_{23}				
B_{12}	B_{13}	B_{23}	B^{a}_{123}			
C_{12}	C_{13}	C_{23}	C^{a}_{123}	C^{b}_{123}		
D_{12}	D_{13}	D_{23}	D^{a}_{123}	D^{b}_{123}	D^{c}_{123}	
E_{12}	E_{13}	E_{23}	E^{a}_{123}	E^{b}_{123}	E^{c}_{123}	E^{d}_{123}

The first three columns in Table 1 represent the binary terms for the three binary subsystems present in the ternary. For the excess quantities the mole fraction terms multiplied by the Redlich-Kister coefficient are $A_{12}x_1x_2$, $E_{13}x_1x_3(x_1 - x_3)^4$, $F_{23}x_2x_3(x_2 - x_3)^5$, etc. The coefficients left over are the three component terms. The number of superscripts on these terms is always two less than the number of subscripts. The minumum number of subscripts allowed for a letter is two. This can only occur with binary terms. The maximum allowable number of

subscripts is equal to one more than the letter's position in the alphabet. However, the actual number of subscripts is equal to the number of components in the system. For example, the maximum number of subscripts for E is six; however, in a ternary system this is limited to three subscripts.

Table 2 is useful in correlating coefficients and superscripts with their appropriate powers. The first mole fraction terms are indicated by the subscripts. For example E^{b}_{123} is a sixth power term in mole fraction. This is because E is the fifth letter in the alphabet. In all cases one gets the power by adding one to the number representing position in the alphabet. The first three mole fraction terms are $x_1x_2x_3$ corresponding to each of the subscripts. The next mole fraction term is calculated from $(V - x_i)^m$ where m is equal to the number of the capital letter which is six for E, minus the number of subscripts, minus the number for each superscript. Thus in this case $m = 6 - 3 - 1 = 2$. V is the sum of each of the first mole fraction terms in this case $V = x_1 + x_2 + x_3$, and i is the first subscript. There is also a term Z^n associated with each superscript; n is the corresponding number associated with the superscript in the above scheme. Z is defined as $(x_j - x_k)$, where j is the second subscript from the left and k is the subscript correlated

with the superscript. The superscript is correlated with the subscript of the Redlich-Kister coefficient from the right. For example, the term E^{ca}_{1234} has (a) correlated with 4 and (c) is correlated with 3. Thus for E^{b}_{123} the complete term is

$$E^{b}_{123}x_1x_2x_3(V - x_1)^2(x_2 - x_3)^1$$

which is

$$E^{b}_{123}x_1x_2x_3(x_2 + x_3)^2(x_2 - x_3)^1$$

This notation can also be used for higher component diagrams. For example:

$$E^{bb}_{1234}x_1x_2x_3x_4(x_2 - x_4)(x_2 - x_3)$$

$$C^{b}_{641}x_6x_4x_1(x_4 - x_1)$$

and

$$D^{ba}_{3254}x_3x_2x_5x_4(x_2 - x_5).$$

Table 2. Redlich-Kister coefficients and their subscripts correlated with their corresponding powers

		A	B	C	D	E	F	G	H
0	1	2	3	4	5	6	7	8	9
a	b	c	d	e	f	g	h	i	j

The Higher Component Systems

For a three component system that includes mole fraction terms up to the seventh power, that is F, there must be at least fifteen terms present. There are also twenty of the four component terms for the excess

quantity. These terms are presented in Table 3, in the order that they are entered into the computer program.

However, the excess quantity is not enough. Expressions for the partial molal quantities are also needed. This can be accomplished as in the two component case by taking the derivative of the excess terms with respect to n, the number of moles.

Table 3. The three and four component Redlich-Kister coefficients

THE THREE COMPONENT TERMS

B^{a}_{123}	C^{a}_{123}	C^{b}_{123}	D^{a}_{123}	D^{b}_{123}	D^{c}_{123}
E^{a}_{123}	E^{b}_{123}	E^{c}_{123}	E^{d}_{123}	F^{a}_{123}	F^{b}_{123}
F^{c}_{123}	F^{d}_{123}	F^{e}_{123}			

THE FOUR COMPONENT TERMS

C^{aa}_{1234}	D^{aa}_{1234}	D^{ab}_{1234}	D^{ba}_{1234}	E^{aa}_{1234}	E^{ab}_{1234}
E^{ba}_{1234}	E^{ac}_{1234}	E^{bb}_{1234}	E^{ca}_{1234}	F^{aa}_{1234}	F^{ab}_{1234}
F^{ba}_{1234}	F^{ac}_{1234}	F^{bb}_{1234}	F^{ca}_{1234}	F^{ad}_{1234}	F^{bc}_{1234}
F^{cb}_{1234}	F^{da}_{1234}				

THE ONE COMPONENT PHASES

Equations of State for Magnesium Oxide

The volume as a function of temperature of MgO is well known at temperatures up to 1700 K, and the volumes tabulated by Touloukian[16] are easily fit by a quartic in (T - 1000 K):

$$V = 11.5643\,[1 + .434332 \times 10^{-4}(T - 1000) + 567479 \times 10^{-8}\,(T - 1000)^2 - .502119 \times 10^{-12}\,(T - 1000)^3 + .821952 \times 10\text{-}15\,(T - 1000)^4]. \quad (34)$$

Figure 1 shows values of the thermal expansion coefficient, α, calculated from this polynomial, the tabulated volumes by Touloukian,[10] and the volume polynomial from Howald, Moe and Roy.[25] It is clear that the volume dependence upon temperature from Howald, et al.[25] has been given excess curvature by the least squares procedure. The straight line between 300 and 1700 K is given by the equation

$$\alpha = 0.0000435 + 1.0 \times 10^{-8}\,(T - 1000). \quad (35)$$

The volumes from the thermal expansion equation and the volume polynomial in temperature agree within ± .001 cm^3/mole. The low temperature data [17,18,19,20] cited by

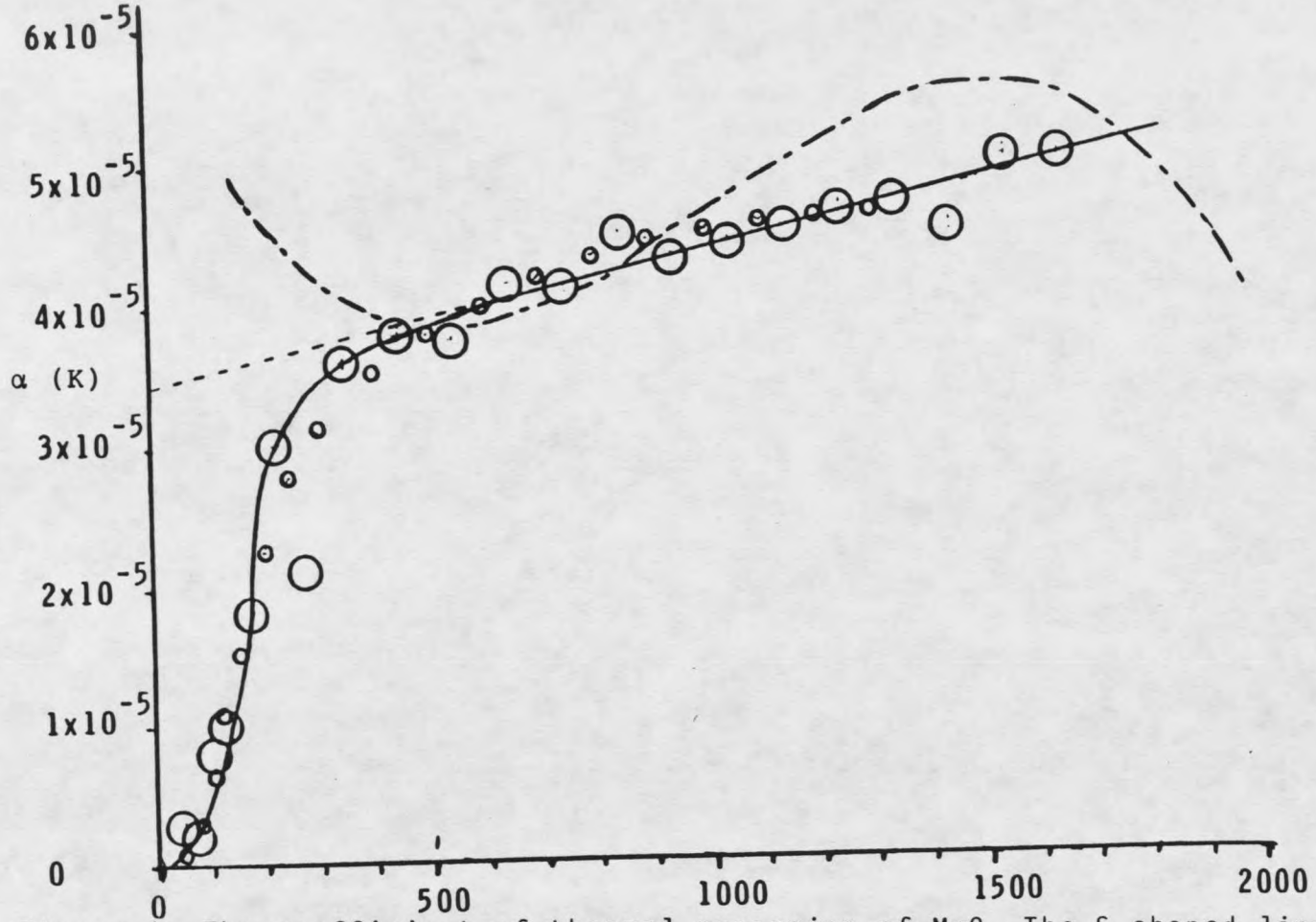

Figure 1. The coefficient of thermal expansion of MgO. The S shaped line with alternating long and short dashes represents the values used in ref.25. The straight dashed line is $.0000435+1.0\times10^{-8}(T-1000)$. The solid line shows the values selected in this work . Above 300K the solid line is that calculated from ref.16,17, and 20.

Touloukian[16] extends down to 4 K so that it is possible to sketch a reasonable curve between 400 and 0 K. The solid line in this region of Figure 1 gives volumes at 0 and 100 K of 11.1996 and 11.2016 cm^3/mole respectively.

However, it is also extremely important to have accurate data on the compressibility of MgO as a function of temperature and pressure. The Murnaghan logarithmic equation of state[21,22] has been widely used[22,23,24,25] to express the pressure dependence of the bulk modulus (K). The equation is

$$K = K_o + NP \tag{36}$$

where K_o is the bulk modulus at a standard pressure, N is a constant and P is the pressure. This equation is accurate and is easily extrapolated to high pressures, so that with a few measurements of K at various pressures a value for N can be determined.

There have been various expressions for the temperature dependence of the bulk modulus. Equations such as

$$K_{oT} = K_{oo} - CT \tag{37}$$

where, K_{oo} is the bulk modulus at a standard temperature and pressure, have been used empirically[24,25] and derived theoretically;[26,27,28] however, they are probably too simple. For example, the values for dK/dT obtained for MgO by Spetzler[24] are 27.2 to 30.1 MPa/K. These values

are inconsistent with the value calculated from Swalin's equation[26]

$$dK_S/dT = 2\gamma^2 C_p/V = 20.7 \text{ MPa/K} \quad (38)$$

where K_S is the adiabatic bulk modulus and is the Gruneisen parameter. The Gruneisen parameter is

$$\gamma = \alpha V/K_T C_V. \quad (39)$$

The difference between the adiabatic bulk modulus, K_S, and the isothermal bulk modulus K_T cannot account for this discrepancy.

Howald, Moe and Roy[25] have used the Murnaghan logarithmic equation of state

$$V = V_o(1 + NP/K_o)^{-1/N}, \quad (40)$$

but a constant value of N results in negative coefficients of thermal expansion at high temperatures and pressures. They solved this problem by including a temperature dependence for N for MgO, $AlO_{1.5}$ and $MgAl_2O_4$. However, the temperature dependence of N in the exponent greatly complicates obtaining derivatives. Also, increasing K to a value large enough to avoid negative values is inconsistent with Spetzler's[24] measurements. Also, using a positive value for dN/dT is not satisfactory, as the following derivation shows. The equation

$$d\alpha/dP = (dK/dT)/K^2 \quad (41)$$

can be easily derived from

$$d^2V/dTdP = d^2V/dPdT \quad (42)$$

and the definitions of α and K,

$$\alpha = (1/V)(dV/dT)_P \tag{43}$$

and

$$K = 1/\beta = -V(dP/dV)_T. \tag{44}$$

If the Murnaghan logarithmic equation of state is used, the expression for the pressure dependence of the coefficient of thermal expansion becomes by substitution,

$$d\alpha/dP = [(dK_o/dT) + P(dN/dT)]/(K_o + NP)^2. \tag{45}$$

The term dK_o/dT is negative and at low pressures is dominant, so that $d\alpha/dP$ is negative at low pressures as is expected. If dN/dT is positive then at higher pressures $d\alpha/dP$ becomes less negative, as it should be. However, with dN/dT being positive, there is some finite pressure at which $d\alpha/dP$ becomes positive. This can not happen, because as P approaches infinity the volume and the coefficient of thermal expansion must approach zero. This can be derived assuming that the nearest neighbor forces for any interatomic potential do not become infinite at a separation greater than zero.

It is entirely possible that the Murnaghan logarithmic equation of state is only valid over a finite temperature range. However, any correct high pressure equation of state must give volumes equal to zero as P approaches infinity, and must represent a mathematical form for the repulsive terms of the interatomic

potentials. Therefore any high pressure equation of state should be somewhat consistent with the Murnaghan logarithmic equation of state. Thus, we were led to consider the Murnaghan logarithmic equation of state as being valid to high pressures.

Spetzler's experimental measurements[24] indicate that dN/dT is zero. If this is correct then the pressure dependence of the thermal expansion coefficient becomes,

$$d\alpha/dP = (dK_o/dT)/(K_o + NP)^2. \tag{46}$$

This can be integrated to give

$$\alpha = -(dK_o/dT)/N(K_o + NP). \tag{47}$$

Thus, both α and β approach zero linearly in $1/(K + NP)$ as the pressure approaches infinity.

Rearranging and integrating this equation for α, we obtain

$$K_{oT} = K_{oT_o} \exp(-N \int_{T_o}^{T} \alpha dT) = K_{oT_o}(V_{T_o}/VT)^N \tag{48}$$

where T_o is a standard temperature at which the low pressure bulk modulus is K_{oT_o}.

While there are usually sufficient data to evaluate V and α at high temperatues, there is very little data for the evaluation of the bulk modulus at these high temperatures. Therefore, if this equation is at all correct, it will be extremely useful.

There is good agreement[24,17,18,19,20] on the value of K_o = 160100 MPa for MgO at 298.15 K. We first used

Spetzler's[24] value of N = 3.9; however, this gives values of dK_o/dT of about -15 MPa/K. This is definitely not steep enough to match either Spetzler's[24] or Soga and Anderson's[29] data. Anderson's 1968 review[30] gives N = 4.50 and 4.58 for single crystal and polycrystalline MgO respectively. We finally chose a value of N = 4.57 for our calculations, which is taken from Carter, et al.,[31] and is consistent with other measurements.

With values of N and $K_{o,298.15}$ chosen, we can calculate K_o at any temperature from the relationship

$$K_{oT} = K_{oT_o}(V_{T_o}/V_T)^N. \tag{49}$$

Most experimental methods give the adiabatic bulk modulus instead of the isothermal bulk modulus, but this can easily be corrected through the equation

$$K_s = K/(1 - \alpha^2 VKT/C_p). \tag{50}$$

This equation gives K_s = 163062 and 150082 MPa at 300 and 1000 K respectively. For temperatures below 300 K, values for α were determined from the curve shown in Figure 1, and C_p values were taken from the JANAF tables[32] and the Barron paper[33] to get $K = K_s$ = 163137 MPa at 0 K. The full set of calculated K_s values is plotted in Figure 2. The calculated curve is in excellent agreement with the 300 and 800 K values of Spetzler[24] and the 296 value of Anderson and Andreatch.[34] Anderson and Andreatch's value[34] at 77 K and all the values of Soga and Anderson[29]

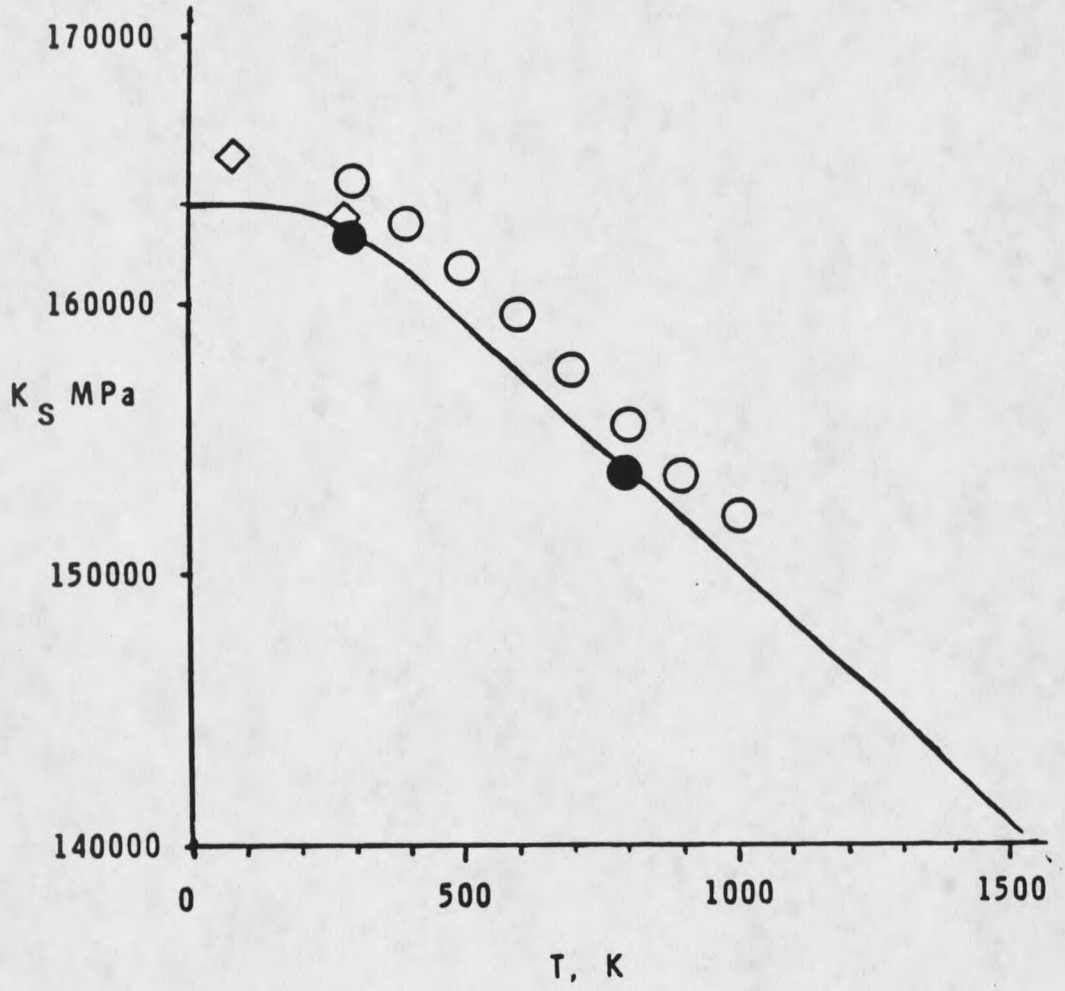

Figure 2. The isoentropic bulk modulus for MgO. The solid line is calculated from the theory presented here. The experimental values are from Spetzler, black circles; Soga and Anderson, open circles; and from Anderson and Andreatch, diamonds.

are about 1% higher that the calculated curve, but this is within the experimental error. Therefore, the data for MgO are in full agreement with the predictions assuming the validity of the Murnaghan logarithmic equation of state to high pressures with a constant value of N = 4.57.

Table 4 provides calculated molar volumes at various pressures for MgO for comparison with the calculated volumes of Howald, et al.[25] The values at 0.1 and 900 MPa agree with Howald, et al.[25] within ± 0.01 cm^3/mole. At 30,000 MPa our values are 0.05 to 0.06 cm^3/mole larger. This is due to the larger value of N that we are using.

Table 4. Calculated molar volumes for MgO

	P,MPa			
T,K	.01	9000	15000	30000
300	11.2464	10.6974	10.4025	9.8223
650	11.3956	10.8094	10.4980	9.8912
1000	11.5643	10.9341	10.6035	9.9665

Once these calculations using the Murnaghan logarithmic equation of state are done it is a simple matter to calculate the volume polynomial's dependence on pressure. The completed volume polynomials for MgO(c) and MgO(l) are given in Table 5, along with the heat capacity

Table 5. The equations of state, heat capacity equations and selected thermodynamic properties of MgO (c) and MgO (l)

MgO (S) VOLUME POLYNOMIAL

11.56431	4.3773181E-5	5.6747946E-9	-5.02119E-13	8.219519E-16
-7.096668E-6	-1.728388E-9	-3.96682E-13	-4.12045E-17	-3.69883E-20
1.402579E-10	6.210500E-14	2.043779E-17	4.563120E-21	2.019368E-24
-3.36068E-15	-2.15203E-18	-9.20887E-22	-2.99147E-25	-1.16580E-28
8.593206E-20	7.114327E-23	3.704788E-26	1.538755E-29	6.128646E-33
-2.00574E-24	-1.96492E-27	-1.16729E-30	-5.66303E-34	-2.35995E-37
2.819661E-29	3.033287E-32	1.941636E-35	1.027253E-38	4.424865E-42

MgO (LIQUID) VOLUME POLYNOMIAL

13.993	.437732E-04	.567479E-08	-.502119E-12	.821952E-15
-.709667E-05	-.172839E-08	-.396682E-12	-.412045E-16	-.369883E-19
.140258E-09	.621050E-13	.204378E-16	.456312E-20	.201937E-23
-.336068E-14	-.215203E-17	-.920887E-21	-.299147E-24	-.116580E-27
.859321E-19	.711433E-22	.370479E-25	.153875E-28	.612865E-32
-.200574E-23	-.196492E-26	-.116729E-29	-.566303E-33	-.235995E-36
.281966E-28	.303329E-31	.194164E-34	.102725E-37	.000000E+00

HEAT CAPACITY C_p

	A[a]	B	C	D	E
MgO (S)	51.0941	.00310468	-5.56218E-07	2.747330E-10	-1.26513E+06
MgO (L)	53.6488	.0032598	-5.84029E-07	2.884697E-10	-1.32839E+06

THERMODYNAMIC PROPERTIES	Y_{1000} J MOL^{-1}	$H_{1000}-H_{298}$ J MOL^{-1}	H_{298} J MOL^{-1}	S_{298} J MOL^{-1} K^{-1}	V_{1000} CM^3
MgO (S)	49.27	3.2974E+4	-6.01490E+5	26.94	11.248
MgO (L)	63.10923	34623.	-551278.3	35.	11.81

[a] THE HEAT CAPACITY EQUATIONS ARE GIVEN BY $Cp = A + B \times 10^{-2}(T-1000) + C \times 10^{-6}(T-1000) + D \times 10^{-9}(T-1000) + E \times 10^{7}(T^{-2}-10^{-6})$

equations and selected thermodynamic values. The heat capacity equation for MgO(c) and the ΔH_{fus} are taken from Howald, et al.[25] The ΔH_{fus} is 57.65 KJ/mole. Thus the solid is fully described and can be used to calculate equilibrium constants for any reaction in which it is involved.

For MgO liquid there are few measurements of volume or heat capacity. From the volume and heat capacity changes in the fusion of the alkali halides we have estimated the volume and the heat capacity of the liquid to be 21% and 5% greater than that of the solid.

In order to compare the equations of state considered here with other proposed equations, we have calculated Gruneisen,

$$\gamma = KV/C_V, \tag{51}$$

and the Anderson-Gruneisen,

$$\delta = (dK_S/dP)_T - 1, \tag{52}$$

parameters for MgO over a wide range of temperatures and pressures. These parameters show a small but not negligible dependence upon both the pressure and temperature. The results of γ are shown as contour lines in Figure 3. Figure 4 shows that the values of the Gruneisen parameter for MgO calculated from our equation of state are approximately consistent with the commonly assumed form

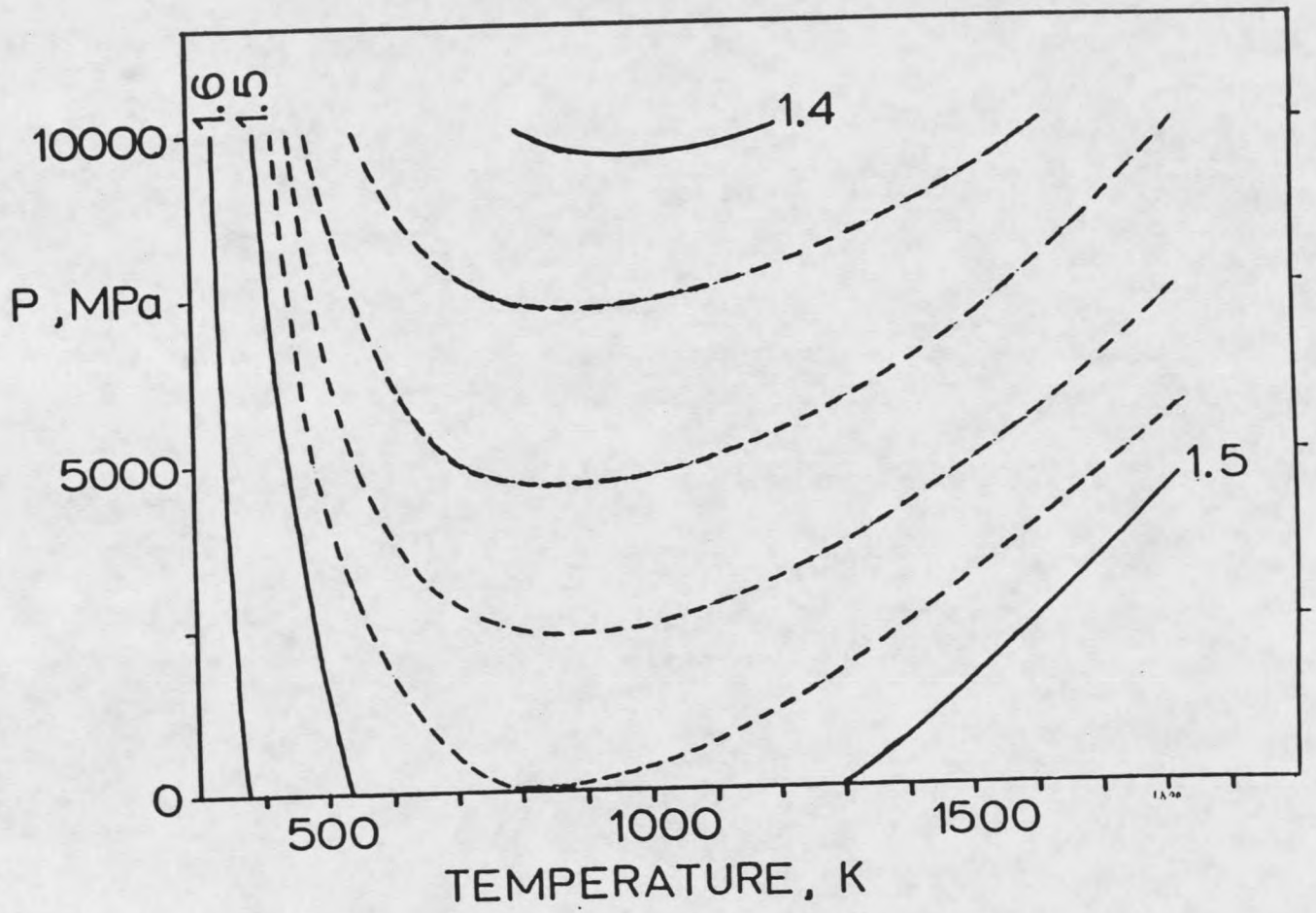

Figure 3. Contour lines for the Gruniesn parameter, γ, for MgO on a P-T field. The contour interval is 0.01, except that at high temperatures dotted lines at 0.02 intervals are also shown.

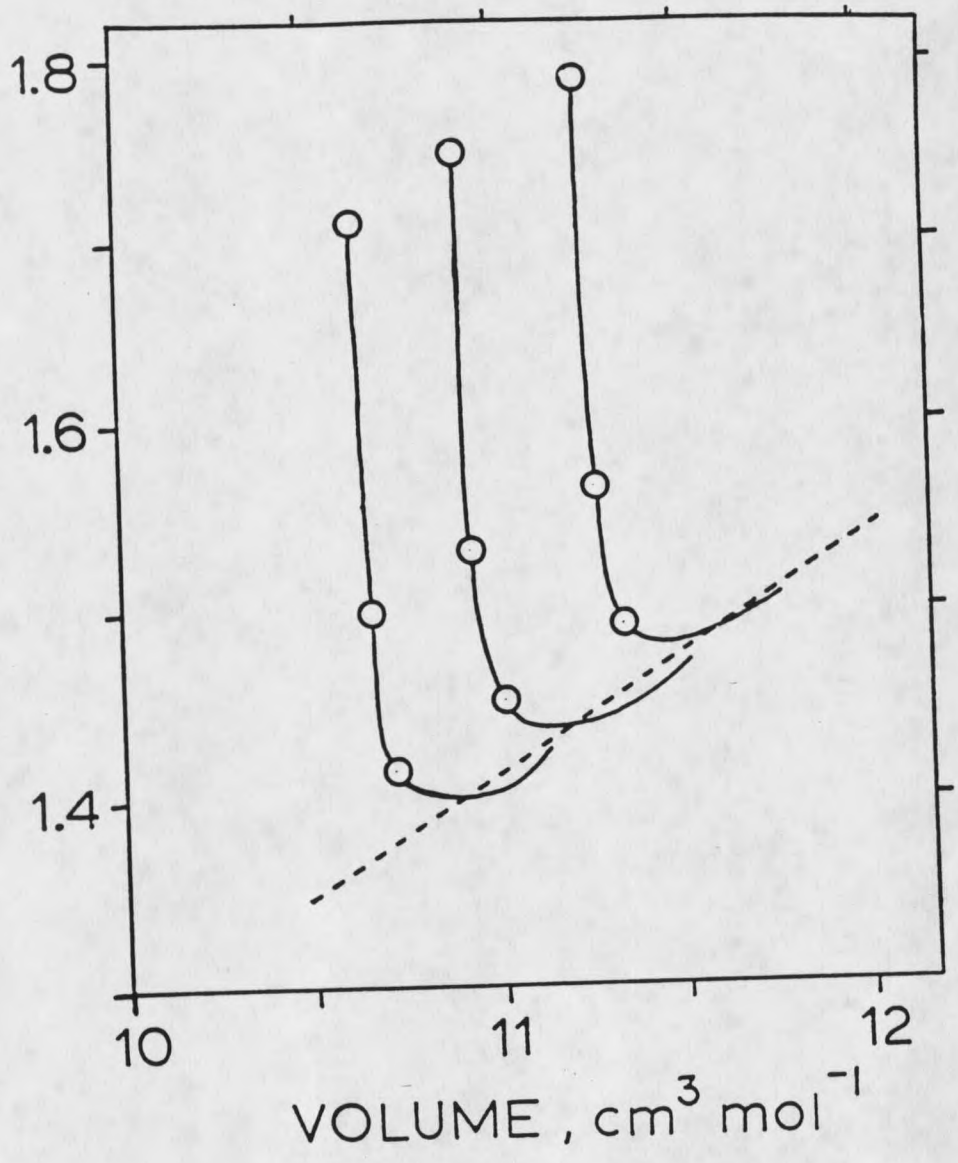

Figure 4. Gruneisen parameters, γ, for MgO plotted versus volume for the three pressures 0.01, 5000, and 10000 MPa. The circles represent calculated values at 300, 400, and 600 K. The dotted line is for $\gamma = 0.12652\ V^{1.0059}$.

$$\gamma = CV^n \tag{53}$$

with n = 1.0059 and C = 0.12652 but only at points above 600 K.

The Anderson-Gruneisen parameter, , is not plotted since there is a related quantity,

$$\delta_T = (-1/\alpha K)(dK/dT)_P, \tag{54}$$

which reduces to $\delta_T = N$ using

$$\alpha = -(dK/dT)_P/NK. \tag{55}$$

Thus the equations of state we have proposed here are equivalent to choosing a constant value for δ_T.

Anderson[35,36,37,38,39] has considered the approximation of αK = constant as an alternative to γ = constant. Our equations give

$$K = -(1/N)(dK_o/dT) \tag{56}$$

which is fully independent of pressure. As Anderson recognizes αK cannot be fully independent of temperature, because α approaches zero at 0 K as shown in Figure 1. The quantity (dK_o/dT) is approximately independent of temperature only above some minimum temperature. Our equation $K_{oT} = K_{oT_o}(V_{T_o}/V_T)^N$ will give reasonable values for K_o at any temperature for which low pressure thermal expansion data are available. This approximation would be better than assuming dK_o/dT is constant.

Equations of State for Silicon Dioxide

There are several known phases of silicon dioxide; these are alpha quartz, beta quartz, coesite, cristobalite, tridymite, stishovite and liquid. One of the problems with the SiO_2 phase diagram is the alpha quartz to beta quartz phase transition. There are various values for the enthalpy change between alpha quartz at 298.15 and beta quartz at 1000 K in the literature, as shown in Table 6. The two standard compilations are the JANAF (Stull and Prophet)[32] and Bulletin 1452, Robie, et al.[40] There is a 380 J/mole difference in these two compilations, and a difference of 200 J/mole is significant in calculating the various equilibria in the SiO_2 phase diagram as shown in Table 7. Thus, it is important to have a well defined enthalpy of transition for the alpha quartz to beta quartz transition.

The 380 J/mole difference between the tabulated values of Stull and Prophet[32] and Robie et, al.[40] is due primarily to the difference between differential thermal analysis and drop calorimetry, as shown by Richet, et al.[41] The differential thermal analysis is rather poor, due to the fact that equilibrium for the alpha to beta quartz transition requires a long period of time, and small changes in temperature have a large effect on the heat capacity of alpha quartz.

Table 6. Values reported for the enthalpy change between alpha quartz at 298.15 K and beta quartz at 1000 K.

45689.3	Compilation	Robie, et al., 1968
45689.3	Compilation	Kelly, 1960
45617.0	Exp. D. C.	Richet, et al., 1982
45579.	Compilation	Richet, et al., 1982
45452.	Compilation	*
45444.3	Compilation	this work
45358.7	Compilation	Barin and Knacke, 1973
45056.2	Exp Cp	Moser, 1936
44967.	Compilation	Robie, et al. 1969
44826.9	Exp DTA	Ghiorso, et al. 1979

*calculation using values for SiO_2 glass and of (Kracek, et al., 1953), (Richet et al., 1982) and (Navrotsky, et al., 1980)

Table 7. Calculated equilibrium constants for the hypothetical reaction between the two equations of state for Beta Quartz; Robie, et al. and ours.
(SiO_2, our = SiO_2, Robie, et al.)

T (K)	K_{eq}
844	.9890
800	.9928
900	.9849
1000	.9787
1100	.9736
1200	.9694
1300	.9658
1400	.9627
1500	.9598
1600	.9568
1700	.9538

The Alpha Quartz to Beta Quartz Transition

The alpha(α) quartz to beta(β) quartz transition was first discovered in 1889 by Le Chatelier.[42] It has an order disorder lambda transition about 746 K and 0.1 MPa. The alpha quartz crystal structure has a threefold screw axis[43,44] in which the ridged tetrahedra are tilted either to the left or the right. The two structures coexist and are known as Dauphine twin domains. The structure of beta quartz is a sixfold screw axis, that corresponds to an average of the two Dauphine twin domains in alpha quartz. Grimmm and Dorner[44] (1975) and Liebau and Bohm[43] (1982) have extensively discussed the motion involved and the domains formed.

There is also evidence for the existence of an incommensurate phase[45,46,47,48,49,50,51,52] 1 to 2 K above the alpha quartz to beta quartz transition at 846 K. However, since the temperature range in which this incommensurate phase is stable is small, its effect on the phase equilibria is negligible compared to the error in these calculations. Therefore for our purposes, this phase can be ignored. There has been some discussion in the literature on whether the alpha quartz to beta quartz transition is a first order or second order lambda transition. A high heat capacity with drops over a small

temperature range is indicative of a lambda transition. The alpha to beta quartz transition has such a heat capacity near 846 K at low pressures (Figure 5), and also along a line of increasing temperature with increasing pressure. Also the volume change upon transition approaches zero as the alpha to beta quartz transition temperature is approached, as shown in Figure 6. However, the alpha to beta quartz transition can still be modelled as first order, which Richet et al.[41] have done. Our results modelling this transition as a lambda transition agree well with Richet's[41] results.

In a normal first order phase transition the enthalpy of transition can be obtained from the volume change of the transition and the pressure dependence of the equilibrium curve, this equation is

$$dP/dT = \Delta H/T\Delta V = \Delta S/\Delta V. \qquad (57)$$

However, in a lambda transition the ΔV and the ΔH of transition are zero, and the heat capacity is very large, possibly approaching infinity. Therefore the above equation is indeterminate.

Since the change in entropy and volume upon transition are zero, the entropy and volume can be treated as an exact differential. By setting $S_\alpha = S_\beta$ and $V_\alpha = V_\beta$, analogous equations to the Clapeyron equation can be derived. These equations are

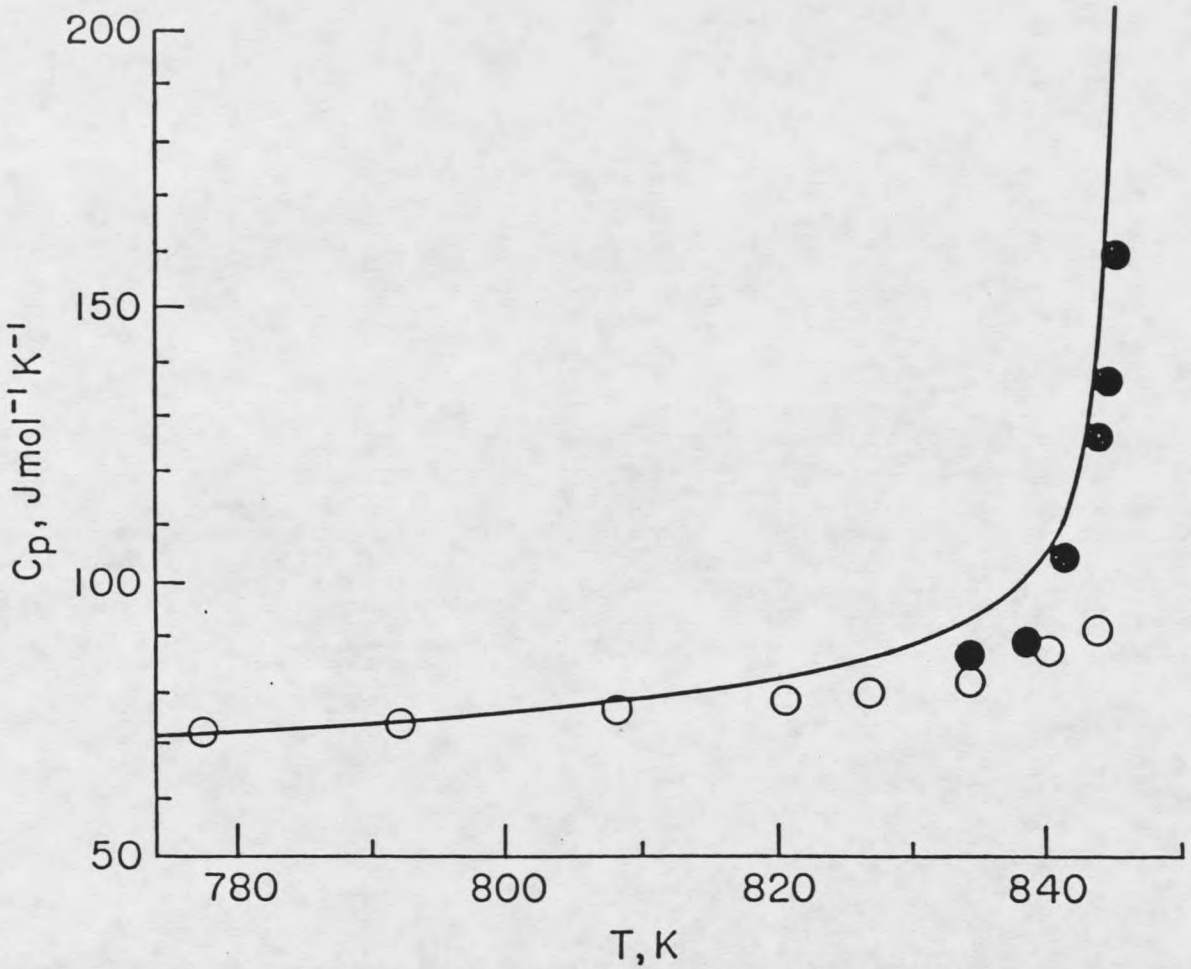

Figure 5. Heat capacity, Cp, for alpha quartz near the lambda temperature. The solid line represents our calculated values. The experimental points of Moser and Sinel'nikov are shown as open and filled circles respectively.

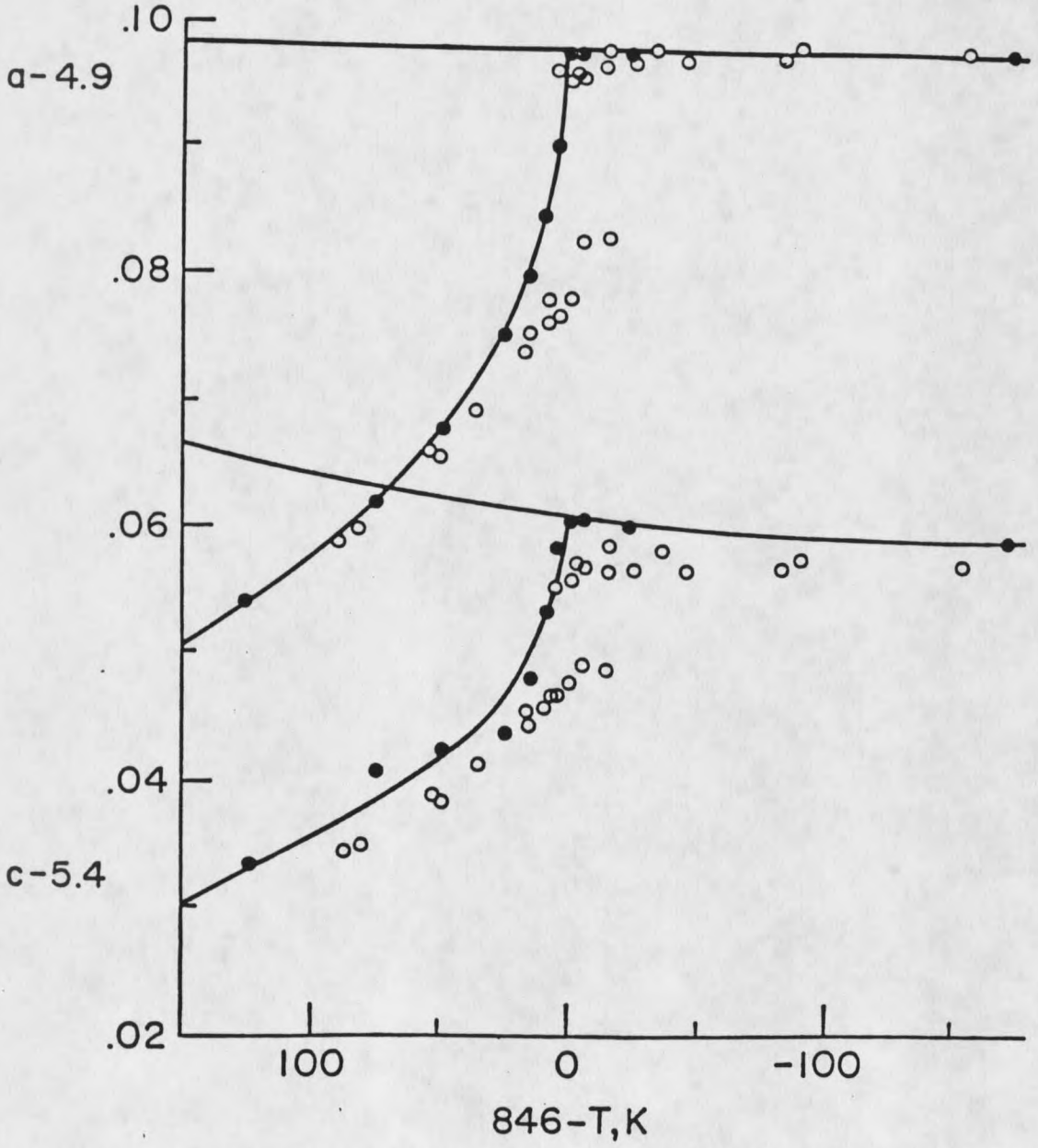

Figure 6. Cell demensions for alpha and beta quartz versus temperature. Our calculated fits to the values of Ackerman and Sorrel, filled circles, are shown as solid lines. Older experimental values of Jay,(1939) and Berger et al.(1966) are shown as open circles.

$$(dT/dP) = -(1/VT)(\Delta\alpha/\Delta C_p) \quad (58)$$

and

$$(dT/dP) = -\Delta\beta/\Delta\alpha. \quad (59)$$

where V_β and S_β are the volume and entropy of beta quartz, V_α and S_α are the volume and entropy of alpha quartz respectively, T is the temperature, α is the coefficient of thermal expansion $(1/V)(dV/dT)_P$, β is the compressibility $(1/V)(dV/dP)_T$, and C_P is the heat capacity. However, since α, β and C_P are increasing rapidly as the transition temperature is approached, see Figures 5 and 6, it is very difficult to get accurate measurements of $\Delta\alpha$, $\Delta\beta$ and ΔC_p.

Pippard[53] in 1956 devised a theory to treat a lambda transition accurately. The Pippard theory treats the surface below the lambda transition temperature as a cylindrical surface. Thus the equations he uses are

$$S = S_o + bT + f'(T/r - P) \quad (60)$$

and

$$V = V_o + aT + f(T/r - P) \quad (61)$$

where r is the equilibrium slope (dT/dP) . We are using the equivalent expressions,

$$S_\alpha = S_\beta + 1/r_o\ f(\theta) \quad (62)$$

and

$$V_\alpha = V_\beta + r/r_o\ f(\theta). \quad (63)$$

where, r_o is the equilibrium slope at 0.1 MPa, S_α and S_β

are the entropies of alpha quartz and beta quartz respectively, V_α and V_β are the volumes of alpha quartz and beta quartz respectively and $\theta = T_\lambda - T$, that is, the amount the temperature is below the lambda transition temperature, T_λ.

The equilibrium slope $(dT/dP)_\lambda$ has been well studied. The initial slope is 0.265 K/MPa as measured by Cohen, Klement, and Adams.[54] Above 1500 MPa the slope is 0.2272 K/MPa and the equilibrium line is straight. So that if the volume and $f(\theta)$ are determined for the transition then the entropy can be calculated. Equations like the Pippard equation have been applied to the alpha quartz to beta quartz transition by various people.[55,56,57] The Pippard relations are used by Dolino, et al.[47,49] and Bachheimer and Dolino,[46] while they call the transiton first order. The main problem with these approaches is the experimental data they used. The Sinelnikov[58] heat capacity data are a distinct improvement over Moser's 1936 data.[59] However, one cannot expect to find good heat capacity measurements for small temperature intervals in a region where long time periods, 20 minutes or more, are required for equilibrium at each temperature. Fortunately, volume measurements are simpler and require only one equilibration per data point. Ackerman and Sorrel[50] have made accurate X-ray

measurements on powdered quartz, obtaining the cell dimensions of both alpha and beta quartz as shown in Figure 6.

Beta quartz is hexagonal so that the volume can be referenced to the two edges of the unit cell, a and c. These dimensions of beta quartz can easily be fit by a quardratic equation in $\theta = T_\lambda - T$. We calculated these equations for (a) and (c) to be

$$a = 4.9978 + 0.30765 \times 10^{-6}\theta \tag{64}$$

and

$$c = 5.4608129 + 0.264750 \times 10^{-4}\theta + 0.822328 \times 10^{-7}\theta^2. \tag{65}$$

The cell dimensions of both these equations are in angstroms. Both (a) and (c) for beta quartz increase with decreasing temperature, and the temperature dependence of each is small. Therefore, extrapolating to 150 K below the lambda transition should introduce little error in the volume of beta quartz, Figure 6. Most of the error in the volume is from the extrapolation of the cell dimension (c). The error in (c) should be well within ± 0.005 angstroms, even out to 150 K below the lambda point. This results in an error of ± 0.0217 cm^3/mole.

The unit cell dimensions of alpha quartz increase very rapidly with increasing temperature, as the lambda transition point is approached. Thus, a simple power

series in $\theta = T_\lambda - T$ will not work. We decided to use a power series with the leading term in $\theta^{(1-A)}$, where (1-A) lies between zero and one. There are enough theories for lambda transitions (Bragg and Williams[61] 1934, through a series of developments,[62,63] up to renormalization group theory by Kandanoff et al.,[64] and Levey et al.,[65]) to justify almost any choice of power from 0.20 through 0.875, even up to 0.95; however the simplest and easiest power to use is 0.5. Thus $(a_\beta - a_\alpha)^2$ and $(c_\beta - c_\alpha)^2$ will both be simple power series in (θ) with no constant term. By dividing by θ and using standard least squares programs we obtained the equations

$$(a_\beta - a_\alpha)^2 = 0.226806 \times 10^{-3}\theta - 0.867408 \times 10^{-7}\theta^2 + 0.259547 \times 10^{-9}\theta^3 - 0.242458 \times 10^{-10}\theta^4 \qquad (66)$$

and

$$(c_\beta - c_\alpha)^2 = 0.0105995 \times 10^{-3}\theta - 0.573545 \times 10^{-7}\theta^2 + 0.373483 \times 10^{-9}\theta^3 - 0.449171 \times 10^{-10}\theta^4. \qquad (67)$$

Figure 6 shows the calculated curves for the cell dimensions of both alpha and beta quartz between 700 and 900 K, and how these curves compare to the measured values of (c) and (a). The scatter in the values of (c) for alpha quartz look bad; however, the largest deviations from the plotted smooth curve are about 0.0025 angstroms

corresponding to an error in (c) or in the volume of alpha quartz of about 0.046%.

From the least squares values of the unit cell dimensions, the molar volumes of alpha quartz can be calculated. From the molar volumes of both alpha and beta quartz we calculated $f(\theta)$ at one degree intervals up to 50 degree intervals from the equation

$$V(T,0,1) - V(T,0,1) = f(\theta) \qquad (68)$$

giving the values shown in Table 8. The volume increase due to disorder in quartz is somewhat larger than 0.60 cm^3/mole since even 150 degrees below the lambda point there is still substantial disorder in equilibrium quartz. The ΔV values of 0.11 to 0.205 cm^3/mole reported by Ghiorso, et al.[66] and Filatov, et. al.[67] for a first order alpha to beta quartz transition result from omitting the very steep and highly curved portions of the last 5 to 15 degrees below the lambda point.

The volumes of both alpha and beta quartz are calculated from the equation

$$V = a^2 c \sin 120. \qquad (69)$$

We used the expressions from (a) and (c) including terms in θ^2. So that $f(\theta)$ logically should include terms from $\theta^{1/2}$ through θ^6; however, a reasonable fit to the values in Table 8 is given by the equation

$$f(\theta) = [0.003515080\theta - 0.158514 \times 10^{-4}\theta^2 + 0.733660 \times 10^{-7}\theta^3 - 0.116609 \times 10^{-9}\theta^4]^{1/2}. \quad (70)$$

We judge from Figure 6 that any errors in the extrapolation of (a) and (c) for beta quartz or in the alpha quartz cell dimensions should be less than 0.005 angstroms. Thus, the values of $f(\theta)$ should be within $\pm$ 0.022 cm^3/mole even as far out as 150 K below the lambda point. The cell dimension (c) of beta quartz contributes to most of the error in $f(\theta)$.

Table 8. The function $F(\theta)$ representing the difference in volume of alpha quartz from a fully disordered beta quartz at the same temperature.

$\theta = T_\lambda - T$ K	0	1	2	3
$f(\theta)$ cm^3/mole	0.	.0159155	.083456	.10197
θ	4	5	10	15	20
$f(\theta)$	.11748	.13105	.18333	.22219	.25398
θ	25	30	40	50	60
$f(\theta)$	.28118	.30510	.34597	.38044	.41022
θ	80	100	150		
$f(\theta)$	.46102	.50446	.59937		

Once the function $f(\theta)$ is known, the entropy of alpha quartz can be calculated by use of the equation

$$S_\alpha = S_\beta - (1/r_o)\, f(\theta). \quad (71)$$

where r_o is the initial slope of the equilibrium curve

between alpha and beta quartz. r_o has been measured by Cohen, et al.[54] in 1974 to be 0.265 ± 0.005 K/MPa. The entropy of beta quartz (S_β) can be calculated from the heat capacity equation for beta quartz

$$C_p = 69.0338 + 0.930215 \times 10^{-2}(T - 1000) - 0.819168 \times 10^{-5}(T - 1000)^2 + 0.547378 \times 10^{-7}(T - 1000)^3 - 0.587077 \times 10^{-10}(T - 1000)^4. \quad (72)$$

This equation can be extrapolated down to 150 K below the lambda point, since the heat capacity for beta quartz has essentially no contribution from the change in disorder.

From the entropy of alpha quartz, S_α, the heat capacity of alpha quartz (C_p) can be calculated. This is possible with the equation

$$\Delta S = C_p \ln(T_1/T_2). \quad (73)$$

We have calculated the heat capacity of alpha quartz over 1 to 10 degree intervals resulting in the smooth curve drawn in Figure 5. The errors in the heat capacity of beta quartz and $f(\theta)$ could result in errors in the heat capacity of alpha quartz as large as 3 J/mole K. But, the errors in the experimental C_p of alpha quartz are over 10 J/mole K. Most of this 3 J/mole K error is from the heat capacity of beta quartz, 3 J/mole K is small, but not negligible. However, the error in the polynomial expansion for $f(\theta)$ fluctuates in sign. Thus much of the

error will cancel out upon integration of the equation. The entropy and enthalpy of alpha quartz near the lambda transition are tabulated in Table 9, along with the literature values from Moser 1936,[54] Robie 1978,[40] and Richet et al. 1982.[41]

Table 9. The entropy and enthalpy changes for alpha quartz near the lambda point.

	ΔS	ΔH	*	**	+
825-846 K	2.6642	2230.	1743.	1569.0	2443.5[++]
800-825 K	2.454	1994.	1925.	1844.0	1925.3
775-825 K	2.369	1866.	1846.	1818.0	1850.7
750-775 K	2.360	1800.	1800.	1791.7	1802.0

* - experimental Cp of Moser, 1936
** - Robie, et al., 1978
\+ - Richet, et al., 1980 compilation dependent on drop calorimetric experiments
++ - The interval used is 826 to 847 K to allow for the use of $T\lambda$ = 847. A correction of 655 J/mole, treated as first order transition has been added as in the published paper

From our enthalpy values for alpha quartz for the range 750 K to 846 K combined with the known heat capacities above and below this range, $H_{1000} - H_{298}$ can be calculated to be 45444.3 ± 70 J/mole. Also the entropy at 1000 K can be calculated to be S_{1000} = 116.215 J/mole K by use of the CODATA[68] value for the entropy of

alpha quartz at 298.15 K, $S_{298.15}$ = 41.46 J/mole K, and our ΔS for the range 750 to 846 K.

In order to check our value of $H_{1000} - H_{298.15}$ with the literature, we needed it to make use of the enthalpy of transformation of quartz to glass. The best experimental values are by Kracek, et al.[69] in 1953 for T = 298.15 K and by Navrotsky, et al.[70] in 1980 for T = 985. Their values are 9121 ± 250 J/mole and 7001 ± 200 J/mole respectively. Thus by transforming to glass at 298.15 K, heating to 985 K, transforming to beta quartz at 985 K and then heating to 1000 K, a value of $H_{1000} - H_{298.15}$ can be calculated to be 45452 ± 300 J/mole which is very close to our value of 45444 ± 70 J/mole. The heat capacity of glass and beta quartz was taken from Richet, et al.[41] for this calculation.

The Equation of State for Beta Quartz

Beta quartz is unusual in that over a 200 K range of temperature at low pressures it has a negative coefficient of thermal expansion, as shown in Figures 6 and 7. It is expected that like H_2O liquid below 277 K beta quartz will have a positive coefficient of thermal expansion at higher pressure. In any case the behavior of the thermal expansion coefficient versus pressure and the bulk modulus (K) versus temperature should not fit the Murnaghan-

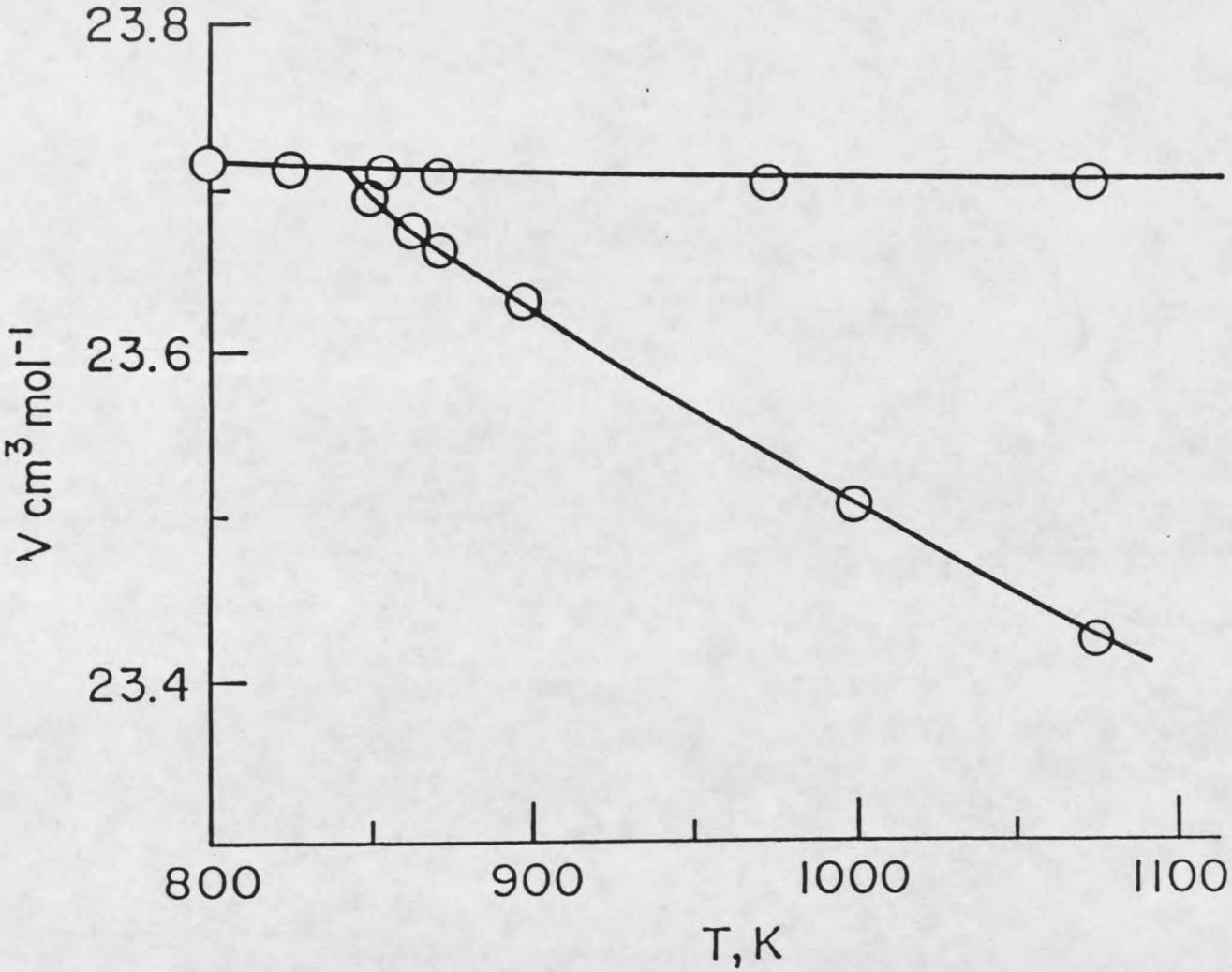

Figure 7. Volumes of Beta quartz at 0.1 MPa and at the lambda point plotted versus temperature.

Hildebrand equation of state as developed earlier in this thesis. Thus experimental values for the bulk modulus as a function of temperature for beta quartz are needed.

Krammer, Pardus, and Frissel[71] have measured the elastic moduli for beta quartz from 863 to 1073 K. These moduli can be used to calculate values of the bulk modulus (K) from the equation

$$K = (2S_{11} + S_{33} + 2(S_{12} + 2S_{13}))^{-1} \quad (74)$$

where S represents the elastic compliance constant. Using the value $V° = 23.70$ cm^3/mole, $K_o = 73046$ MPa from Kammer, et al.,[71] and estimating $N = 6$, the volume at the lambda point at 1073 K and 897 MPa can be calculated to be $V = 23.42$ cm^3/mole from the Murnaghan logarithmic equation of state

$$V = V_o(1 - NP/K_o)^{-1/N}. \quad (75)$$

Below 1200 MPa a cubic equation in pressure (P) can be used to describe the temperature of the lambda transition. The equation we are using is

$$T_\lambda = 846 + 0.265P - 0.11393229 \times 10^{-4}P^2 - 2.4632558 \times 10^{-9}P^3. \quad (76)$$

Since the volume of beta quartz and the volume at the lambda transition are known only up to 1073 K, as shown in Figure 7, it is necessary to extrapolate these curves to much higher temperatures. For the volume at the lambda point, we have assumed a linear relation with temperature

to extrapolate up to 1700 K, even though the volume has a very slight curvature at lower temperatures. The equation for the linear region is

$$V_\lambda = 24.54953 - 0.00105T. \quad (77)$$

To extrapolate the volume of beta quartz at 0.1 MPa ($V_{0.1}$) we have assumed that the volume goes through a minimum and that the thermal expansion coefficient becomes positive as the temperature reaches 1600 K. The polynomial equation

$$\begin{aligned} V = {} & 23.7013 - 0.105873 \times 10^{-5}(T - 1000) \\ & + 0.854633 \times 10^{-8}(T - 1000)^2 \\ & - 0.188601 \times 10^{-10}(T - 1000)^3 \\ & + 0.144073 \times 10^{-13}(T - 1000)^4 \end{aligned} \quad (78)$$

fits the data of Ackerman and Sorrell 1964[60] very well below 1373 K and extrapolates nicely to 2000 K. These extrapolations give a maximum value of K_o = 100,000 MPa at 1650 K, which is reasonable behavior for a material with K_o increasing with increasing T in the experimentally accessible region. The full 35 volume, temperature and pressure parameters are given in Table 10 for beta quartz. The volume and entropy contour lines from alpha and beta quartz are shown in Figures 8 and 9. The contour lines for the beta quartz volume and entropy are nearly vertical and horizontal because the slopes of these lines are $1/\alpha K$

Table 10. The equations of state, heat capacity equations and selected thermodynamic properties of alpha and beta quartz.

SiO_2 (C, BETA QUARTZ)

23.701266	-.1058728E-5	.854633E-8	-.188601E-10	.1440728E-13
-.1520712E-4	.2042034 E-7	-.519449E-10	.974922 E-13	-.714101E-16
.2441776 E-8	-.806657E-11	.1837775E-13	-.490703E-16	.492830 E-19
-.116290E-11	.3979281E-14	-.368804E-17	.917195 E-20	-.127623E-22
.2140223E-15	-.80183 E-18	.596339 E-21	-.701148E-24	.1175194E-26

SiO_2 (C, ALPHA QUARTZ)

24.340296	3.238095 E-4	7.855450 E-7	1.018418 E-9	5.083011E-13
-1.218243E-4	-5.371956E-7	-1.357596E-9	-1.73248E-12	-8.66629E-16
1.170823 E-7	5.474543E-10	1.376992E-12	1.886086E-15	9.986443E-19
-7.99760E-11	-3.38035E-13	-8.22533E-16	-1.14072E-18	-6.00664E-22
3.031544E-14	1.203374E-16	2.743039E-19	3.586603E-22	1.754802E-25
-5.78773E-18	-2.23346E-20	-4.71042E-23	-5.49837E-26	-2.30557E-29
4.329322E-22	1.658714E-24	3.241953E-27	3.236415E-30	1.010065E-33

HEAT CAPACITY (Cp)

A	B	C	D	E
(C, BETA QUARTZ)				
69.0387884	9.302148 E-3	-.819168 E-5	.5473777 E-7	-.587077E-10
(C, ALPHA QUARTZ)				
98.469291	.175798	.31970680E-3	2.1971990E-7	-.501216E-10

THERMODYNAMIC PROPERTIES	Y_{1000} J/MOL	H_{1000}-H_{298} J/MOL	H_{298} J/MOL	S_{298} J/MOL K	V_{1000} CM^3
(C, ALPHA QUARTTZ)	70.84657	47620.06	-910700.	41.46	24.3403
(C, BETA QUARTZ)	76.31535	39899.69	-905155.39	52.63	23.701

THE HEAT CAPACITY EQUATIONS ARE GIVEN BY $Cp=A+B(T-1000)+C(T-1000)^2+D(T-1000)^3 + E(T-1000)^4$.

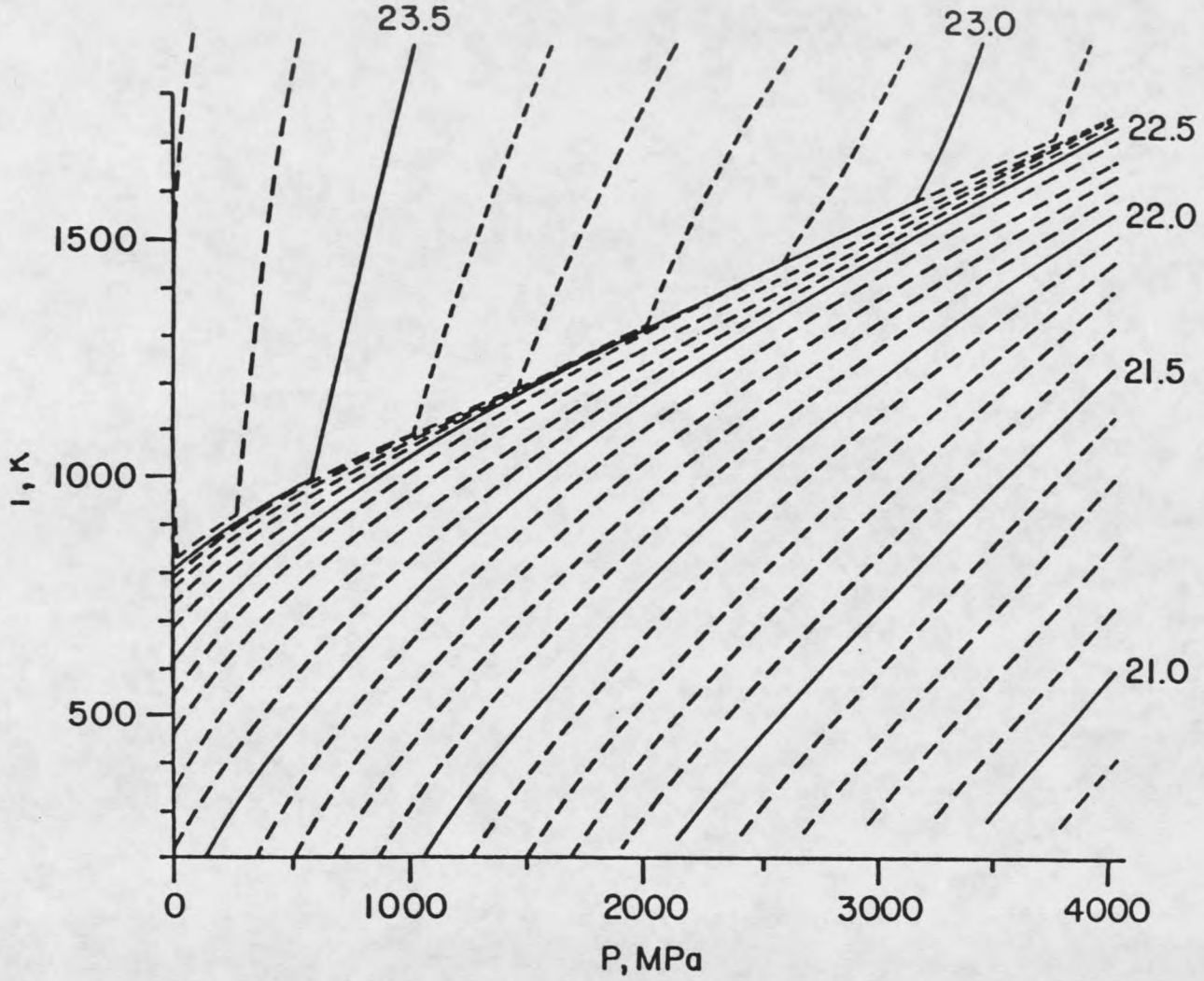

Figure 8. Our calculated contour lines for the volume of beta quartz.

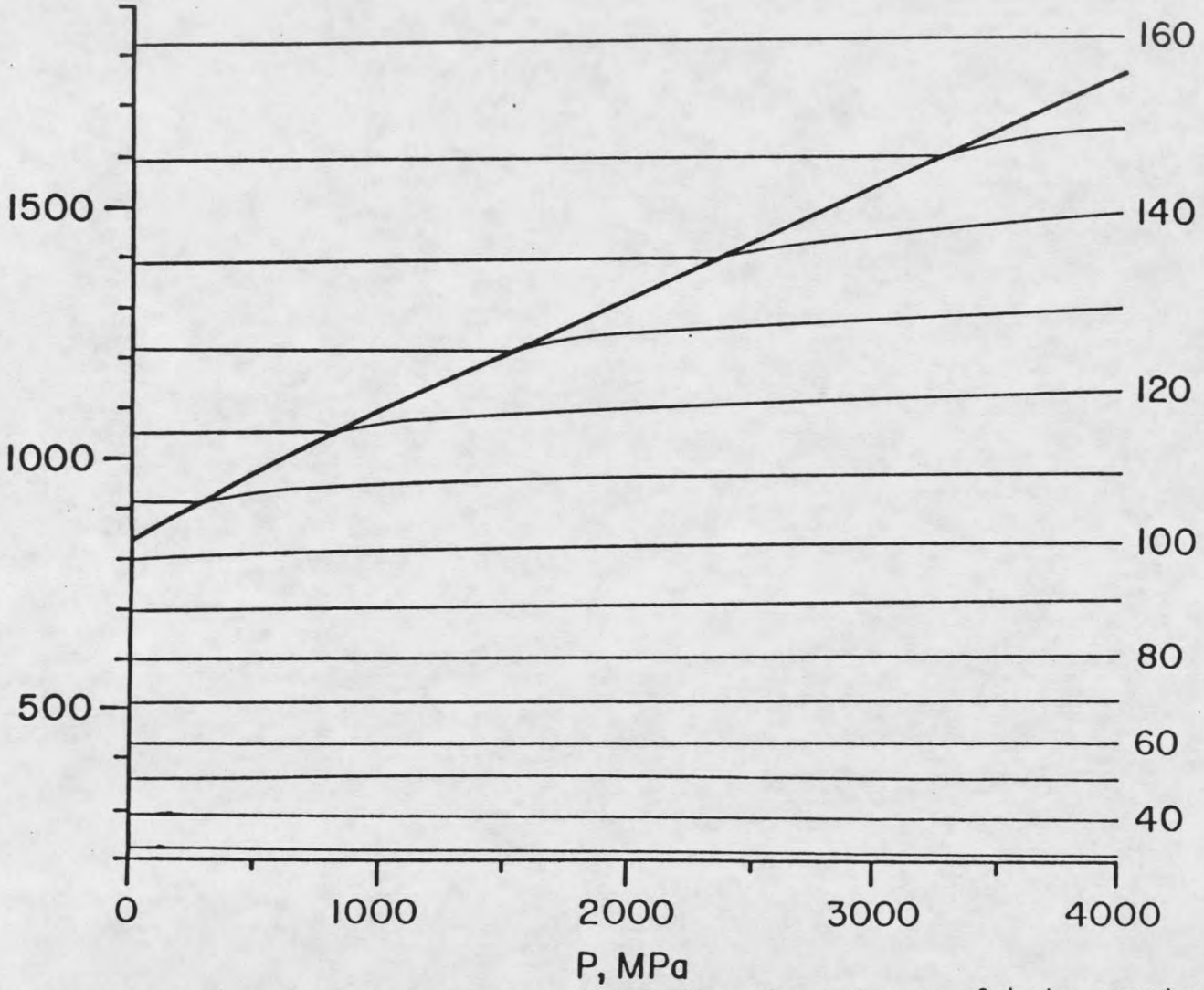

Figure 9. Our calculated contour lines for the entropy of beta quartz.

and $\alpha VT/C_p$ respectively, and the thermal expansion coefficient is very small.

The alpha quartz-beta quartz-coesite triple point at 1643 K and 3400 MPa is a convenient place to compare various equations of state. However, the only other treatment of beta quartz with enough detail to compare with our equation of state is the Murnaghan logarithmic equation of state which we calculated earlier. These two equations of state are compared in Table 11 along with the change in volume and entropy values for beta quartz going to coesite at 1653 K and 3440 MPa from Mirwald and Massone[72].

Equation of State of Alpha Quartz

For alpha quartz, as the lambda point is approached, the bulk modulus approaches zero and the thermal expansion coefficient and the heat capacity approach infinity. According to the Pippard theory[53] the volume and the entropy slopes are both limited by the equilibrium slope $(dT/dP)_\lambda$ which = (r). Therefore, as the volumes and the entropy contour lines approach the lambda transition they must bend sharply as shown in Figures 8 and 9 and Klement's Figure 6.

Table 11. Comparison of the thermodynamic values for beta quartz and coesite at high pressures and temperatures.

T K	P MPa	Quartz	ref.	beta Quartz	Coesite	ΔQ^*
1643	3400	H	**	-740206	-746483	-6277
			+	-739240	-748258	-9018
		S	**	151.50540	147.69553	-3.80978
			+	153.45105	148.05736	-5.39369
		V	**	22.96967	20.91757	-2.05210
1653	3440	H	**	-738539	-744944	-6405
			+	-737578	-746712	-9134
			++			-6900
		S	**	151.08281	148.12198	-2.96083
			+	153.93282	148.49823	-5.43459
			++			-4.2
		V	**	22.96209	20.91458	-2.04751
			+	21.67548	20.48325	-1.19223
			++			-3.1

*) The change in the H in (J/mole) , S in (J/mole K) and V in (cm^3/mole)
**) This Work
+) Howald, et al., 1985
++) Mirwald and Massone, 1980

The volume and entropy of alpha quartz both have terms in $\theta^{0.5}$ near the lambda transition where, $\theta = (T_\lambda - T)$. These terms are very difficult to represent accurately with a power series in temperature and pressure as θ approaches zero. Therefore, we have chosen to model alpha quartz with Pippard's theory 50 to 60 K below the

lambda transition. The thermodynamic properties are calculated from the equations

$$V_{alpha} = V_{beta} - r/r_o\ (f(\theta)) \quad (79)$$

$$S_{alpha} = S_{beta} - 1/r\ (f(\theta)) \quad (80)$$

where $r = (dT/dP)_\lambda$ the equilibrium slope, $r_o = 0.265$, $\theta = (T_\lambda - T)$ and $f(\theta)$ is given in Table 8. The choice of $1/r_o$ and r/r_o allows for the curvature in the equilibrium slope. The slope drops to 0.227231 for a pressure greater than 12000 MPa and r/r_o compensates for this by decreasing the change in volume of transition instead of increasing the change in entropy of transition with increasing temperature and pressure.

The equation of state for beta quartz should extrapolate reasonably well to 50 to 60 K below the transition temperature of 846 K. Then with the $f(\theta)$ values from Table 8, values for the volume and entropy of alpha quartz can be calculated at these temperatures and a series of pressures. Fitting a reliable power series is simple if good volume data are available along three of the edges of the area to be fit. At low pressures the volume and the bulk modulus are well known for alpha quartz, $K_o = 37200$ MPa, as reported by Weaver, et al.,[73] Soga[74] and McSkimmn, et al.[75] The values at $\theta = 55$ and 60 give the volumes and (dV/dT) along the upper edge from the Pippard theory. A few

intermediate temperatures for a good least squares fit need to be estimated; but, even estimates should be accurate to at least within ± 0.2 cm^3/mole. The equations of state obtained can then be checked against the entropy values at $T_\lambda - T = 60$ K and against the $(dT/dP)_S$ values measured at 800 and 1000 K by Boehler.[76] The contour lines for alpha quartz in Figures 8 and 9 are a third attempt in a series of successively better approximations.

Two major tests of the accuracy for the equation of state for alpha quartz are its match with the volumes and entropies from the Pippard theory shown in Table 12, and how $(dT/dP)_\lambda = \alpha VT/C_p$ compares to the experimental values of Boehler[76] shown in Figures 10 and 11.

Equation of State for Coesite

The quartz coesite equilibrium has been widely studied. This equilibrium provides a very stringent test of the equations of state since the change in enthalpy, ΔH, and the change in entropy, ΔS, are small, and very small changes in them can cause very large changes in the equilibrium slope ($\Delta V/\Delta S$). The volume and bulk modulus of coesite are well known.[73,77] The equation of state for coesite is shown in Table 13.

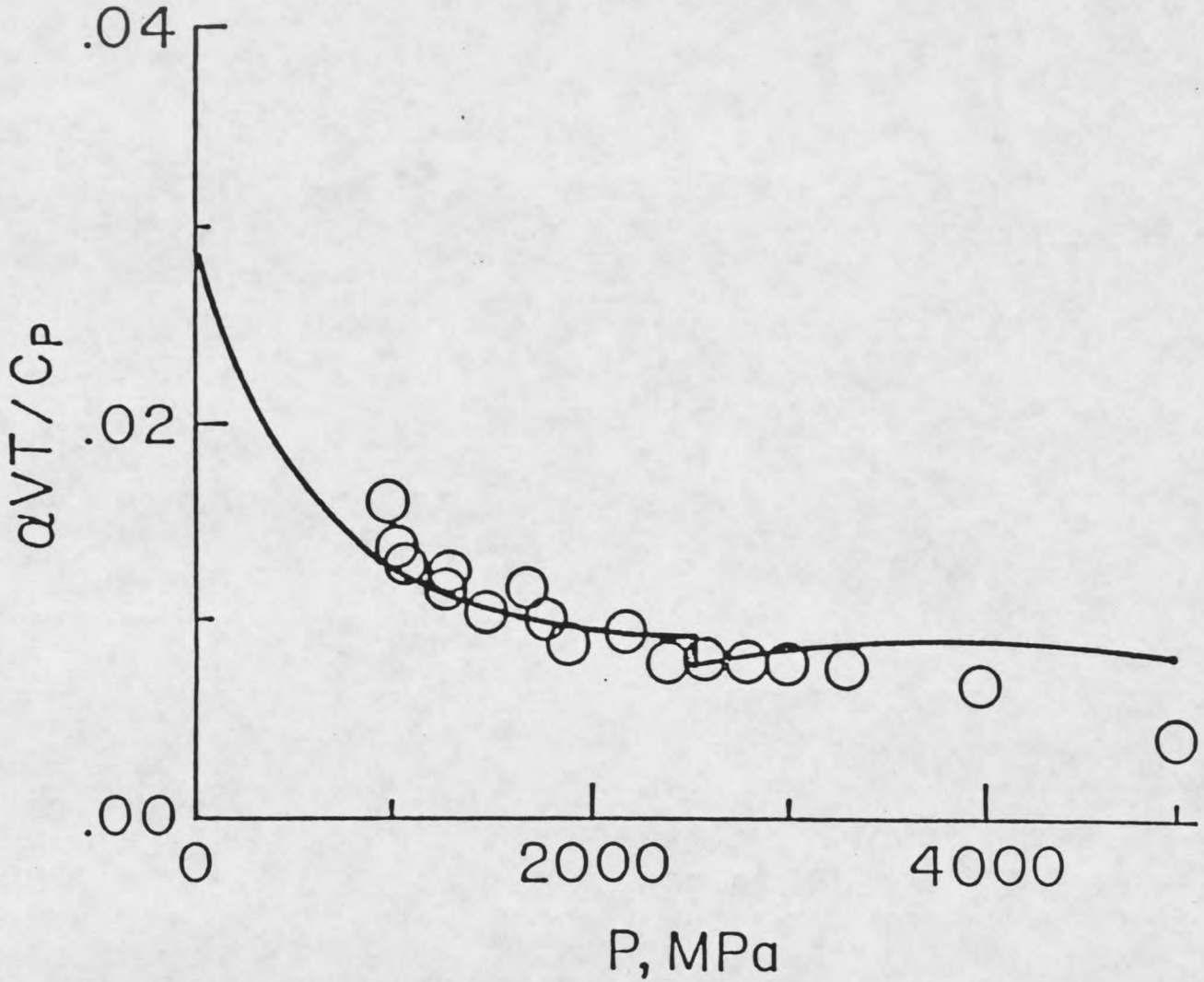

Figure 10. $(dT/dP)_\lambda = \alpha VT/Cp$ at 800 K. The solid line is our calculated curve. The open circles are the experimental values of Boehler.

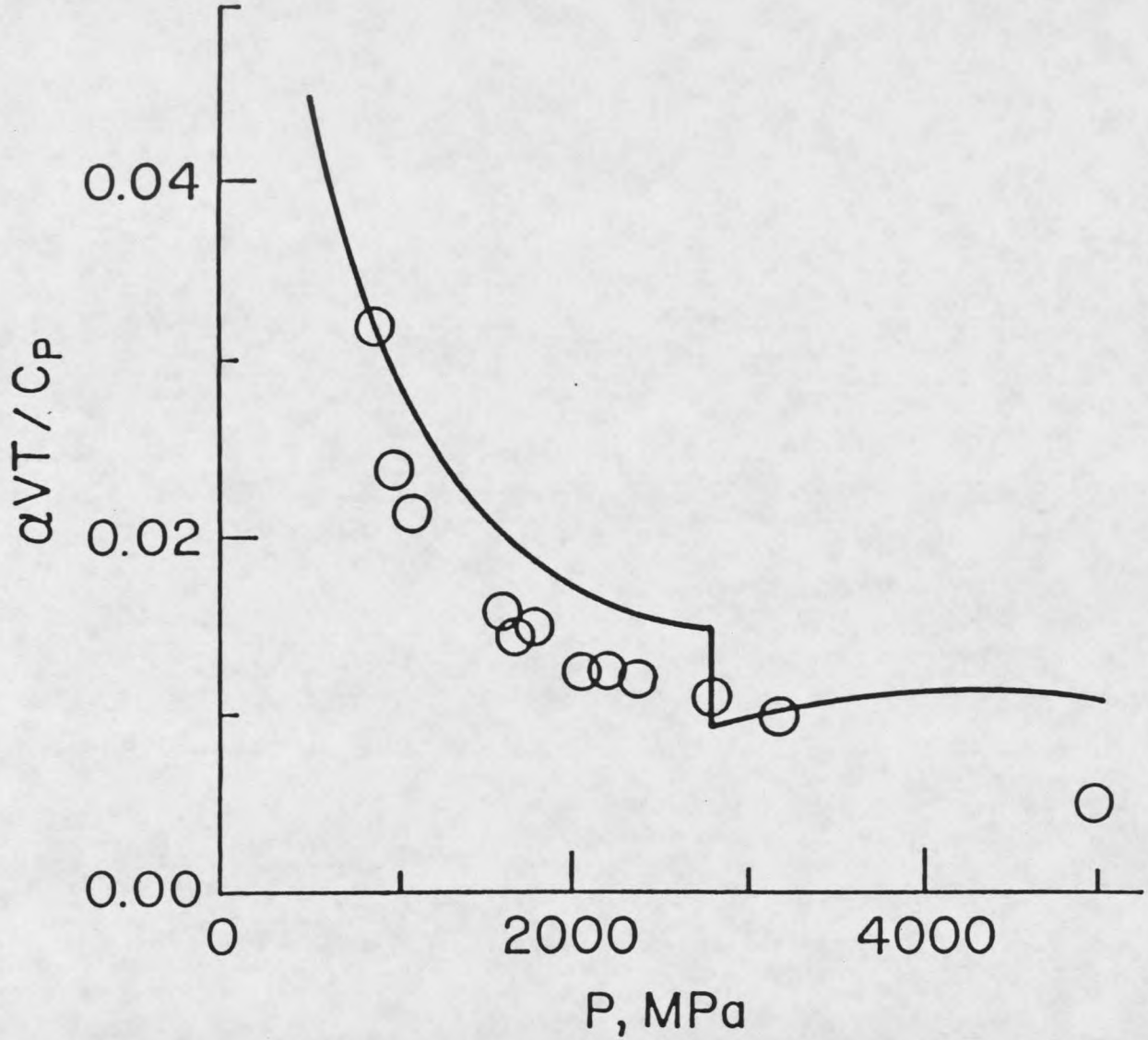

Figure 11. $(dT/dP)_\lambda = \alpha VT/Cp$ at 1000 K. The solid line is our calculated curve. The open circles are the experimental values of Boehler.

Table 12. Comparison of the polynomial fit and Pippard calculations for the thermodynamic properties of alpha and beta quartz 60 K below the lambda transition.

P MPa	T K	Material	H	S	V
0.1	786	beta quartz	-879756	99.91288	23.72101
		Pippard theory	-1281	-1.548	-.41022
		alpha quartz*	-881037	98.36490	23.31228
		alpha quartz**	-881052	98.36416	23.31228
2000	1265	beta quartz	-800119	132.4389	23.18649
		Pippard theory	-2023	-1.548	-.35175
		alpha quartz*	-802142	130.8909	22.83474
		alpha quartz**	-802356	130.8132	22.77600
3400	1583	beta quartz	-744774	148.67349	22.95617
		Pippard theory	-2515	-1.5487	-.35175
		alpha quartz*	-747289	147.12549	22.60442
		alpha quartz**	-747813	146.85953	22.54784

*) Values calculated from the beta quartz equation of state and the Pippard equations.
**) Values calculated from the alpha quartz equation of state

In order to accurately fit the measured equilibria between quartz and coesite, we had to successively adjust the heat capacity equation through successively adjusting its entropy and enthalpy. The heat capacity equation for coesite listed in Table 13 is

$$C_p = 9.0E\ (T/800) - 1.23583 + 0.625 \times 10^{-2}(T - 1000)$$
$$- 0.409460 \times 10^{-5}(T - 1000)^2$$
$$- 0.747870 \times 10^{-9}(T - 1000)^3$$
$$+ 0.195243 \times 10^{-10}(T - 1000)^4$$
$$+ 0.48 \times 10^{6}(1/T^2 - 1 \times 10^{6}) \qquad (81)$$

Figure 12 shows that the heat capacity is not unreasonably large or small over the temperature range under consideration.

Table 13. The equation of state, heat capacity equations and selected thermodynamic properties of coesite and high coesite.

SiO_2 (COESITE)[a]

0.208005E+02	0.300153E-04	0.480077E-09	-.255108E-13	-.689626E-16
-.111596E-04	-.230112E-08	-.272670E-12	-.783177E-16	0.648684E-19
0.420456E-09	0.145340E-12	0.420059E-16	0.294235E-19	-.269232E-22
-.167317E-13	-.672272E-17	-.390897E-20	-.397802E-23	0.378781E-26
0.511098E-18	0.198214E-21	0.196687E-24	0.234987E-27	-.227515E-30
-.929361E-23	-.322891E-26	-.478139E-29	-.617087E-32	0.602315E-35
0.713800E-28	0.218545E-31	0.437280E-34	0.588345E-37	0.000000E+00

HEAT CAPACITY (Cp)

A	B	C	D	E
SiO2 (COESITE)[b]				
-1.235835	.00625	-.040946E-4	-.074787E-8	.195243E-10

THERMODYNAMIC PROPERTIES	Y_{1000} J MOL^{-1}	H_{1000} -H_{298} J MOL^{-1}	H_{298} J MOL^{-1}	S_{298} J MOL^{-1} K^{-1}	V_{1000} CM^3
SiO2(COESITE)	68.77690	43080.19	-907213.9	40.46715	20.8005
SiO2(HIGH COESITE)	71.32204	43080.19	-903599.8	43.01228	20.8005

THE HEAT CAPACITY EQUATIONS ARE GIVEN BY Cp= A+B(T-1000)+C(T-1000)^2 +D(T-1000)^3 +E(T-1000)^4. [a]THE EQUATION OF STATE FOR COESITE AND HIGH COESITE ARE THE SAME EXCEPT FOR THE ENTROPY AND PLANCK FUNCTION. [b]THE HEAT CAPACITIES FOR COESITE AND HIGH COESITE HAVE THE ADDITIONAL TERMS .48E6(T^{-2}-10^{-6}) AND 9.0x E(800/T) WHERE E IS AN EINSTEIN TERM.

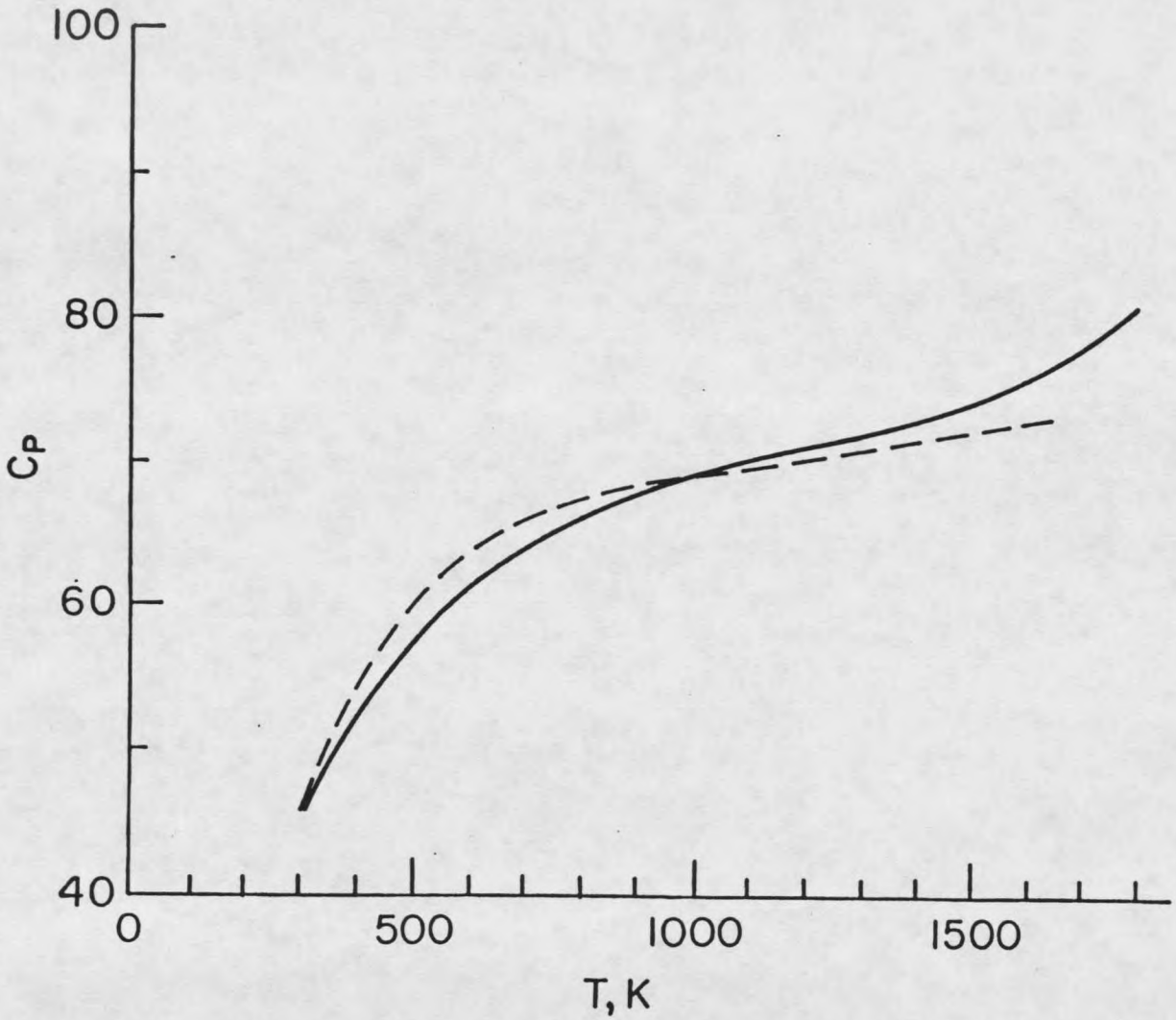

Figure 12. Heat capacity values for coesite (solid line) and cristobalite (dashed lines).

The calculated entropy value for coesite at T = 298.15 K is $S_{298.15}$ = 40.4672 ± 0.2 J/mole K, which agrees with the value reported by Holm, Kleppa and Westrum[78] of $S_{298.15}$ = 40.376. Our calculated enthalpy value for coesite at 298.15 K is $H_{298.15} = \Delta H_f$ = -907213.9 ± 200 J/mole. This enthalpy value along with the heat capacities for both quartz and coesite gives ΔH_{970} = 1103 ± 200 J/mole for beta quartz going to coesite. This can be compared to the values from Holm, et al., ΔH_{970} = 2930 ± 630 J/mole, and from Navrotsky, ΔH_{970} = 1339 J/mole. It is worth noting that a 200 J/mole shift in the enthalpy causes a substantial change in the slope and appearance of the equilibrium lines in Figure 13.

Our calculated values of the equilibrium are in good agreement with the measured equilibria up to 1400 K. Above 1400 K both alpha quartz and beta quartz going to coesite give calculated ΔS values and values of the equilibrium slope that are too negative and that are too small compared to the measured data of Boyd and England[79] and Mirwald and Massone.[72] Since there must be a substantial increase in the entropy of alpha quartz as it approaches the lambda point, the only reasonable way to accomodate the higher slope is to increase the entropy of coesite at higher temperatures. We accomplished this by making a first order transition in coesite with an entropy

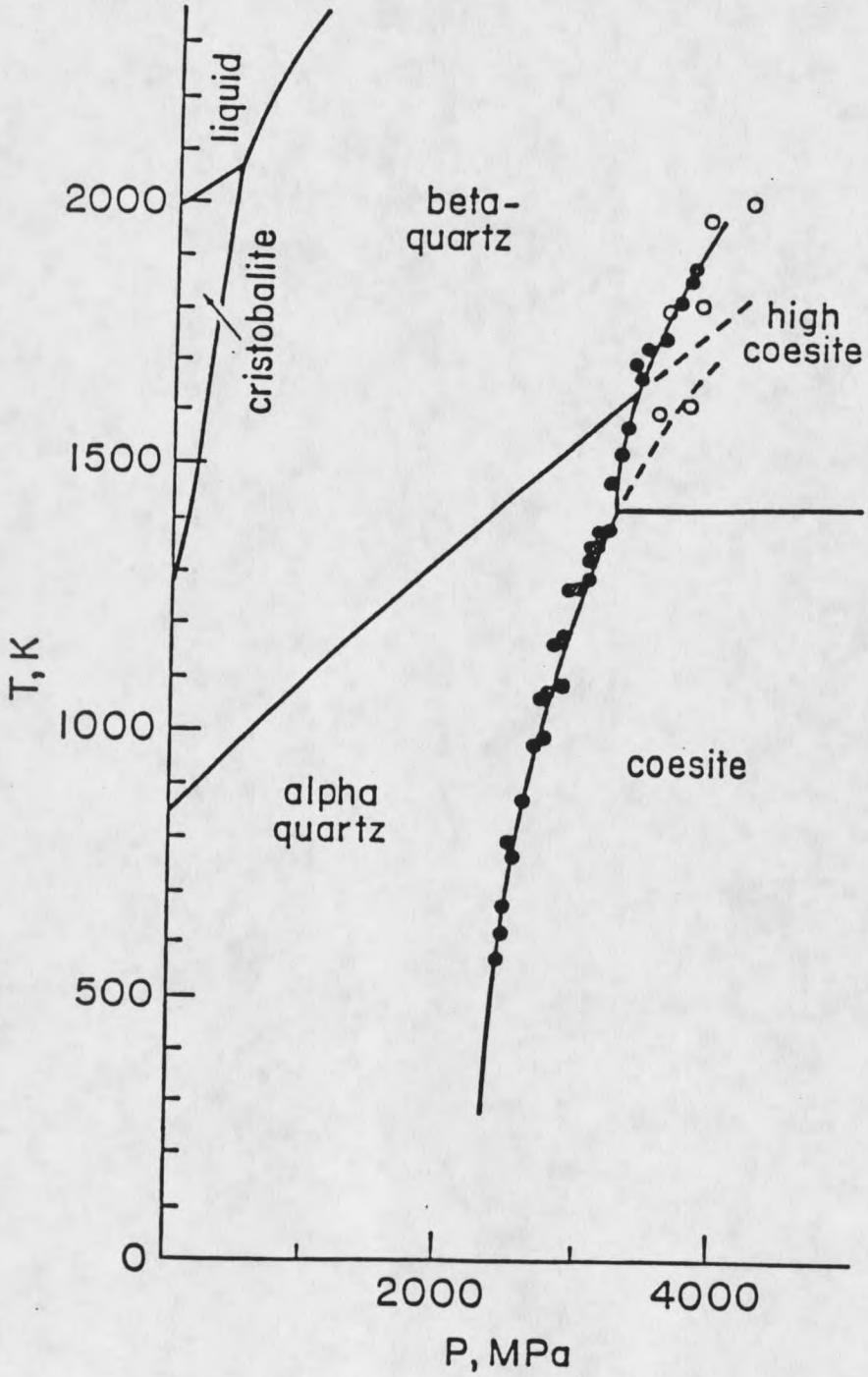

Figure 13. Calculated phase diagram for SiO_2. Filled circles are from (Boehler, 1982; Bohen and Boetcher, 1982; Mirmald and Massone, 1980) with the values of Boyd and England, 1960, as open circles.

of transition equal to ΔS_{trans} = 2.5451 ± 0.2 J/mole K. The assumed transition in coesite is shown in Figure 13, with the continuation of the quartz to low coesite calculations included as dotted lines.

The Equation of State for Cristobalite

Eliezer, et al.[80] first treated cristobalite in 1978. This treatment was based upon the JANAF[32] values, except for an increase of 0.11 J/mole K in the entropy of cristobalite to bring the quartz cristobalite equilibrium point to 1175 K. We now have good heat capacity values for alpha and beta quartz and there is reasonable agreement in the changes of enthalpy for cristobalite as shown in Table 14. Thus the enthalpy changes for quartz going to cristobalite at various tempratures can be converted to changes in enthalpy for alpha quartz going to low cristobalite at 298.15 K. The best enthalpy changes in the literature for the reaction

$$SiO_2(\text{beta quartz}) = SiO_2(\text{cristobalite}) \qquad (82)$$

are by Holm, et al.[78] ΔH_{trans} = 1882.8 ± 630 J/mole at 970 K, and by Navrotsky, et al.[70] ΔH_{trans} = 907.928 ± 250 J/mole at 985 K. Converting these values to $\Delta H_{283.15}$ using our heat capacities yields 2356 ± 600 J/mole and 1389 ± 250 J/mole for Holm's and Navrotsky's values respectively. These values along with Kracek's[69] ΔH_{298} =

2636 ± 290 J/mole from enthalpies of solution data at 298.15 K are in very poor agreement. Certainly they are worse than the enthalpies from the quartz to glass transition. This indicates that the problem is with the cristobalite samples rather than the methodology.

Table 14. The thermodynamic properties of cristobalite

	this work	*	**	***	+	++
S_{298} +++	43.363	43.363	43.40	43.40	42.635	
H_{298}	-907916	-907864	-908346	-908346		-908346
T lambda	535	525	523	543	535	
S_{600}	83.954	84.300	84.60	83.789	83.178	83.138
$H_{600}-H_{298}$	18062	18232	17973	18008	18037	17635
S_{1000}	118.216	118.167	118.61	117.80	117.36	117.69
$H_{1000}-H_{298}$	44985	44859	44735	44769	44890	44786
$H_{1000}-H_{1000}$ quartz	1456	21116	2122	1925		
$H_{298}-H_{298}$ quartz	2785	2836	2354	2389		2354

*) Richet, et al., 1982
**) Robie, et al., 1978
***) Stull and Prophet, 1971
+) Moseman and Pitzer, 1941
++) Elizer, et al., 1978
+++) S.I. units ,J/mole and J/mole K are used throughout this table

It appears that the entropy of the cristobalite is better known than the enthalpy, so that the enthalpy of

cristobalite at 298.15 K should be adjusted to fit what is known of the equilibrium between quartz and cristobalite, instead of adjusting the entropy. We have accepted Richet's[41] value for the entropy of low cristobalite of $S_{298.15}$ = 43.363 J/mole K. However, their transition temperature for the quartz to cristobalite equilibrium is too low at T_{eq} = 1108 K. Beta quartz is stable at 1141 and changes to tridymite at 1150 K in the presence of alkali silicates. Alkali silicates dissolve SiO_2 and should catalyze the transformation of quartz to cristobalite. Therefore the transition temperature needs to be even higher than 1141 K. The quartz to cristobalite transformation has been observed at 1163 K by Holmquist (1961), so that the equilibrium must be between 1163 and 1141 K. We picked 1160 for the equilibrium; thus, giving $H_{298.15}$ = -907915 for low cristobalite. Then the change in enthalpy for the alpha quartz to cristobalite transition is 2785 ± 200 J/mole, which agrees well with Kracek's value[69] but is higher than either Holm's[78] or Navrotsky's[70] values.

Using the available drop calorimetry data between 541.65 and 1834 K,[81,41] the heat capacity for cristobalite was fit to the following polynomial

$$C_p = 9.0\ E\ (T/800) - 1.49773 + 0.327610 \times 10^{-3}(T - 1000) + 0.201540 \times 10^{-5}(T - 1000)^2 + 0.601119 \times 10^{-8}(T - 1000)^3 + 0.127126 \times 10^{-11}(T - 1000)^4 + 0.48 \times 10^{6}(1/T^2 - 1 \times 10^{-6}); \quad (83)$$

where E represents an Einstein term, and the $1/T^2$ term keeps the higher polynomial powers from becoming excessively large within the region of 400 to 2000 K which the equation represents.

The literature values for $S_{600} - S_{298.15}$ for cristobalite are summarized in Table 14 and range from 40.3 to 41.2 J/mole K, so that the error in ΔS is the largest error in the enthalpy for cristobalite. Therefore we decided to treat the second order transition in cristobalite with the Pippard relations. The equation is

$$S_{low(450)} = S_{high(450)} - 1/r\ (V_{high(450)} - V_{low(450)}) \quad (84)$$

The equilibrium slope for this transition has been measured by Cohen and Klement[82] to be $(dT/dP) = 0.51$ K/MPa. The volume of high cristobalite at low pressure is described by the polynomial

$$V = 27.430 + 0.605751 \times 10^{-5}(T - 1000) - 0.86013 \times 10^{-8}(T - 1000)^2 + 0.15697 \times 10^{-10}(T - 1000)^3 - 0.884294 \times 10^{-14}(T - 1000)^4 \quad (85)$$

fit from the data of Johnson and Andrews[83] as cited in Skinner 1966,[84] and Touloukian 1967.[16] Graphical interpolation results in a volume of low cristobalite at 450 K of 26.04 cm^3/mole.[83,85] The change in volume is then $\Delta V = 27.181 - 26.04 = 1.141$ cm^3/mole yielding a change in entropy of 2.237 J/mole K. The low cristobalite entropy of Moseman and Pitzer[81] at 450 K, $S_{low} = 63.443$ J/mole K can be corrected to 64.194 J/mole K by using the better heat capacity of Leadbetter and Wright.[83] This value for S_{low} then yields an entropy of 66.431 J/mole K for high cristobalite from the Pippard equations. Using the heat capacity of high cristobalite gives $S_{high(600)} = 83.954$ and $S_{high(1000)} = 118.216$ J/mole K.

The high pressure volumes for cristobalite came from the Murnaghan-Hidebrand equation of state with $K_o = 14237$ MPa and N = 6. This value for K_o is an estimate chosen to give a reasonable value for the speed of sound in cristobalite and in SiO_2 liquid. The full polynomial equation of state for cristobalite is given in Table 15 along with the SiO_2(l) equation of state.

Table 15. The equations of state, heat capacity equations and selected thermodynamic properties of cristobalite and liquid quartz.

SiO_2 (LIQUID)

0.256903E+02	0.882893E-04	0.403999E-08	-.115153E-12	0.130579E-15
-.621362E-04	-.277794E-07	-.622431E-11	-.130836E-14	-.497927E-18
0.818605E-08	0.647971E-11	0.272915E-14	0.126817E-17	0.732965E-21
-.779195E-12	-.958310E-15	-.630580E-18	-.421055E-21	-.291350E-24
0.407254E-16	0.784452E-19	0.682613E-22	0.528631E-25	0.390861E-28
-.101736E-20	-.314107E-23	-.322660E-26	-.267420E-29	-.203681E-32
0.922540E-26	0.473867E-28	0.538327E-31	0.462225E-34	0.357553E-37

SiO_2 (C, CRISTOBALITE)

27.438	6.0575144E-6	-8.601635E-9	1.569704E-11	-8.84294E-15
.7023787E-4	-3.158457E-9	4.231581E-12	-6.83298E-15	3.541668E-18
1.6423549E-8	1.364669E-12	-1.75038E-15	2.550793E-18	-1.21353E-21
-3.58174E-12	-3.89561E-16	4.879866E-19	-6.69296E-22	3.000796E-25
4.927630E-16	6.014507E-20	-7.45014E-23	9.915851E-26	-4.30461E-29
-3.42292E-20	-4.40513E-24	5.426761E-27	-7.11521E-30	3.036980E-33
8.964361E-25	1.185093E-28	-1.45570E-31	1.893393E-34	-8.00699E-38

HEAT CAPACITY (Cp)

A	B	C	D	E
SiO_2 (L)				
71.00826	.0184709	-.532714E-5		
(C, CRISTOBALITE)[a]				
-1.497734	3.276100 E-4	2.015400 E-6	.601119 E-8	-1.27126E-12

THERMODYNAMIC PROPERTIES	Y_{1000} J MOL^{-1}	$H_{1000}-H_{298}$ J MOL^{-1}	H_{298} J MOL^{-1}	S_{298} J MOL^{-1} K^{-1}	V_{1000} CM^3
SiO2(L)	74.416376	44673.87	-904213.5	46.861	27.27
(C, CRISTOBALITE)	74.27571	43940.87	-906871.21	42.677	27.38

THE HEAT CAPACITY EQUATIONS ARE GIVEN BY $Cp=A+B(T-1000)+C(T-1000)^2+D(T-1000)^3+E(T-1000)^4$. [a]CRISTOBALITE ALSO HAS THE TERMS $.48\times10^6(T^{-2}-10^{-6})$ +9.0 E(T/800), WHERE E IS AN EINSTEIN TERM.

Equation of State for Silicon Dioxide Liquid

For liquid SiO_2 the heat capacity equation was fit to Richet's drop calorimetry measurements.[41] The heat capacity equation is

$$C_p = 71.0083 + 0.0184709(T - 1000) - 0.532714 \times 10^{-5}(T - 1000)^2. \quad (86)$$

The equation is valid over the range 400 to 2100 K.

The enthalpy of fusion for cristobalite is 8621 ± 150 J/mole at 1966 K. This value is arrived at from the measurements of ΔH for the quartz to glass transformation by Kracek[69] and Navrotsky,[70] the heat capacity of SiO_2 glass[41] and our heat capacity of cristobalite and liquid. Richet's value for the enthalpy of fusion of cristobalite is ΔH_{fus} = 8920 ± 1000 J/mole. Our entropy value for SiO_2 liquid is $S_{2000(l)}$ = 172.9484 J/mole K and Richet's is 172.915 J/mole K. Thus there is overall good agreement between our value and Richet's.

There are a variety of reported values for the physical properties of SiO_2 liquid. Thus, the thermal expansion coefficient between 2208 and 2438 K is $\alpha = 1.03 \times 10^{-4}$ K^{-1} as measured by Bacon, Hasapis and Wholley.[86] Bucaro and Dardy have measured the compressibility of SiO_2 liquid between 1650 and 2000 K to be $\beta = 8.5 \times 10^{-13}$ MPa,[86] and the ultrasonic velocity is C = 6000 m/sec[87] between 2060 and 2160 K. Using these

measured values and our calculated constant pressure heat capacity, C_P, we calculate the constant volume heat capacity C_V from the equations

$$C_V = C_P - TV\alpha^2 K_T \tag{87}$$

and

$$C_V = C_P/(1 + TM\alpha^2 c^2/C_P) \tag{88}$$

where V is the volume, α is the thermal expansion coefficient, K_T is the isothermal bulk modulus, c is the ultrasonic speed and M is the molecular weight of SiO_2. The constant volume heat capacity calculated from equation (87) is C_V = -616.36 J/mole K, and from equation (88) is C_V = 55.46 J/mole K. These values of C_V are obviously incorrect, and at least two of the three reported values of K_T, α and c must be wrong. For one thing the bulk modulus is too large. The bulk modulus of beta quartz is on the order of 5×10^4 MPa. One would expect the bulk modulus of SiO_2 liquid to be in this range if not smaller. The values of the thermal expansion coefficient and the ultrasonic speed are also in error as is shown by the results of equation (88). Consequently we have decreased the bulk modulus a factor of 100 to 1.11525×10^4 MPa and the thermal expansion coefficient to 8.8384×10^{-5} K^{-1}. With these changes the constant volume heat capacity and the ultrasonic speed are C_V = 79.262 J/mole K and c = 2343.9 m/sec. Both of these values are now reasonable.

Equations of State for Aluminum Oxide

In order to describe Al_2O_3 in binary and higher order phase diagrams we need to use the formula $AlO_{1.5}$. Aluminum oxide dissolves in oxide melts at very low concentrations contributing two Al^{+3} for every mole of aluminum oxide. The aluminum ions are not necessarily associated with each other. Therefore, in order to give Henry's Law behavior one must describe Al_2O_3 as $AlO_{1.5}$.

Henry's Law states that the activity of a solute is directly proportional to the mole fraction

$$a = Kx \tag{89}$$

where K is the Henry's Law constant. If we use Al_2O_3 then the activity of alumina is described by the square of the mole fraction. Since two Al^{+3} are dissolved per Al_2O_3

$$a = \gamma K x^2 \tag{90}$$

The activity can also be described at any concentration by the equation

$$a = \gamma x \tag{91}$$

thus, in dilute solutions

$$\gamma = Kx. \tag{92}$$

However, we are using R. K. coefficients to describe log such that

$$\log \gamma = \log Kx. \tag{93}$$

Therefore, as x approaches zero log γ approaches negative

infinity, which is impossible. Choosing $AlO_{1.5}$ as the formula for aluminum oxide avoids this problem.

Aluminum Oxide (C, Corundum)

The heat capacity equation for $AlO_{1.5}$ (c, corundum), listed in Table 16, was obtained through least squares fitting of the tabulated data of Stull and Prophet.[32] The equation is valid over the range 250 to 2400 K. The temperature dependence of the volume of $AlO_{1.5}$ was calculated from the accurate NBS X-ray data[87] and from the relative volumes measured by Engberg and Zehms.[88]

Howald, Moe and Roy[25] first calculated the equation of state for corundum in 1983. At this time they included a temperature dependence of N in the Murnaghan logarithmic equation of state.[21,22] Their value of N = 4.0 for corundum gives differences of as much as ± 4% between the measured and the calculated values of K_s at various temperatures, and a (dK_s/dT) of about -11 which is half that measured by Soga and Anderson.

If the discrepancies described above are real it indicates a small error in the Murnaghan-Hildebrand equation of state. In order to check this discrepancy we repeated the calculation with other parameters and additional data. We recalculated the volume as a function of temperature using constraints to force the thermal expansion coefficient to continually increase with

Table 16. The equations of state, heat capacity equations and selected thermodynamic properties of aluminum oxide corundum and liquid.

$AlO_{1.5}$ (LIQUID)

16.23	0.40000000E-4	4.499999E-10	4.500196E-15	3.379152E-20
-5.879075E-6	-8.81860E-10	-6.61392E-14	-3.31059E-18	-1.24850E-22
1.036895E-10	2.799532E-14	3.779063E-18	3.412825E-22	2.324960E-26
-2.23345E-15	-8.70313E-19	-1.69433E-22	-2.21229E-26	-2.17263E-30
5.167876E-20	2.610551E-23	6.561746E-27	1.105066E-30	1.386229E-34
-1.11168E-24	-6.68757E-28	-1.98662E-31	-3.93645E-35	-.574006E-38
1.482980E-29	9.853453E-33	3.214079E-36	6.971421E-40	1.103936E-43

$AlO_{1.5}$ (S,CORUNDUM)

0.130133E+02	0.275994E-04	0.397122E-08	-.186255E-11	0.117407E-14
-.431438E-05	-.627682E-09	-.123187E-12	0.302827E-16	-.288620E-19
0.492851E-10	0.137846E-13	0.257387E-17	-.129451E-20	0.139498E-23
-.790190E-15	-.775852E-18	0.872600E-22	0.327643E-24	-.146650E-27
0.336497E-19	0.145582E-21	0.119748E-25	-.174437E-28	-.426406E-31
-.209256E-23	-.175490E-25	-.729901E-29	-.638203E-32	0.143614E-34
0.507648E-28	0.802517E-30	0.567430E-33	0.648833E-36	0.000000E+00

HEAT CAPACITY (Cp)[a]

A	B	C	D	E
$AlO_{1.5}$ (LIQUID)				
94.69605	.019816	-.123850E-04		
$AlO_{1.5}$(S,CORUNDUM)[b]				
2.47207	.00482352	.545513 E-6	-.708193 E-9	.165569 E-12

THEMODYNAMIC QUANTITIES	Y_{1000} J MOL^{-1}	$H_{1000}-H_{298}$ J MOL^{-1}	H_{298} J MOL^{-1}	S_{298} J MOL^{-1} K^{-1}	V_{1000} CM^3
$AlO_{1.5}$ (LIQUID)	50.16645	34333.9	-824498.8	69.82366	16.238
$AlO_{1.5}$ (S,CORUNDUM)	51.11802	38982.328	-837846.	25.44894	13.0133

[a] THE CAPCITY EQUATION IS GIVEN BY $(Cp) = A + B(T-1000) + C(T-1000)^2 + D(T-1000)^3 + E(T-1000)^4$. [b] $AlO_{1.5}$(S,CORUDUM) HAS AN ADDITIONAL EINSTEIN TERM 7.5E(T/708).

increasing temperature. A graph of the thermal expansion coefficient versus temperature is shown in Figure 14. We included the extensive single crystal measurements on corundum cited by Simmons and Wang[89] which included $K_{s,298.15} = 250800$, $N = 4.27$ and an extensive series of measurements on the temperature dependence of K as published by Tefft.[90]

With $N = 4.27$ and $K_{298.15} = 250800$ we were able to calculate the temperature dependence of K_s. The calculated K_s values are plotted in Figure 15 along with the experimental values. The slope of the Murnaghan-Hildebrand line is still smaller than that indicated by the experimental data. However, this line is well within ±2% of the experimental values. An older calculation giving a line with even more curvature can be found in Howald, et al.[25]

The uncertainties present in the thermal expansion coefficient for corundum can introduce uncertainties of about ±2% in K_s through the equation

$$K_s = K[C_p/(C_V - \alpha^2 VKT)] \tag{94}$$

Also, it is not certain whether the high temperature values reported for K_s are good to better than ± 2%. Thus, while the Murnaghan-Hildebrand equation of state does not fit the measured slopes (dK_s/dT) of Soga and

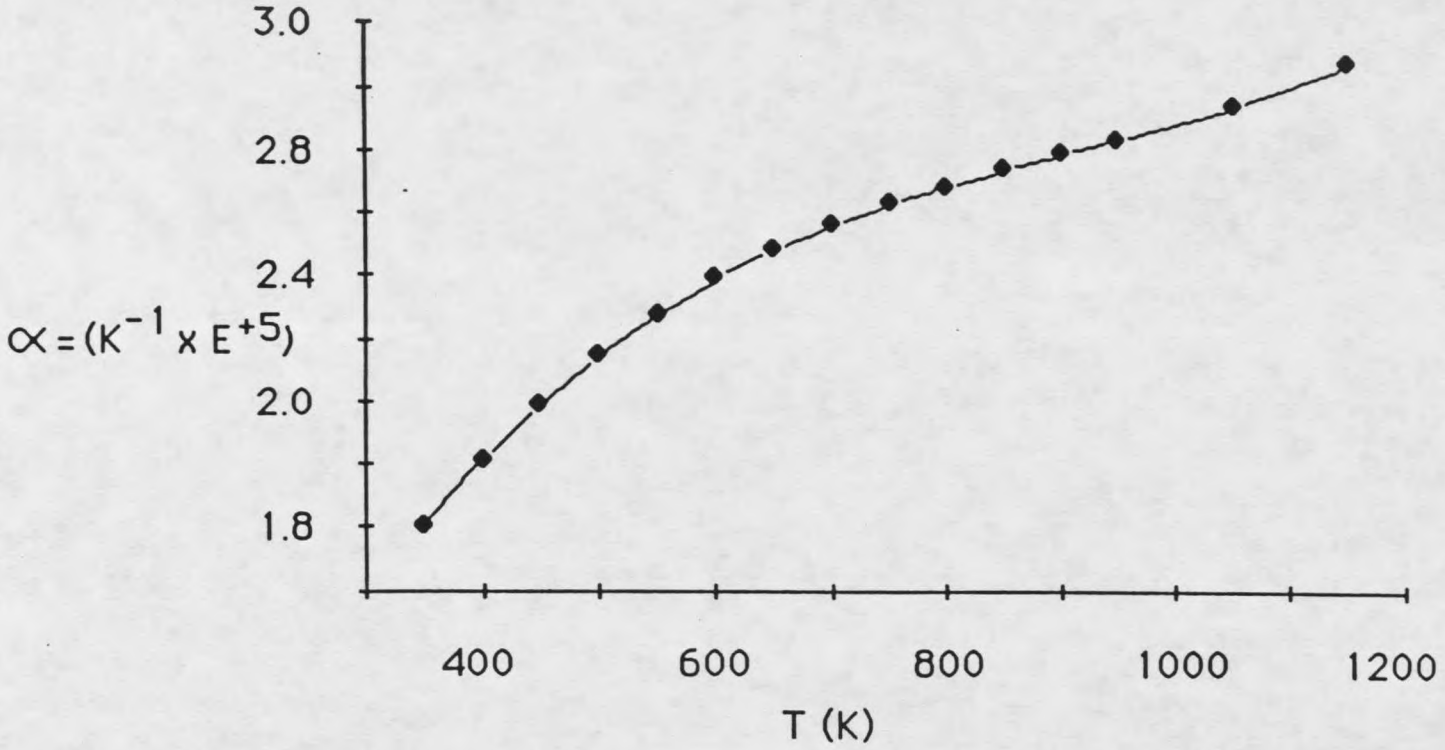

Figure 14. The thermal expansion coefficient of aluminum oxide versus temperature.

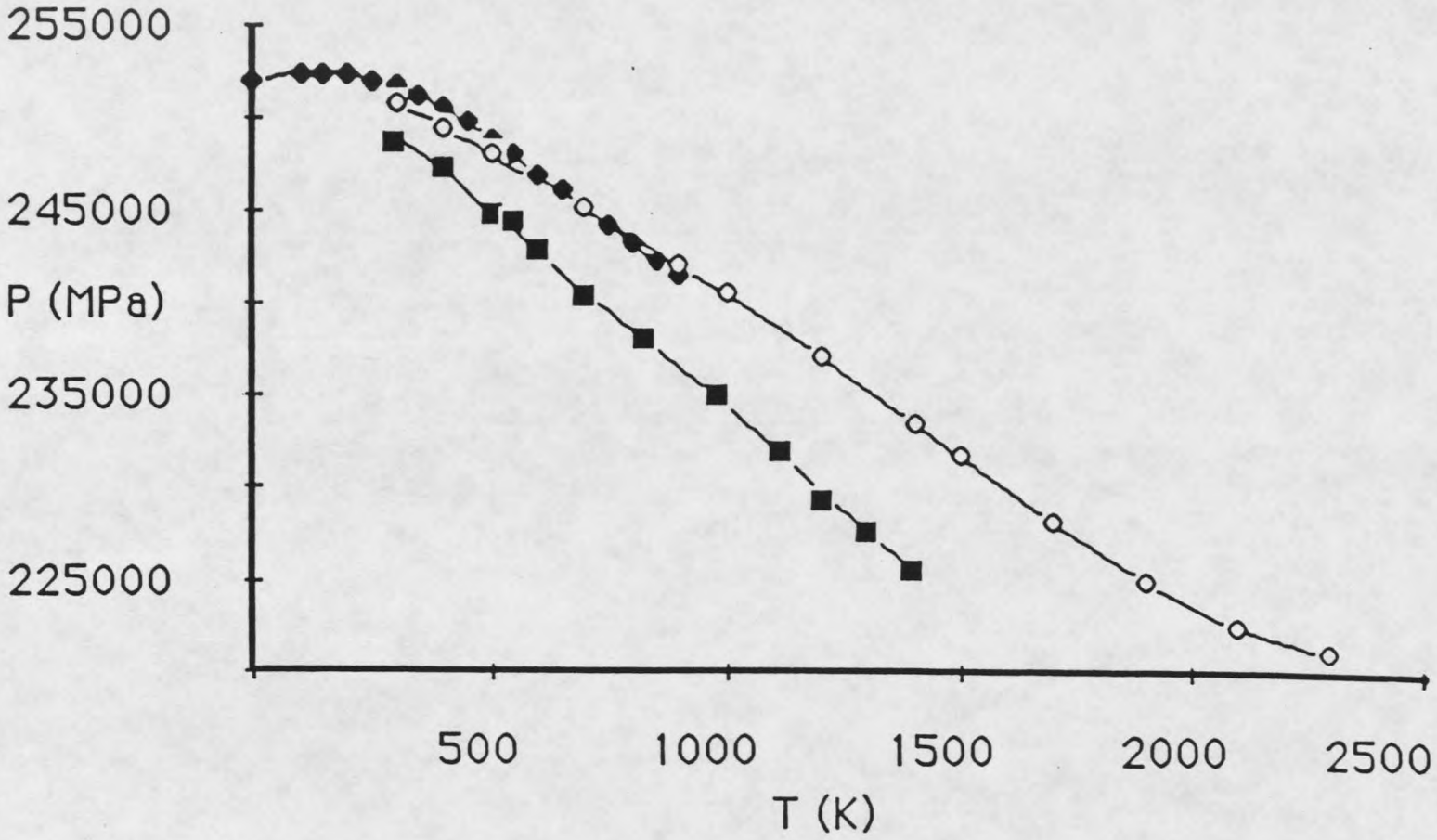

Figure 15. The adiabatic bulk modulus of $AlO_{1.5}$ versus temperature. The filled circles are values from Tefft (1966), the open circles are our calculated values and the solid diamonds are the values of Soga and Anderson (1967).

Anderson[29] and Tefft,[90] it nevertheless falls within the experimental errors present.

We have used the Murnaghan logarithmic equation of state[21,22] to calculate the pressure dependence of the volume of corundum. We then fit these calculated points by least squares procedures. The full 35 term polynomial is given in Table 16.

Aluminum Oxide (Liquid)

There is a lack of good experimental values for the enthalpy of fusion of $AlO_{1.5}$. This is due mainly to the high temperature at which it melts, 2327 K. Shpilrain's[91] work explains the discrepancies about the melting point by using a high heat capacity for the liquid, so the enthalpy of fusion is small at equilibrium but, 50 to 150 K above the melting point, is substantially larger. We have decided to use Shpilrain's heat capacity equation

$$C_p = 27.66 - .00296\ (T - 1000\ K) \qquad (95)$$

as a basis for our heat capacity equation. However, Shpilrain's equation does not extrapolate well to low temperatures, so we changed the equation to give reasonable values at these temperatures. The heat capacity equation is given in Table 16. We are also using Shiplrain's[91] heat of fusion of $AlO_{1.5}$, ΔH = 12.85 Kcal/mole.

There is no experimental data on the volume of $AlO_{1.5}$ liquid. Thus, the equation of state for $AlO_{1.5}$(l) in Table 16 is calculated from estimates of V_o, K_o, α and N. The volume of $AlO_{1.5}$(l) was estimated to be 25% larger than the volume of $AlO_{1.5}$ (c, corundum). K_o and N were estimated to be 170,000 MPa at 1000 K and 5, respectively. With these estimates we were able to calculate the equation of state using the Murnaghan-Hildebrand equation of state.

The Stoichiometric Phases

Forsterite

The heat capacity equation for forsterite, Mg_2SiO_4, shown in Table 17 was calculated from the high temperature enthalpy data of R. L. Orr.[92] An Einstein term was included to fit the low temperature heat capacity data of K. K. Kelly.[93] This equation is valid up to 2000 K and extrapolates well up to the melting temperature of Forsterite at 2100 K. The enthalpy of formation of Forsterite at 298.15 K is -2168486.75 J/mole. This value is calculated from the enthalpy of solution with hydrofluoric acid,[94] and from the enthalpies of formation of MgO and cristobalite.

The temperature dependence of the volume shown in Table 17 is calculated from the tabulated data of

Touloukian et al.[16] The pressure dempendence of the volume is calculated using the Murnaghan-Hildebrand logarithmic equation of state with N = 5.0 and $K^{\circ}_{298.15}$ = 128134 MPa as experimentally determined by Graham and Barsch.[95]

Table 17. The equation of state, heat capacity equation and selected thermodynamic properties of forsterite (Mg_2SiO_4).

Mg_2SiO_4 (C, FORSTERITE)				
44.900	0.38494257E-4	8.5512090E-9	1.432073E-13	-6.64640E-16
-8.767975E-6	-2.026311E-9	-6.45672E-13	-9.93583E-17	1.968706E-20
2.306197E-10	9.769012E-14	4.053964E-17	1.071385E-20	7.874807E-25
-7.39389E-15	-4.53815E-18	-2.31366E-21	-8.45035E-25	-1.73786E-28
2.494164E-19	1.966847E-22	1.170763E-25	5.312951E-29	1.530971E-32
-7.25419E-24	-6.67828E-27	-4.39426E-30	-2.27676E-33	-7.66702E-37
1.170027E-28	1.170020E-31	8.138615E-35	0.4533533E-37	1.645590E-41

HEAT CAPACITY (Cp)[a]

A	B	C	D	E
17.149773	.01588391	7.14404 E-6	-.324016 E-8	9.39570E+5

THERMODYNAMIC PROPERTIES	Y_{1000} J MOL^{-1}	$H_{1000}-H_{298}$ J MOL^{-1}	H_{298} J MOL^{-1}	S_{298} J MOL^{-1} K^{-1}	V_{1000} CM^3
Mg_2SiO_4 (C, FORSTERITE)	172.51588	109559.	-2168486.8	95.1900	43.790

[a] THE HEAT CAPACITY EQUATION IS GIVEN BY A + B(T-1000) + C(T-1000)^2 + D(T-1000)^3 + E(1/T^2 -10^{-6}). [b] FORSTERITE ALSO HAS AN ADDITIONAL EINSTEIN TERM 10E(T/500).

Enstatite (Magnesium Silicate)

The stochiometric compound $MgSiO_3$ has three different crystal structures corresponding to Clinoenstatite,

orthoenstatite and protoenstatite. The volume data for these three phases is taken from Touloukian, Kirby and Taylor's[16] tabulated thermal expansion data for nonmetallic substances. The bulk moduli for these phases were taken from Clark,[96] and values of N are estimates. The heat capacity equations for the enstatites listed in Table 18 are from K. K. Kelly[93] and K. K. Kelly.[97]. These equations are good over the range 298.15 to 1800 K. Figure 16 shows the calculated equilibria between the various enstatites using our equations of state.The experimental points are those of Grover [98] and Boyd and England.[99]

Spinel (Magnesium Aluminate)

The heat capacity equation for spinel, $MgAl_2O_4$, in Table 19 is from Bulletin 1452[40] and then adjusting these values for Mg-Al disorder as described by Howald, et al.[25] The temperature dependence of the volume of $MgAl_2O_4$ is given in Table 19. This equation was obtained by least squares fitting of the values reported by Clark[96] from the work of Rigby, et al.[100] The pressure dependence of the volume is from Schreiber,[101] Chang and Barsch[102] and Anderson, Schrieber and Lieberman.[103] The bulk modulus is K_T° =200900 MPa and (dK/dP) = N = 4.19. Thus, the volume of spinel can be calculated at any temperature and pressure using the Murnaghan-Hildebrand equation of state.

Table 18. The equations of state, heat capacity equations and selected thermodynamic properties of the three forms of $MgSiO_3$; enstatite, protoenstatite and orthoenstatite

$MgSiO_3$ (C,PROTO ENSTATITE)				
32.997	2.9510326E-5	-2.68003E-10	-4.12588E-12	3.813557E-15
-.1034629E-4	-1.668996E-9	-8.50053E-14	1.994086E-1	-2.10916E-19
2.942106E-10	8.591046E-14	9.850342E-18	-8.48925E-21	1.007556E-23
-9.89823E-15	-4.12356E-18	-7.21290E-22	3.122188E-25	-4.53786E-28
2.742496E-19	1.405211E-22	3.087455E-26	-7.90949E-30	1.486818E-32
$MgSiO_3$ (C,ENSTATITE)				
32.1346	4.1944547E-5	1.3826728E-8	-3.09543E-14	-1.00521E-15
-1.155055E-5	-2.778779E-9	-1.22745E-12	-2.82446E-16	-1.78068E-19
3.870193E-10	1.688601E-13	9.135715E-17	3.643220E-20	2.064981E-23
-1.57082E-14	-9.80906E-18	-6.24682E-21	-3.47599E-24	-1.99796E-27
6.561695E-19	5.162945E-22	3.714745E-25	2.574122E-28	1.539655E-31
-2.23521E-23	-2.01031E-26	-1.56209E-29	-1.23274E-32	-7.60931E-36
3.961003E-28	3.815435E-31	3.093022E-34	2.619277E-37	1.648066E-40
$MgSiO_3$ (C,CLINOENSTATITE)				
32.0476	3.3448084E-5	5.0511436E-9	-3.89573E-12	8.830467E-21
-1.104299E-5	-2.033051E-9	-4.60007E-13	1.909745E-16	2.925781E-20
3.351322E-10	1.122201E-13	3.381681E-17	-7.36881E-21	-2.90019E-24
-1.19992E-14	-5.75027E-18	-2.13649E-21	1.952870E-25	1.928241E-28
3.487301E-19	2.056186E-22	8.695828E-26	-1.57312E-30	-7.64917E-33

HEAT CAPACITY (Cp)				
A	B	C	D	E
PROTOENSTATITE				
123.586	.0168455	-.164109E-4	.159434E-7	-.151109E7
ORTHOENSTATITE				
123.586	.0168455	-.164109E-4	.159434E-7	-.151109E7
CLINOENSTATITE[a]				
55.721425	.01195776	-.9537309E-5	-.229344 E-8	[b].397042 E-10

THERMODYNAMIC PROPERTIES	Y_{1000} J/MOL	H_{1000}-H_{298} J/MOL	H_{298} J/MOL	S_{298} J/MOL K	V_{1000} CM^3
PROTOENSTATITE	117.1442	77235.	-1548467.0	66.2475	31.599
CLINOENSTATITE	116.55215	75126.1	-1548597.8	67.86	31.470
PROTOENSTATITE	117.98970	77235.	-1547400.	66.7835	32.384

THE HEAT CAPACITIES ARE GIVEN BY THE EQUATION $(Cp)=A+B(T-1000)+C(T-1000)^2+D(T-1000)^3+E(T^{-2}-10^{-6})$. [a] CLINOENSTATITE HAS AN EINSTEIN TERM 8.5(1000/T)
[b]THIS TERM IS $E(T-1000)^4$

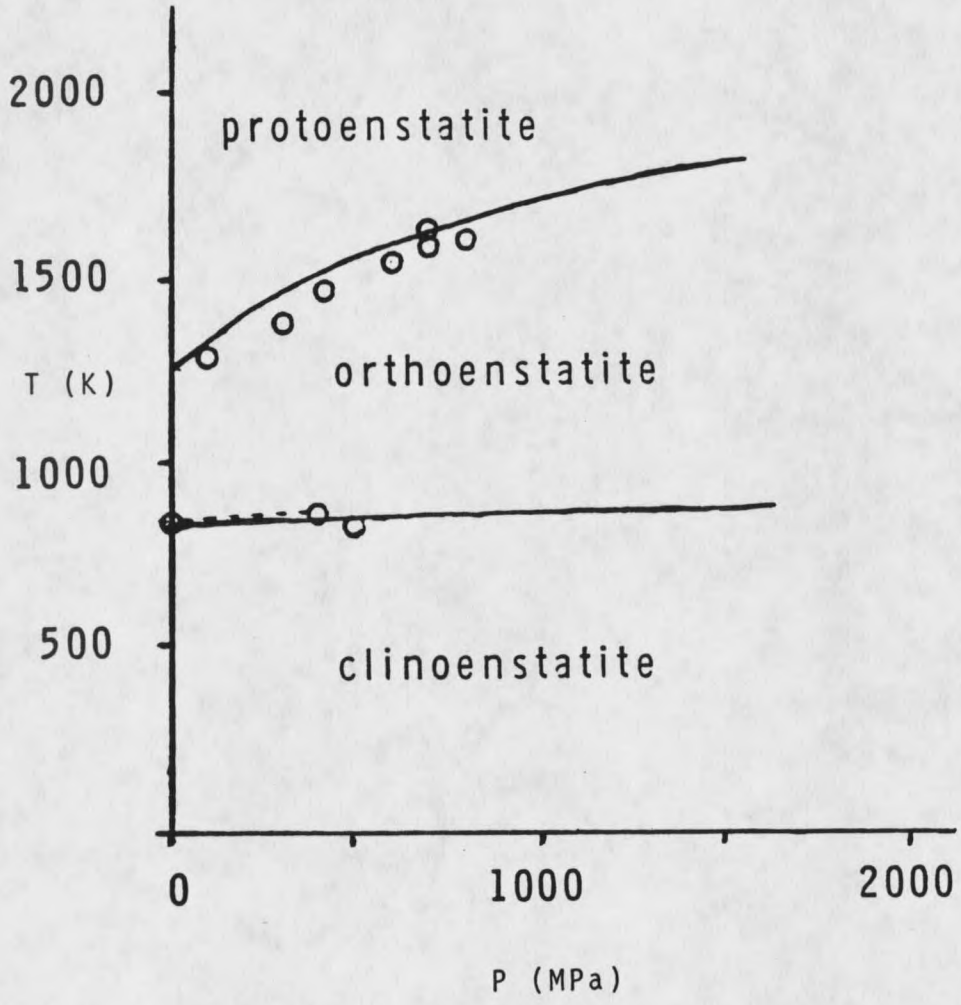

Figure 16. The calculated phase diagram for $MgSiO_3$. The experimental points shown are those of Grover 1972, and Boyd and England 1965.

Table 19. The equation of state, heat capacity equation and selected thermodynamic properties of spinel ($MgAl_2O_4$).

$MgAl_2O_4$ (C, SPINEL)

.404136E+02	.285336E-04	.419510E-08	-.146062E-11	-.457875E-17
-.535877E-05	-.793759E-09	-.164180E-12	.260203E-16	.341202E-20
.745188E-10	.199552E-13	.532159E-17	-.197197E-21	-.124942E-24
-.124816E-14	-.483529E-18	-.157824E-21	-.856107E-26	.270666E-29
.224941E-19	.113512E-22	.436263E-26	.557514E-30	-.236600E-34
-.389813E-24	-.236766E-27	-.102675E-30	-.187940E-34	-.770728E-39
.449630E-29	.304801E-32	.142237E-35	.309217E-39	.247142E-43

HEAT CAPACITY (Cp)[a]

A	B	C	D
185.173	.0370550	-.574449 E-4	3.52436 E-8

THERMODRNAMIC QUANTITIES	Y_{1000} J MOL^{-1}	$H_{1000}-H_{298}$ J MOL^{-1}	H_{298} J MOL^{-1}	S_{298} J MOL^{-1} K^{-1}	V_{1000} CM^3
$MgAl_2O_4$ (C, SPINEL)	153.580	112079.	-2300553.	80.63002	40.4136

[a] THE HEAT CAPACITY IS GIVEN BY $(Cp) = A + B(T-1000) + C(T-1000)^2 + D(T-1000)^3$.

Contour lines for the volume of $MgAl_2O_4$ are shown in Figure 17. Diferences from Figure 2. of Howald, Moe and Roy are due to the adoption of a Murnaghan-Hildebrand equation of state. Spinel undergoes disproportionation at higher temperatures according to the reaction

$$MgAl_2O_4 = MgO(c) + 2AlO_{1.5}(c). \qquad (96)$$

The contour lines showing ΔV for the disproportionation of spinel are shown in Figure 18. The equilibrium line in the pressure-temperature plane shows substantial

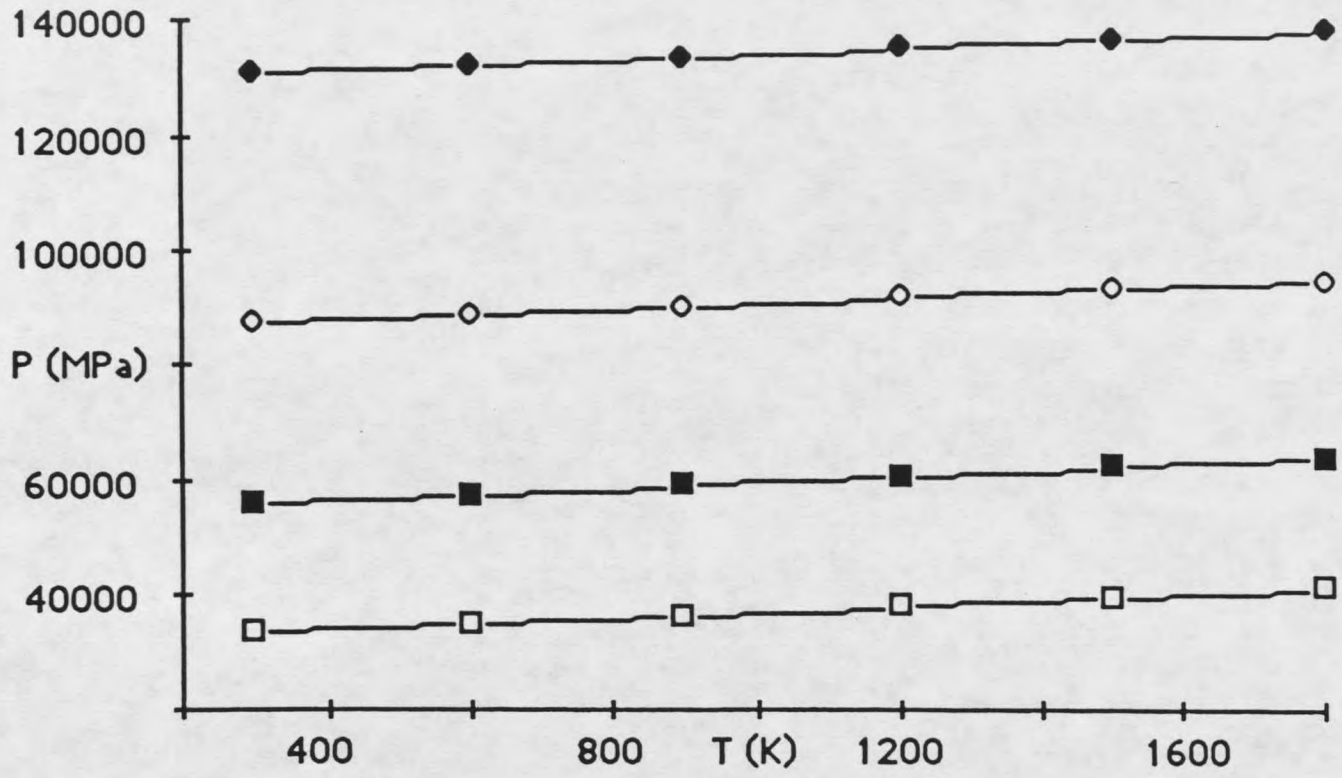

Figue 17. Contour lines for the volume of $MgAl_2O_4$, spinel as a function of temperature as reported by Howald, et al.

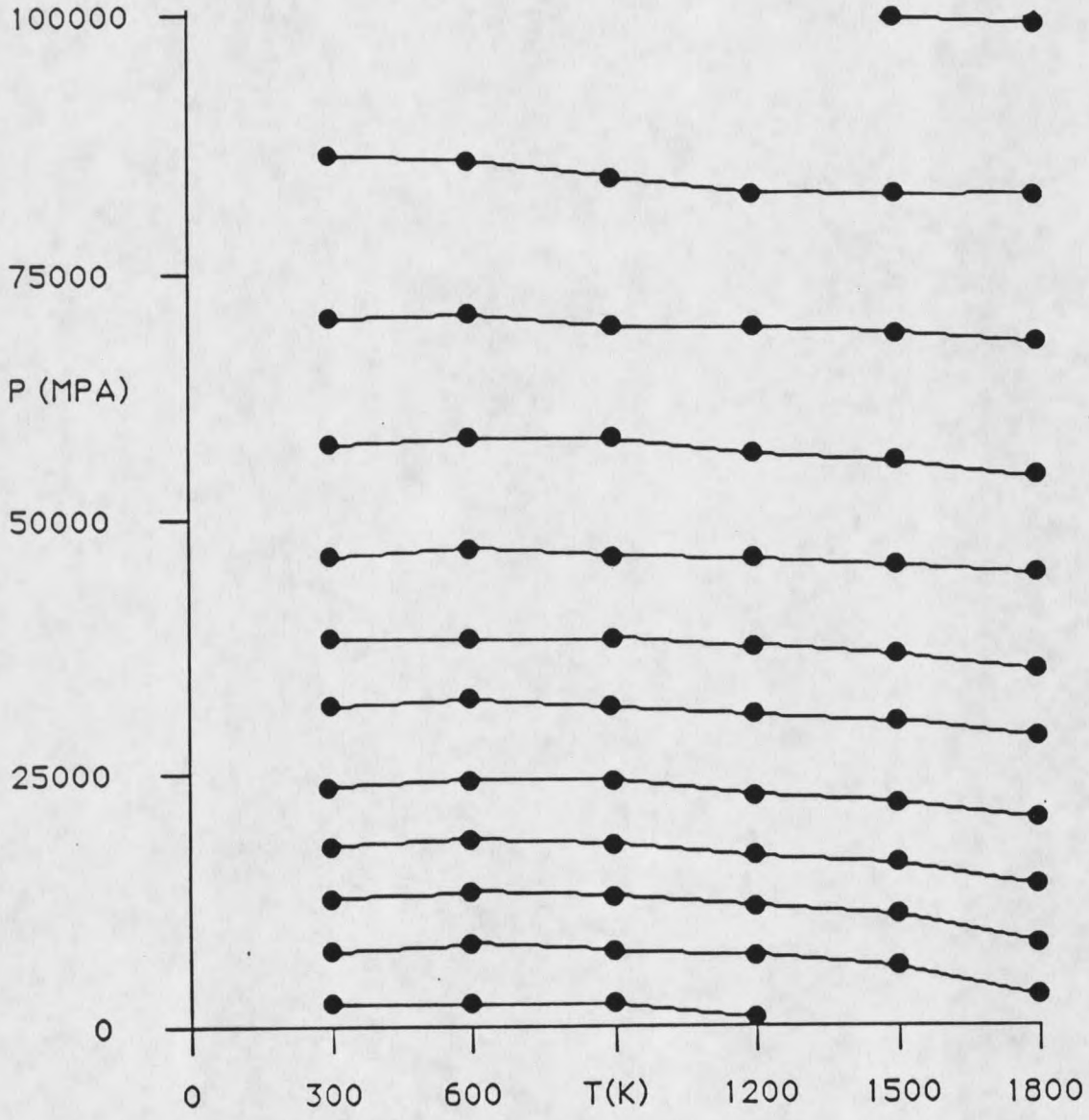

Figure 18. Countour lines showing ΔV for the reaction $MgAl_2O_4(c) = MgO(c) + 2AlO_{1.5}(c)$.

curvature, as shown in Figure 19. This is due primarily to the ΔS of the reaction shown in Table 20. The ΔS of disproportionation is large and negative due to the entropy of disorder between the Mg and Al cations, caused by the interchange of these ions within the spinel crystal structure.

Cordierite

It is essential to have a reasonable equation of state for cordierite, $Mg_2Al_4Si_5O_{18}$, since it shows up in the ternary phase diagram at high temperatures. In order to calculate the equation of state for cordierite we fit the volumes by least squares at the following temperatures: T = 300, 400, 900, 1400 and 1500 K. We were able to calculate the volumes at these temperatures from the coefficient of thermal expansion data listed in Memoir 97.[96] In order to calculate the pressure dependence of the volume listed in Table 21 we had to estimate values of N and K of 4.8 and 120,000 MPa respectively, since there is no pressure data available for cordierite.

The heat capacity equation for cordierite in Table 21 is taken directly from Robie, et al., Bulletin 1452[40] along with the selected thermodynamic properties.

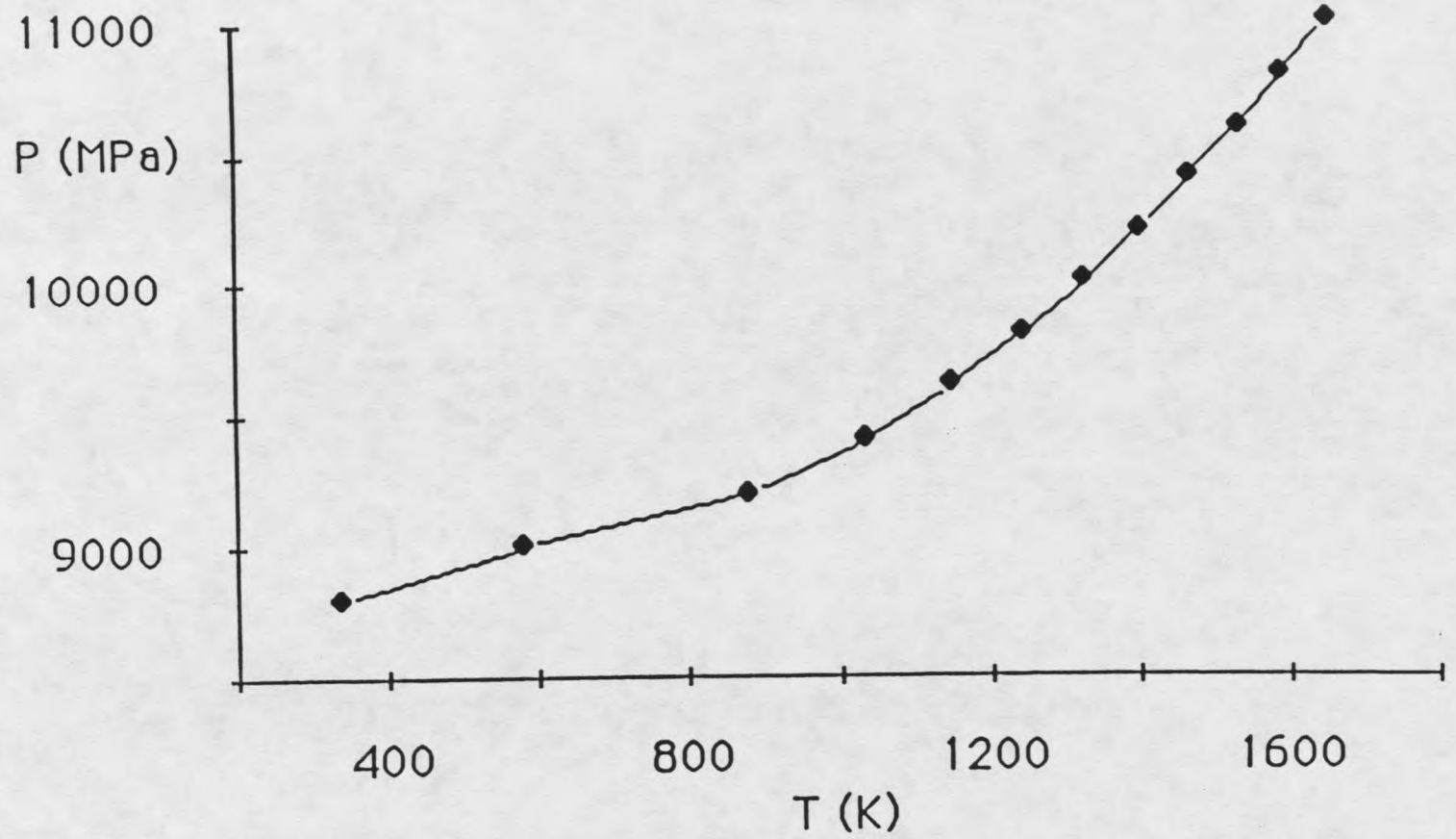

Figure 19. Equilibrium line for the spinel disproportionation as calculated in this work.

Table 20. ΔS and ΔV of disproportion for $MgAl_2O_4$

T (K)	P (MPa)	ΔV (cm^3/mole)	ΔS (J/mole K)
577.5	9000.	-2.654	-1.3997
1097.	9500.	-2.620	-4.6693
1326.	10000.	-2.600	-6.6834
1502.	15000.	-2.580	-7.9860

Table 21. The equation of state, heat capacity equation and selected thermodynamic properties of cordierite ($Mg_2Al_4SiO_{18}$).

$Mg_2Al_4Si_5O_{18}$ (C, CORDIERITE)

0.234078E+03	0.899349E-05	0.451668E-08	-.285238E-11	-.230909E-14
-.848087E-05	-.442406E-09	-.229776E-12	0.132829E-15	0.109807E-18
0.207740E-09	0.193252E-13	0.105119E-16	-.553999E-20	-.120853E-23
-.559773E-14	-.444596E-18	-.928989E-21	0.374617E-24	-.106071E-26
-.856411E-20	-.114674E-21	0.261934E-24	-.248256E-28	0.170194E-30
0.237592E-22	0.225578E-25	-.422462E-28	-.429451E-32	-.923538E-35
-.140682E-26	-.129101E-29	0.233536E-32	0.537906E-36	0.000000E+00

THE HEAT CAPACITY (Cp)[a]

A	B	C	D	E
698.34	.043339	-8.211200E+6	-5.0003E+3	

THERMODYNAMIC QUANTITIES	Y_{1000} J MOL^{-1}	$H_{1000}-H_{298}$ J MOL^{-1}	H_{298} J MOL^{-1}	S_{298} J MOL^{-1} K^{-1}	V_{1000} CM^3
$Mg_2Al_4Si_5O_{18}$	693.26	433303.	-9161524.	407.20	234.078

[a] THE HEAT CAPACITY EQUATION IS GIVEN BY $Cp = A + B(T-1000) + C(1/T^2 - 10^{-6}) + D(1/(T)^{1/2} - 1/(1000)^{1/2})$

THE BINARY SYSTEMS

In describing ternary systems it is necessary to have equations of state for all the single component subsystems, and to be able to calculate activities in the inherent binary subsystems. The MgO-SiO_2-$AlO_{1.5}$ ternary phase diagram includes the three binary subsystems: MgO-SiO_2, MgO-$AlO_{1.5}$ and SiO_2-$AlO_{1.5}$. To calculate the activities of these systems one must have Redlich-Kister coefficients for the activity coefficient (α) and the excess enthalpy H^e as discussed in the introduction.

The Magnesia-Silica Binary

The first system that I shall discuss is the MgO-SiO_2 binary. This binary system is an extremely important system for which a substantial amount of accurate data is available. However, one major problem with this system is the lack of direct calorimetric data for the enthalpies of fusion for MgO, Mg_2SiO_4 and $MgSiO_3$. If we had accurate enthalpies for these compounds we could calculate an excess enthalpy for the liquid at two compositions. However, the best published values for the heats of fusion of these three compounds have come mostly from analysis of phase equilibria, and it is possible that

the $MgO-SiO_2$ system is as well known as the other systems listed in Table 22.[104-109]

Table 22. Published estimates of the enthalpy of fusion of various compounds in the $MgO-SiO_2$ system.

T (K)	solid	ΔH_f (kJ/mole)	system	reference number
3105	MgO	57.65 ± 8	MgO-CaO	104
		60.97 ± 16	$MgO-SiO_2$	a
		77.1	$MgO-SiO_2$	105
		77.4	$MgO-ZrO_2$	32,106
		95.4		107
1830	$MgSiO_3$	48.8 ± 3	$MgO-SiO_2$	a
		60.4 ± 15	$MgO-SiO_2$	b
		61.5	$MgSiO_3-CaSiO_3$	106,40
		75.3 ± 21	$MgSiO_3-TiO_2$	32,108
2156	Mg_2SiO_4	58.6	$Mg_2SiO_4-Fe_2SiO_4$	109
		71.1 ± 21	$Mg_2SiO_4-TiO_2$	32,108
		92.88 ± 12	$MgO-SiO_2$	a
		118.5 ± 26	$MgO-SiO_2$	b

a) This work final value
b) This work first estimate

It is possible to get enthalpy of mixing data for the liquids from the heats of solution of glasses near 985 K. There is one recently published value in this system,[110] giving an enthalpy of vitrification of 42 kJ/mole for $MgSiO_3$. The heat capacities of the liquid, glass and solid should give an enthalpy of fusion somewhat larger than this, about 48 kJ/mole. Combination of this value with the enthalpy of 57.6 kJ/mole for the heat of fusion of MgO leads to an excess enthalpy of mixing of -20 kJ at $x = 0.5$ for the $MgO\text{-}SiO_2$ liquid. The mixing of MgO and silica liquids should be exothermic and various published models[111,112,3] agree roughly on the magnitude. This is true even though the heat of solution of glass was not available when the models in Table 23 were proposed.

Table 23. Excess enthalpies of mixing of MgO and SiO_2 for various models at a molefraction of 0.5.

H^e (kJ/mole)	Model
-18.7	Lin-Pelton
-26.6	This work
-27.	Michels
-0.7	Hoch

Figure 20 shows four calculated curves for the excess enthalpy at 2123 K in this system. The curve with the shallowest minimum and the least curvature is a Toop-Samis[1] calculation with the enthalpy given by the

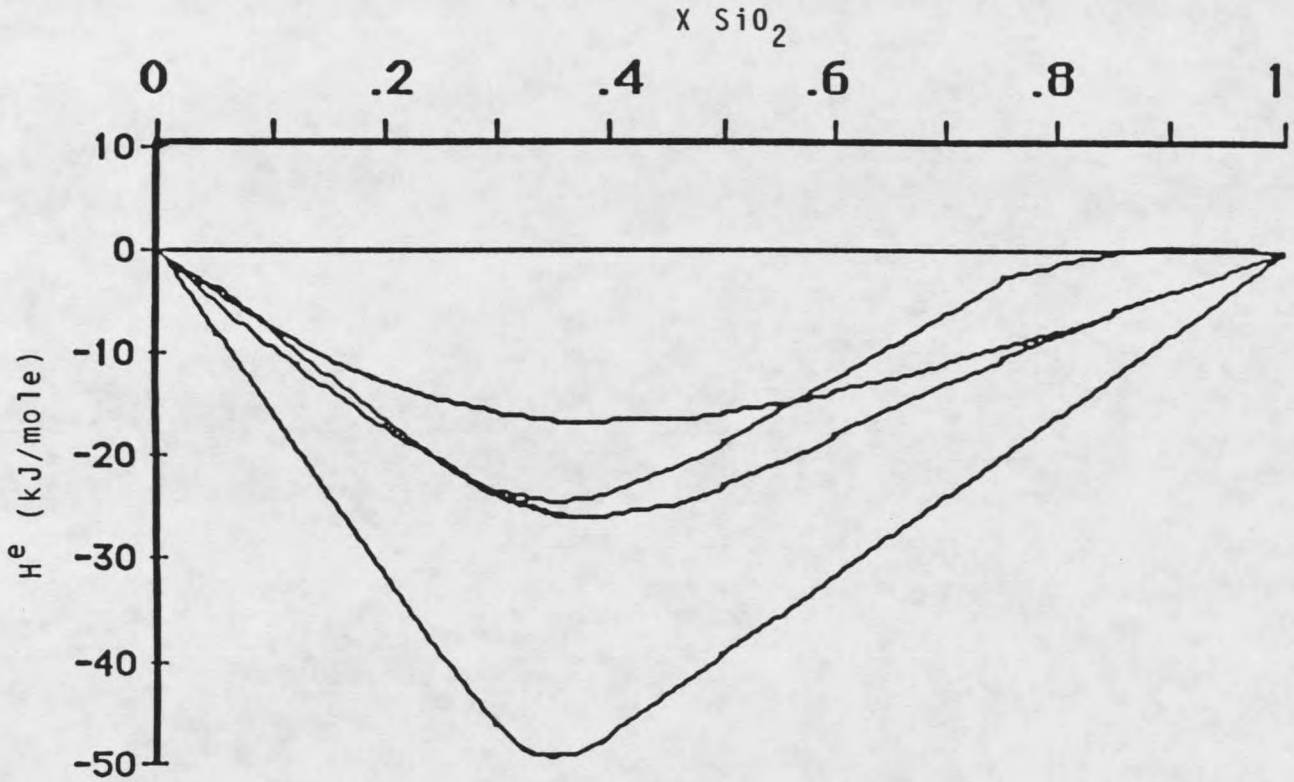

Figure 20. Various calculated excess enthalpies for the MgO-SiO_2 phase diagram.

number of moles of O^- multiplied by 2000 J/mole and an equilibrium constant of K = 0.103716. The curve that goes slightly positive at high concentrations of SiO_2 is that of Lin and Pelton,[3] and the other middle curve represents our final selected curve. The curve with the deepest minimum and largest curvature at x = 1/3 is a modified Lin-Pelton calculation selected to illustrate the behavior expected for more negative enthalpies of mixing. Our final selected enthalpy values shown in Figure 20 are calculated from two sets of Redlich-Kister parameters for the separate regions $x < 2/3$ and $x > 2/3$.

The four curves in Figure 20 represent the range of enthalpy curves seriously being considered for this system. It is desirable to have more information on the depth of the minumum and on the extent of the curvature in this region. The extreme behaviors shown in Figure 20 can be easily eliminated from what is known of the excess free energy.

The temperature of 2123 K was selected for Figure 21 since this is the temperature of the MgO, forsterite eutectic. At this temperature a liquid with an MgO mole fraction near 0.7 is in equilibrium with the two solids MgO and Mg_2SiO_4. In order to show the free energy data with a high degree of accuracy we have chosen to plot the function

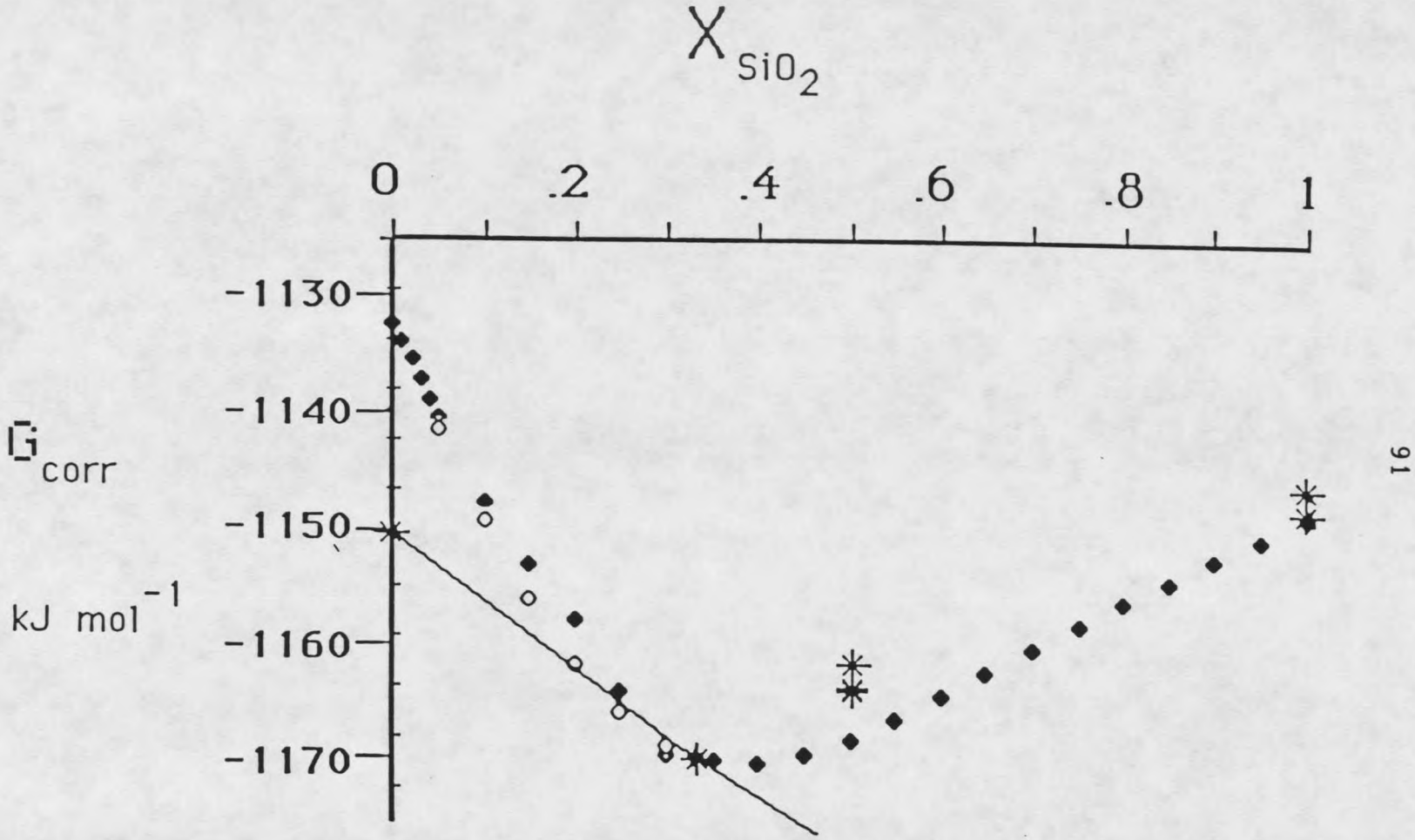

Figure 21. Corrected Gibbs free energy (G/T-382.14) versus mole fraction of SiO_2 for the system MgO-SiO_2

$$G - 382.14x_{MgO} = -YT/1000 + H_{298} - 382.14x_{MgO} \quad (97)$$

where G is the Gibbs free energy in J/mole of metal, H is the enthalpy, Y is the Planck function and x is the mole fraction of MgO. The values for the solids enstatite, MgO and SiO_2 are from previous discussions in this thesis.

Since 2123 K is the eutectic temperature, the tangent of the curve of the liquid phase, at about x_{MgO} = .7 to 0.69, must pass through the points MgO and $Mg_2$4. curve; because, they are at equilibrium at this temperature. This tangent must pass below the points for the $MgSiO_3$ solids Its intercept must be at a point determined by the enthalpy of fusion of MgO. This indicates that the curve has a broad minimum and it is possible to sketch a reasonable curve for the liquid. A smooth curve that meets these conditions will come close to matching our final curve. The points shown as diamonds are calculated from our final two sets of Redlich-Kister coefficients. Enthalpy values can be estimated from free energy curves at different temperatures through the Gibbs-Helmholtz equation

$$(d(G/T)/dT)_p = -H/T^2. \quad (98)$$

However, this yields larger uncertainties. For example ΔH_{fus} = 99000 ± 36000 for forsterite and 93000 ± 40000 for protoenstatite. In order to do better we need a usable entropy model.

As a first approximation the $x_{MgO} = 0.7$ can be considered as an ideal solution of 0.1 mole MgO in 0.30 moles of liquid Mg_2SiO_4. This yields a positive entropy of mixing of 1.87 J/K. Converting from a reference state of pure undissociated Mg_2SiO_4 to SiO_2 liquid introduces a substantial uncertainty. Nevertheless, the excess entropy will be positive, but less than the value 5.08 J/mole K. The uncertainty in the excess free energy is substantial unless the heat of fusion of MgO is fixed. But, it is in the range of -30 ± 3 kJ/mole. These values combine to give -24 ± 8 kJ/mole for the excess enthalpy at $x_{MgO} = 0.70$, accurate enough to eliminate both the highest and lowest curves in Figure 20.

The Enthalpy of Fusion of Magnesium Oxide

If the free energy curve has a broad minimum as shown in Figure 21, then the liquidus curve for forsterite should be reasonably symmetric, and the mole fraction of MgO at the 2123 K eutectic should be between $x_{MgO} = 0.69$ and 0.70. Some disproportionation of the orthosilicate is probably present. However, at these basic compositions a Flood-Knapp[2] model with three species should be adequate. Thus, we can consider the liquid as an ideal solution of MgO, Mg_2SiO_4 and $Mg_3Si_2O_7$. Without an enthalpy of fusion for MgO the amount of disproportionation of orthosilicate and the enthalpy are

uncertain. But, the reaction

$$2Mg_2SiO_4(l) = Mg_3Si_2O_7 + MgO(l) \quad (99)$$

should have a positive ΔH, a ΔS approximately equal to zero, and thus, an equilibrium constant less than one. If z is the number of moles of $Mg_3Si_2O_7$ present then there are $3x - 2 + z$ moles of MgO and $1 - x - 2z$ moles of Mg_2SiO_4 present in the liquid; with a total of $2x - 1$ moles. Thus, the equilibrium constant for the above reaction is

$$K = (3x - 2 + z)(z)/(1 - x - 2z)^2. \quad (100)$$

Therefore, when $x_{MgO} = 0.7$ and assuming that the equilibrium constant is greater than zero and less than one then z can range from 0 to 0.08 as shown in Table 24. The activity of MgO liquid is determined from the mole fraction of MgO present in the liquid. Thus,

$$x_{MgO} = a_{MgO} = (3x - 2 + z)/(2x - 1) \quad (101)$$

which reduces to $a_{MgO}(liquid) = 0.25 + 2.5z$ at $x_{MgO} = 0.7$ and $a_{MgO}(liquid) = 0.18421 + 2.6316z$ at $x_{MgO} = 0.69$. Therefore, the activity of MgO is between 0.25 and 0.45 in the eutectic liquid at 2123 K. Using the melting point of 3105 K for MgO and the Gibbs-Helmholtz equation

$$\ln (K_2/K_1) = (\Delta H/R)(1/T_2 - T_1) \quad (102)$$

along with the activities of MgO at 2123 yields an enthalpy of fusion for MgO of 60.97 ± 16 kJ/mole. This agrees well with the value 57.650 ± 8 kJ/mole from Howald

and Chang.[104] Certainly values above 90 kJ/mole are excluded and the Janaf value of 77.4 ± 15 kJ/mole[32] is barely acceptable. Thus, we feel justified in proceeding with calculations based upon the 57.65 ± 8 kJ/mole value.

Table 24. Calculated equilibrium constants for reaction: $2Mg_2SiO_4$ (l) = $Mg_3Si_2O_7$ + MgO(l) at x MgO = 0.7, where z is the number of moles of $Mg_3Si_2O_7$.

a (MgO)	z	K_{99}
.25	0.0	0.0
.275	.01	.0140
.30	.02	.0355
.325	.03	.0677
.35	.04	.115
.375	.05	.1875
.40	.06	.2963
.425	.07	.4648
.45	.08	.7347
.475	.09	1.1875

The Entropy of Mixing

With the properties of MgO liquid confirmed at the previously selected values[104] the excess G/T for the eutectic can be calculated to be -14.2613 at x_{MgO} = 0.70. This can be divided into excess entropy and an excess enthalpy term in various ways. Assuming ΔS = 0 for the reaction

$$3Mg_2SiO_4 + SiO_2 = 2Mg_3Si_2O_7, \qquad (103)$$

the Flood-Knapp[2] model calculates the excess entropy and excess enthalpy to be 3.189 J/mole K and -23500 J/mole

respectively. The Toop-Samis model[1] yields 11.428 J/mole K and -6015 J/mole for the excess entropy and enthalpy of mixing. The ideal mixing of the three types of oxygen atom present in the Toop-Samis model[1] seriously overestimates the entropy of mixing. The Lin-Pelton model[3] corrects for this by using separate terms for the mixing of negative centers and polymeric anions. The Lin-Pelton equation is

$$\begin{aligned} S^e = R[&[(x - z)\ln((x - z)/(1 - z)) \\ &+ (1 - x)\ln((1 - x)/(1 - z) \\ &+ (2 - 2x - z) \\ &\quad \ln((2 - 2x - z)(1 - z)/((2 - 2x)(1 - x))) \\ &+ [(2 - 2x)(1-x)/(1-z) - (2 - 2x - z)] \\ &\quad \ln[((2 - 2x)(1 - x)/(1 - z) - (2 - 2x - z)) \\ &\quad /((2 - 2x)(1 - x)/(1 - z))]] \end{aligned} \qquad (104)$$

where x is the mole fraction of MgO, and z is 1/2 the number of O^- ions present. The first two terms account for the mixing of negative centers and O^{-2} where (1 - x) is the SiO_{2n}^{-m} ion and (x - z) is the number of O^{-2} present, yielding 1-z total moles. The last two terms are mixing of O^{-2}, O^o and O^- with the number of moles of Si-O-Si(n_{Si-Si}) equal to (2 - 2x)(1 - x)/(1 - z). However, a much simpler equation for the excess entropy can be arrived at by using N(Si-Si) = (2 - 2x). This yields what we call a modified Lin-Pelton model with the excess

entropy being

$$S^e = -R[(x - z)\ln((x - z)/(1 - z)) + (1 - x)\ln((1 - x)/(1 - z) + (2 - 2x - z)\ln((2 - 2x - z)/(2 - 2x)) + z\ln(z/(2 - 2x)); \quad (105)$$

where $2 - 2x - z$ = moles of O^o and $z = (1/2)O^-$. The parameter z can be evaluated by minimizing the free energy function with the excess enthalpy proportional to z. The choice of $H^e = -39005z$ gives $G/T = -14.261$ at $x_{MgO} = 0.70$ with $S^e = 5.49448$ J/mole K and $H^e = -18611$. Computations with this parameter at 1830 K and 2163 K yield enthalpies of fusion of $\Delta H_{fus} = 118500 \pm 8000$ for forsterite and $\Delta H_{fus} = 60400 \pm 8000$ J/mole for protoenstatite with the uncertainty due to the uncertainty of ± 4 J/mole K in the excess entropy. The excess entropy at x = 0.7 and T = 2123 K with the original Lin-Pelton model is 3.9805 J/mole K, increasing to 4.5000 J/mole K if the enthalpy is adjusted to bring G/T to -14.2613 J/mole K. $S^e = 5 \pm 4$ J/mole K is a reasonable estimate of the excess entropy in the liquid near $x_{MgO} = 0.7$.

A simple model like the one parameter modified Lin-Pelton model can not describe the excess enthalpy at all compositions and temperatures. However, a set of Redlich-Kister coefficients can fit each of the models considered, and so they can fit the differences between

various models and presumably correct any of the models to exact values. For example it is quite easy to introduce negative curvature for G/T to the high silica end of the phase diagram, so that the amount of liquid-liquid immiscibility decreases with increasing temperature.

Similarly, the various models proposed for the entropy of mixing in this system all have at least a hint of a local minimum near the orthosilicate composition of $x_{MgO} = 2/3$ for a type of M shaped curve. Several of these are shown in Figure 22. Using separate sets of Redlich-Kister coefficients for the nonideal parts of the two humps for the excess entropy gives us the flexibility to fit any curve of this type.

The Heat Capacity

The disproportionation equilibria give a substantial temperature dependence for the enthalpy in the neighborhood of the minimum at $x_{MgO} = 0.7$. This must obviously be reflected in terms of the excess heat capacity of mixing. We used the single parameter modified Lin-Pelton model to calculate the temperature and composition dependence of this part of the heat capacity. However, adding this C_p^e for $x = .5$ to the heat capacities of MgO and SiO_2 liquids gives a heat capacity for $MgSiO_3$(liquid) of $C_p = 100$ J/mole K, which is substantially less than that reported by White,[115]

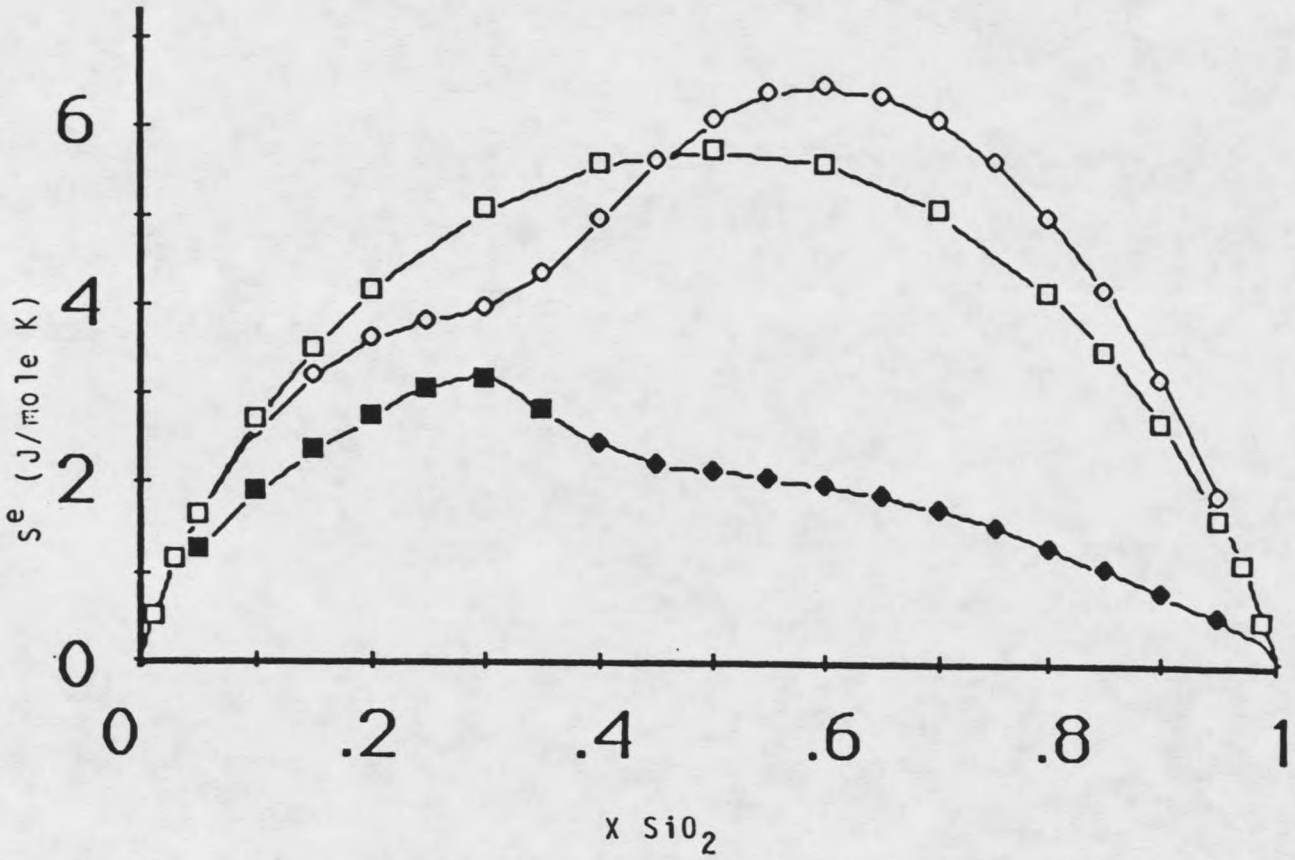

Figure 22. Entropy of mixing versus the molefraction of SiO_2 in the system MgO-SiO_2. Circles, open squares and filled squares are from Lin and Pelton, ideal mixing and this work respectively.

C_p^e = 130.7 J/mole K. This discrepancy was corrected by adding 25 J/mole K to the first Redlich-Kister term for the excess heat capacity. The resulting curve of C_p versus mole fraction at 2123 K is shown in Figure 23 to demonstrate that it is a reasonable choice. The C_p^e curve is shaped like the excess entropy curve, since it is calculated from the excess entropy from the Lin-Pelton model.

With the heat capacity of the liquid phase chosen, it can be combined with the measurements of White[113] for the heat capacity of the glass to convert the measured heat of vitrification of Navrotsky[110] to a heat of fusion of 48.8 kJ/mole at 1830 for $MgSiO_3$. This is just barely consistent with the value of 60.4 ± 15 kJ/mole given above. We have accepted the lower value for our final calculations and to fix the enthalpy curve in Figure 20. It is worth noting that using a higher enthalpy of fusion for MgO only makes this discrepancy worse. A heat of fusion for $MgSiO_3$ of 48.8 ± 3 kJ/mole for $MgSiO_3$ corresponds to H^e= -23.91 ± 4 kJ/mole at x = 2/3 and 1830 K. This determines our final selected values of H^e = -25.199 ± 4 kJ/mole and S^e = -2.295 J/mole at x = 2/3 and 2123 K, and an enthalpy of fusion for forsterite of ΔH_{fus} = 92.88 ± 12 kJ/mole at 2156 K.

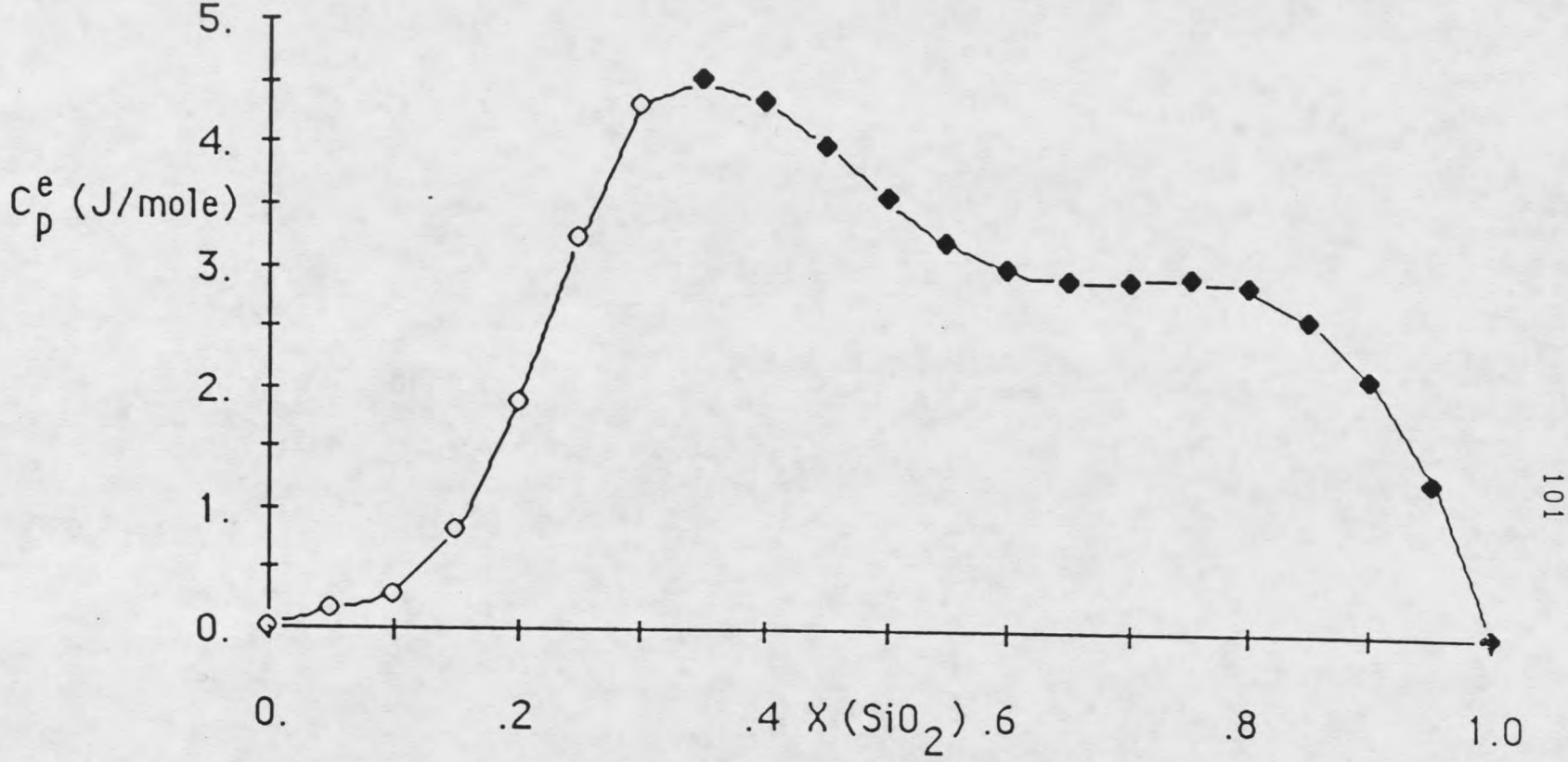

Figure 23. Excess heat capacity versus molefraction of SiO_2 at 2123 K for the MgO-SiO_2 system.

The Phase Diagram

With choices made for the excess enthalpy and the heat capacity of mixing, every measurement of solid liquid equilibria gives a value for the activity coefficients and the entropy. The resulting excess entropy values have already been displayed in Figure 22. Also, the calculated activities at 2000 K can be compared with the measurements of Kambayashi and Kato[114] as shown in Figures 24 and 25. Except for the problem already evident at high concentrations of MgO by their failure to fit the known phase equilibria, the agreement is fair. The phase equilibria measurements are more reliable than the effusion measurements.

There are reliable density measurements of the liquid by J. F. Riebling,[115] so that the phase diagram can be extended to higher pressures. The calculated phase diagrams at .1 and 2000 MPa are shown in Figures 26 and 27. Table 25 gives the Redlich-Kister coefficients for both the acidic and basic sides of the phase diagram.

The Alumina-Silica Binary

The thermodynamic properties of the alumina-silica binary have been modelled by Howald and Eliezer[116] in 1978. We are using their equations of state for the various stoichiometric phases. The Redlich-Kister coefficients

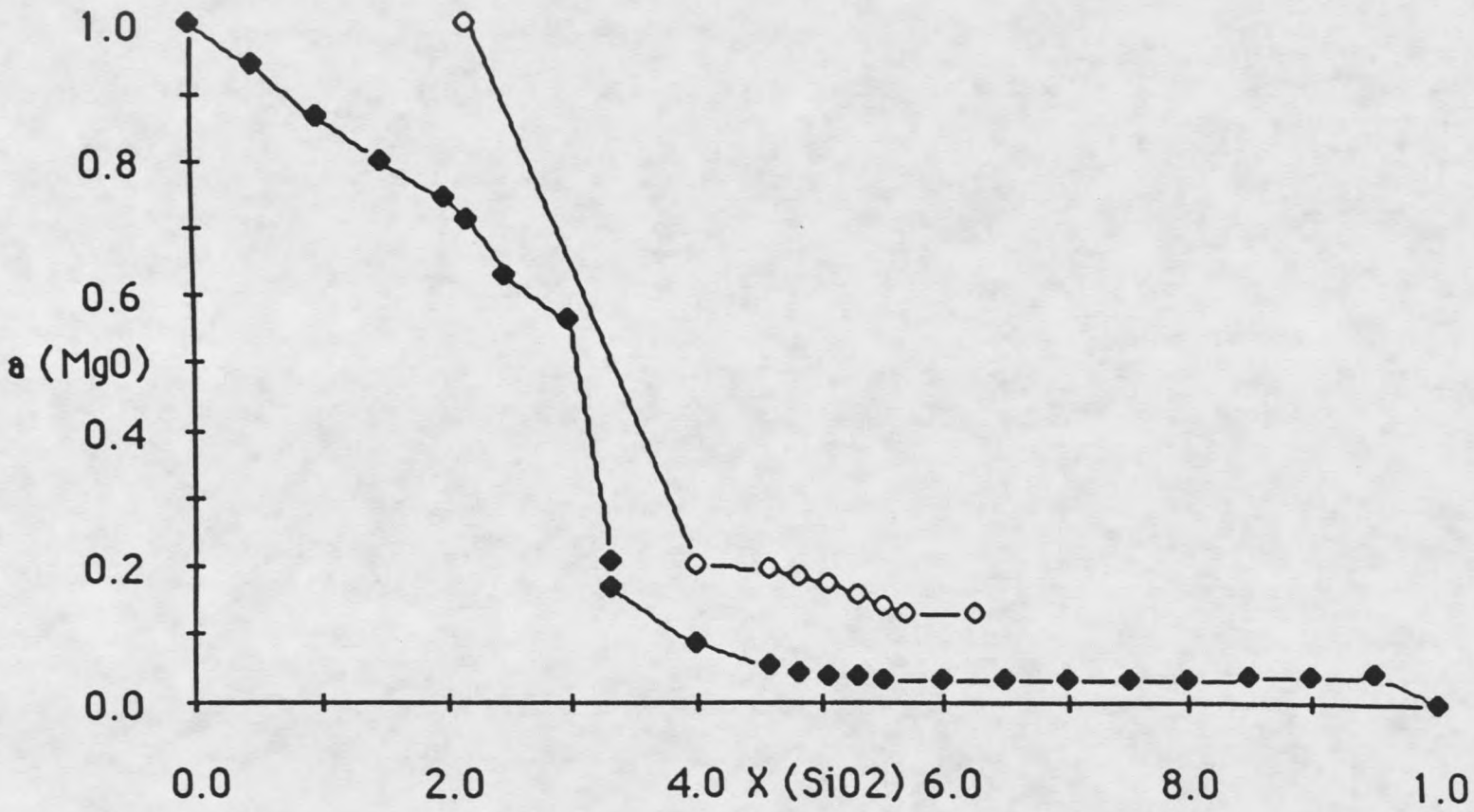

Figure 24. Activities of MgO. Filled diamonds are calculated from our Redlich-Kister coefficients, open circles are from S. Kambayashi and E. Kato.

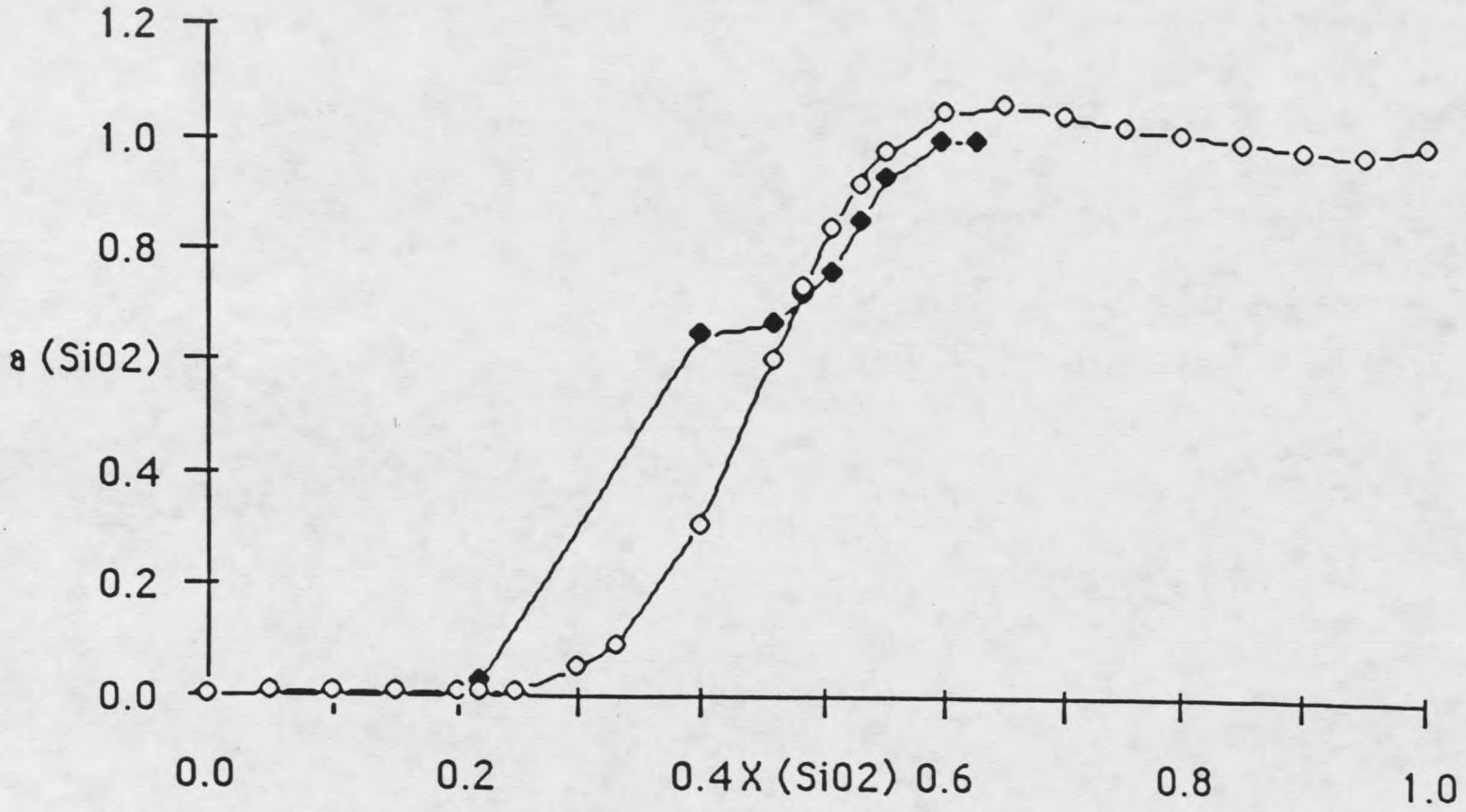

Figure 25. Activities of SiO_2. Open circles are calculated from our Redlich-Kister coefficients, filled diamonds are from S. Kambayashi and E. Kato.

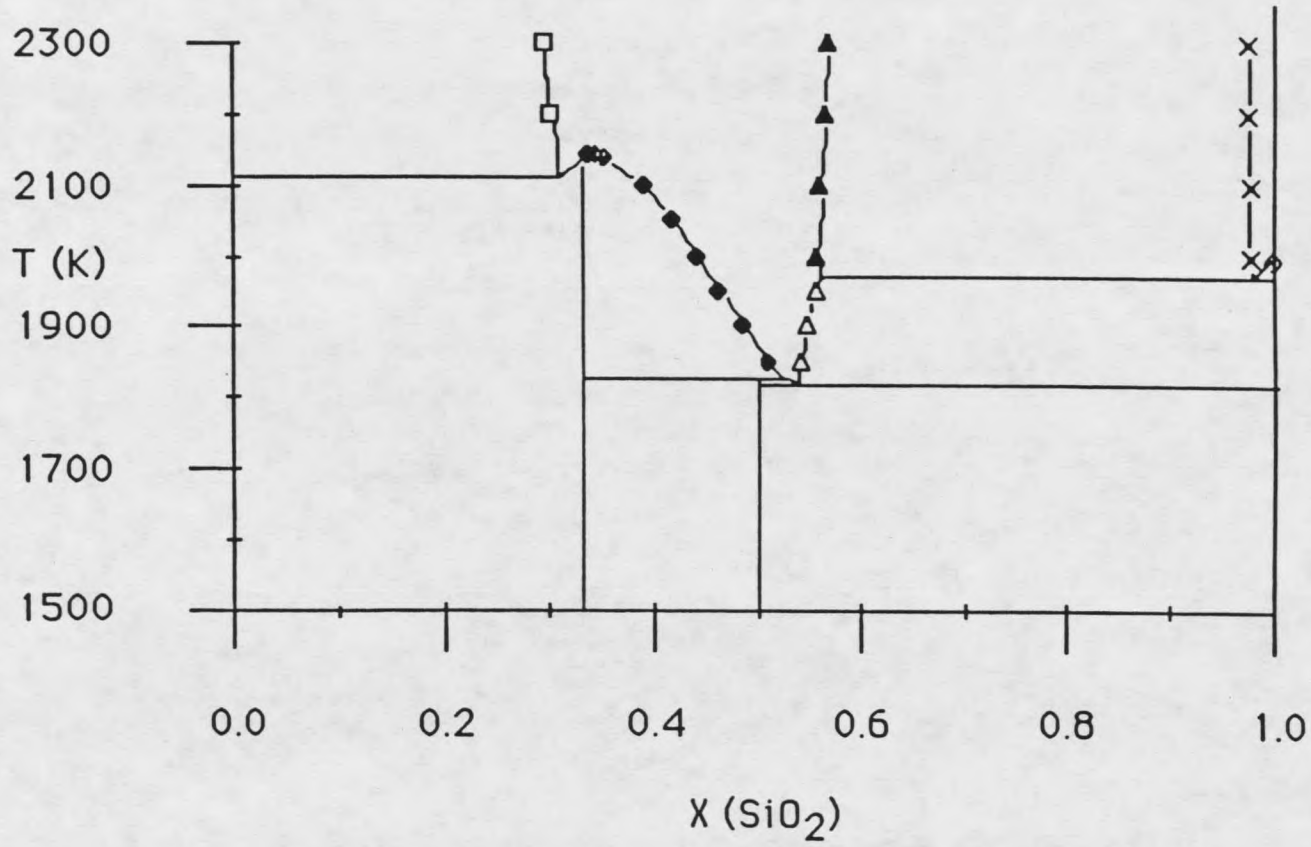

Figure 26. The calculated phase diagram at 0.1 MPa for the MgO-SiO_2 system.

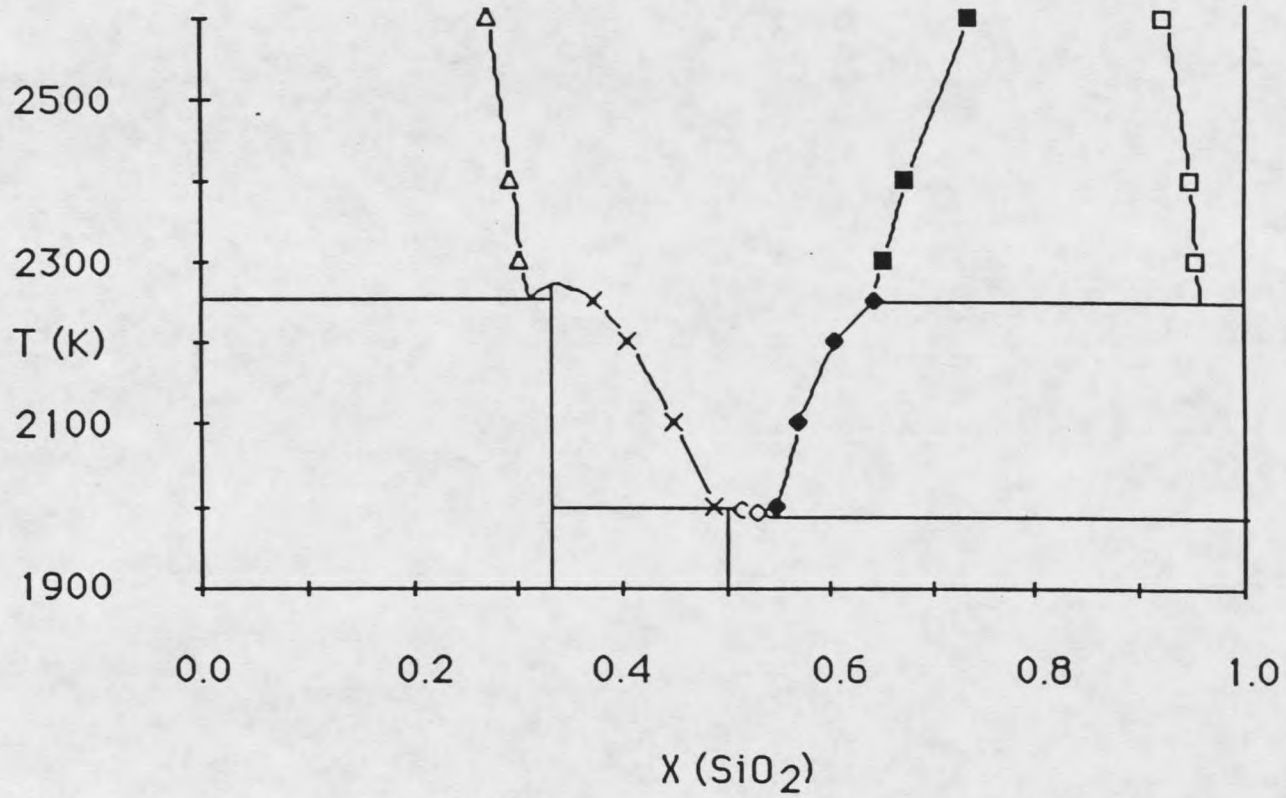

Figure 27. The Calculated phase diagram at 1000. MPa for the MgO-SiO_2 system.

Table 25. Redlich-Kister coefficients for acidic and basic $MgO-SiO_2$.

	A	B	C	D	E	F
a) log γ	-4.284510	-5.0782545	-.7017948	5.5773431	6.9039075	2.197768
b) log γ	-.328548	-37.588266	87.678091	-78.884975	22.121726	2.197768
a) H	-106333.59	-106101.23	-21837.49	171288.1	238689.37	100752.46
b) H	-16426.745	-818763.25	1850296.	-1459206.2	238689.37	100752.46
a) Cp	11.870530	15.174986	14.355571	-20.8517	-65.6362	-38.9678
b) Cp	46.80464	427.70785	-918.31275	649.06314	-65.6362	-38.9678
c) dCp/dT	.002539050	.002055004	.0132324	-.023815	-.003681462	.0096971585
c) d^2Cp/dT^2	-4.225033E-7	-1.992977E-6	8.4855E-7	3.8824667E-6	-1.025983E-6	-1.55113E-6
c) V	-5.7079297	-9.6020113	-3.206035	22.275335	10.892596	-15.26825
c) dV/dT	-.0010398796	.0097664152	.0032609281	-.022656	-.011079	.0155296
c) dV/dP	.00010398796	-.9766415E-3	-.3260928E-3	.00226567	.0011079	-.00155296

a) acidic coefficients
b) basic coefficients
c) coefficients for both the acid and the base

for the liquid and solid phases calculated by Howald and Eliezer[116] are listed in Table 26. However, the heat capacity of the liquid has been refined and the equation changed. This made it necessary to change the Redlich-Kister coefficients for the liquid. Chang, Howald and Roy[117] made these changes in 1982. These values for the Redlich-Kister coefficients for log γ and enthalpy are also shown in Table 26.

Table 26. Redlich-Kister coefficients for the $AlO_{1.5}$-SiO_2 solid and liquid systems.

Phase	Quantity	Ref.	A	B	C
(l)	log γ	Howald, et al.	1.330516	-0.212719	.096297
	enthalpy		26778.		
(s)	log γ		3.134095	-9.233145	10.646443
	enthalpy		35974	99035.	
(l)	log γ	Chang, et al.	1.330266	-.211929	.0959393
	enthalpy		26853.8		
(l)	log γ	this work	.8634264	-.2353337	.1233324
	enthalpy		9000.0		
(s)	log γ		3.134095	-9.233145	10.646443
	enthalpy		35974	99035.	

Since then we have found that the enthalpy Redlich-Kister coefficent for the liquid in this binary is much too large. We have reduced the enthalpy coefficient from 26853.8[118] to 9000 J/mole and have recalculated the log γ coefficients for the liquid as shown in Table 26.

The first step in calculating the Redlich-Kister coefficients for the alumina-silica binary is to calculate the equilibrium constants for the reactions

$$AlO_{1.5}(c, \text{corundum}) = AlO_{1.5}(l) \qquad (106)$$

and

$$SiO_2(c, \text{cristobalite}) = SiO_2(l) \qquad (107)$$

at the temperatures where Davis and Pask[118] measured the equilibrium between mullite and the alumina and silica liquid. This can easily be done from the equations of state of the reactants and products in reactions (106) and (107).

The equilibrium constant for the melting of mullite is given by

$$K_{eq} = \frac{(a_{SiO_2(l)})^{1/4}(a_{AlO_{1.5}(l)})}{a_{mullite}} \qquad (108)$$

The activity of mullite is given by the equation

$$a_{mullite} = (a_{SiO_2(s)})^{1/4}(a_{AlO_{1.5}(s)}), \qquad (109)$$

so that the equilibrium expression becomes

$$K_{eq} = \frac{(a_{SiO_2(l)})^{1/4}(a_{AlO_{1.5}(l)})}{(a_{SiO_2(s)})^{1/4}(a_{AlO_{1.5}(s)})} \qquad (110)$$

The activities of the solids can be calculated from the Redlich-Kister coefficients for log γ for the solid phase in Table 26. The equilibrium constant, K_{eq}, can be

calculated from the equilibrium constants for the melting of SiO_2 and $AlO_{1.5}$. The equation is

$$K_{eq} = (K_{SiO_2})^{1/4} K_{AlO_{1.5}}. \qquad (111)$$

Normally once this is done the activities and mole fractions of the liquid can be calculated. However, allowing for non-stoichiometry of the mullite phase complicates the calculation substantially. We must allow for two separate equilibria between the solid and liquid phase. These can be chosen as the melting of cristobalite and corundum as shown for reactions (106) and (107).

The two equilibrium concentrations, $x_6(c)$, the mole fraction of the solid alumina; and $x_6(l)$, the mole fraction of the liquid alumina, are those which give the four activities $a_7(c)$, $a_7(l)$, $a_6(c)$ and $a_6(l)$; where the subscripts 6 and 7 represent $AlO_{1.5}$ and SiO_2 respectively. These activities must satisfy the two equilibrium constant expressions

$$x_6(l)/x_6(c) = K_6 \qquad (112)$$

and

$$x_7(l)/x_7(c) = K_7 \qquad (113)$$

where K_6 and K_7 are the equilibrium constants for reactions (112) and (113).

The concentrations and activities for equilibrium at a selected temperature and pressure can be obtained by successive approximations by any of a variety of

mathematical procedures for the minimization of the free energy. Convergence in these calculations is not a trivial problem for highly nonideal solutions. Our current computer program uses a form of the Murtagh and Sargent[119] constrained minimization which is not as efficient for the two component systems as the alternate calculations of mole fractions from activities for the two phases as used by Howald and Eliezer.[116] Eventually a better convergence program incorporating some of the features of White[120] and Murtagh and Sargent[119] will need to be written.

Once convergence has occurred and the activities of the liquid are calculated, the change in the logarithm of the activity coefficient for both the alumina and the silica can be calculated from the equation

$$\Delta \log \gamma = (a_{new}/a_{old}) \qquad (114)$$

where a_{new} is the new activity and a_{old} is the old activity. These changes in log γ can be fit to Redlich-Kister coefficients by a least squares calculation giving the change in the Redlich-Kister coefficients. These coefficients can then be added on to the old coefficients for log γ to give the new Redlich-Kister coefficients for the liquid shown in Table 26.

THE TERNARY SYSTEM: MAGNESIA-SILICA-ALUMINA

With the Redlich-Kister coefficients for the two component systems and the equations of states for the compounds present in this system, we can now proceed to describe the three component system $MgO\text{-}SiO_2\text{-}Al_{1.5}$. The first step in this process is to calculate the Redlich-Kister coefficients for the ternary. There are a variety of methods for doing this; however, the most commonly used interpolation methods are by Kohler[121] and Toop.[122]

The Kohler[121] procedure for calculating the Redlich-Kister coefficients has terms of the form $x_1/(x_2 + x_3)$ in it. These terms cannot be expressed as a finite power series in mole fraction, because as x_1 approaches one $x_2 + x_3$ approaches zero. Thus, the term $x_1/(x_2 + x_3)$ approaches infinity. Toop[122] also developed a method of interpolation, but his method has one set of terms in the Kohler form. What we are using is the Toop interpolation with the set of terms in the Kohler form dropped. Thus, we have a modified Toop or a Toop-Muggianu interpolation.[123] This interpolation method is very useful in calculating Redlich-Kister coefficients for ternary diagrams, and is easily expressed in terms of extended Redlich-Kister notation. The Toop-Muggianu is

exactly a Toop interpolation if the solution formed along one binary edge is ideal or parallel to an ideal solution.

The modified Toop interpolation calculates the ternary Redlich-Kister coefficients from the appropriate binary Redlich-Kister coefficients and also calculates these coefficients so that they give well-behaved Redlich-Kister coefficients for the pseudobinaries. A pseudobinary is a line through the ternary through one vertex, holding the ratio of two of the components constant while varying the third. Thus, it forms a straight line through the apex of one of the pure components and through the baseline connecting the other two components.

For example, assume we want to calculate the Redlich-Kister coefficients for the imaginary ternary $|w,y,z\rangle$. If the binary $|w,y\rangle$ is close to ideal then we can easily calculate the Redlich-Kister coefficients along the pseudobinary $|w_2\ y,z\rangle$. The pseudobinary $|w_2\ y,z\rangle$ corresponds to a straight line through pure z and the point w_2 y along the w,y binary edge. The Redlich-Kister coefficients for the binaries are

$$|w,z\rangle = |A_{wz},B_{wz},C_{wz},D_{wz}\rangle \qquad (115)$$

$$|y,z\rangle = |A_{yz},B_{yz},C_{yz},D_{yz}\rangle \qquad (116)$$

The Redlich-Kister coefficients along the pseudobinary $|w_2\ y,z\rangle$ can be calculated from the equation

$$|w_2\ y,z\rangle = |2/3\ w,z\rangle + 1/3|y,z\rangle \qquad (117)$$

which becomes

$$|w_2\ y,z\rangle = |(2/3)A_{wz} + (1/3)A_{yz}, (2/3)B_{wz} + (1/3)B_{yz}, (2/3)C_{wz} + (1/3)C_{yz}, \ldots\rangle \qquad (118)$$

The modified Toop interpolation calculates the three component terms as listed in Tables 1 and 3 so that they give this behavior in the terms calculated for the pseudobinaries. This is done by multiplying the Redlich-Kister coefficients for the two binaries by the matrix MTOOP shown in Table 27. This equation is

$$|z,w,y\rangle = |MTOOP||B_{zw}, C_{zw}, D_{zw}, E_{zw} \ldots B_{yw}, C_{yw}, D_{yw}, E_{yw} \ldots\rangle \qquad (119)$$

This matrix is programmed into the computer for up to seventh power terms in mole fraction, and it handles up to nine component systems. The computer can easily rotate the subscripts for the three component terms to give the pseudobinaries along another axis. This is done by the equation $|N_{123}\rangle = |CMM||N_{231}\rangle$, where N is the vector of Redlich-Kister coefficients and CMM is the 15 by 15 matrix shown in Table 28.

In the system $MgO\text{-}SiO_2\text{-}AlO_{1.5}$ the components SiO_2 and $AlO_{1.5}$ both act as acids. This leads us to calculate the Redlich-Kister coefficients for the ternary along the pseudobinaries $|AlO_{1.5\ x}\ SiO_{2\ y}, MgO\rangle$ with a modified Toop interpolation. With the matrix CMM we can rotate the

Table 27. The matrix MTOOP for calculating ternary Redlich-Kister coefficients.

1	-2	3	-4	5	1	-2	3	-4	5
0	7/2	-21/2	21	-35	0	7/2	-21/2	21	-35
0	1/2	-3/2	3	-5	0	-1/2	3/2	-3	5
0	0	37/4	-37	185/2	0	0	37/4	-37	185/2
0	0	10/4	-10	25	0	0	-10/4	10	-25
0	0	1/4	-1	5/2	0	0	1/4	-1	5/2
0	0	0	175/8	-875/8	0	0	0	175/8	-875/8
0	0	0	67/8	-335/8	0	0	0	-67/8	335/8
0	0	0	13/8	-65/8	0	0	0	13/8	-65/8
0	0	0	1/8	-5/8	0	0	0	-1/8	5/8
0	0	0	0	781/16	0	0	0	0	781/16
0	0	0	0	376/16	0	0	0	0	-376/16
0	0	0	0	106/16	0	0	0	0	106/16
0	0	0	0	16/16	0	0	0	0	-16/16
0	0	0	0	1/16	0	0	0	0	1/16

subscripts to get any order for the subscripts that we want. For this ternary it is the $|6,7,4\rangle$ ternary coefficients that are used by the computer. They can be used to calculate the excess enthalpy(H^e) along the $|4\text{-}6,7\rangle$ pseudobinary, where 4, 6 and 7 represent MgO, $AlO_{1.5}$

Table 28. The transformation matrix, CNN, from the Redlich-Kister vector N^n_{123} to the vector N^n_{312}.

1	1	-1	1	-1	1	1	-1	1	-1	1	-1	1	-1	1
0	-(1/2)	(3/2)	-1	2	-3	-(3/2)	(5/2)	-(7/2)	(9/2)	-2	3	-4	5	-6
0	-(1/2)	-(1/2)	-1	0	1	-(3/2)	(1/2)	(1/2)	-(3/2)	-2	1	0	-1	2
0	0	0	(1/4)	-(3/4)	(9/4)	(3/4)	-(7/4)	(15/4)	-(27/4)	(3/2)	-3	(11/2)	-9	(27/2)
0	0	0	(1/2)	-(1/2)	-(3/2)	(3/2)	-(3/2)	-(1/2)	(9/2)	3	-3	1	3	-9
0	0	0	(1/4)	(1/4)	(1/4)	(3/4)	(1/4)	-(1/4)	-(3/4)	(3/2)	0	-(1/2)	0	(3/2)
0	0	0	0	0	0	-(1/8)	(3/8)	-(9/8)	(27/8)	-(1/2)	(5/4)	-3	-(27/2)	-(27/2)
0	0	0	0	0	0	-(3/8)	(5/8)	-(3/8)	-(27/8)	-(3/2)	(9/4)	-2	-(9/4)	(27/4)
0	0	0	0	0	0	-(3/8)	(1/8)	(5/8)	(9/8)	-(3/2)	(3/4)	1	-(3/4)	-(9/2)
0	0	0	0	0	0	-(1/8)	-(1/8)	-(1/8)	-(1/8)	-(1/2)	-(1/4)	0	(1/4)	(1/2)
0	0	0	0	0	0	0	0	0	0	(1/16)	-(3/16)	(9/16)	(27/16)	(81/16)
0	0	0	0	0	0	0	0	0	0	(1/4)	-(1/2)	(3/4)	0	-(27/4)
0	0	0	0	0	0	0	0	0	0	(3/8)	-(3/8)	-(1/8)	(9/8)	(27/8)
0	0	0	0	0	0	0	0	0	0	(1/4)	0	-(1/4)	-(1/2)	-(3/4)
0	0	0	0	0	0	0	0	0	0	(1/16)	(1/16)	(1/16)	(1/16)	(1/16)

and SiO_2 respectively. The calculated Redlich-Kister coefficients for excess enthalpy from the Toop interpolation are shown in Table 29 along with the final selected coefficients.

Table 29. Calculated Redlich-Kister coefficients for excess enthalpy from the Toop-Muggianu interpolation along with our final selected values for the $MgO-SiO_2-AlO_{1.5}$ ternary at 1800 K.

Coefficient	H^e Toop-Muggianu	H^e Final Values
B^a	61840.73	58082.73
C^a	36477.38	-2173532.6
C^b	-77664.28	793583.72
D^a	-27662.38	1590207.6
D^b	50574.75	-710619.25
D^c	-58146.47	535636.53
E^a	104838.4	104838.4
E^b	-346939.8	-346939.8
E^c	339367.6	339367.6
E^d	15143.46	15143.46
F^a	-72416.5	-72416.5
F^b	362082.9	362082.9
F^c	-724165.9	-724165.9
F^d	724165.9	724165.9
F^e	-362082.9	-362082.9

We corrected the ternary Redlich-Kister coefficients in the following manner. First, we needed to determine the magnitude of the change needed to correct the Redlich-Kister coefficients. We looked at the pseudobinary through pure $AlO_{1.5}$ and the MgO-SiO_2 edge at $x_{MgO} = 0.5$. The excess enthalpy along the MgO-SiO_2 binary is straight along the acidic side to a first approximation. Thus, if the excess enthalpy at the point $x_6 = 0$, $x_4 = 0.5$ and $x_7 = 0.5$ along the $|6,4\rangle$ binary is z, then at $x_4 = 1/3$ the excess enthalpy is 2/3 z along the $|6,4\rangle$ binary. We can draw a straight line through the points $x_6,x_4,x_7 = 0,1/3,2/3$; $x_6,x_4,x_7 = 1/3,1/3,1/3$ (the center of the graph) and $x_6,x_4,x_7 = 2/3,1/3,0$. If at the mullite composition the excess enthalpy is Y, $H^e = Y$, then at $x_6,x_4,x_7 = 1/3,1/3,1/3$ the excess enthalpy should be

$$H^e = (1/2)Y + (1/3)Z + \Delta. \qquad (120)$$

The Δ contribution to the excess enthalpy is small compared to Y and Z because it is the mixing of $AlO_{1.5}$ and SiO_2. Thus the Δ contribution is negligible. Also along the pseudobinary $|6,7\text{-}4\rangle$, which passes through the center, the excess enthalpy at the point $|6,7,4\rangle = |1/3,1/3,1/3\rangle$ should be approximately (2/3)Y.

We repeated this calculation at seven different points in the ternary diagram. These points are listed in

Table 30, along with the excess enthalpies calculated from the Toop interpolation's Redlich-Kister coefficients and the final values from the final set of Redlich-Kister coefficients chosen for this ternary. To change the Redlich-Kister coefficients we fit the changes in the excess enthalpy that we wanted to Redlich-Kister coefficients and then just added these coefficients on to the Redlich-Kister coefficients calculated from the Toop interpolation. The changes desired at the seven selected symmetrical points are used to adjust the first six ternary Redlich-Kister coefficients: B^a, C^a, C^b, D^a, D^b and D^c. When one has binaries like $MgO\text{-}SiO_2$ with E and F terms, it is necessary to include them in the ternary. However, they do not have to be adjusted. One avoids serious problems with ternaries by not trying to fit high order ternary terms with limited data available.

The Redlich-Kister coefficients for log γ in the ternary were calculated by a modified Toop interpolation. We corrected the log γ values from the known equilibria within the ternary phase diagram using a method similar to that for the excess enthalpy corrections. The log γ Redlich-Kister coefficients are listed in Table 31 for this ternary diagram. The calculated contour lines and the phase fields for the ternary phase diagram are shown in Figures 28 and 29, respectively.

Table 30. Calculated excess enthalpies at 1800 K using the Redlich-Kister coefficients from the Toop-Muggianu interpolation and our final selected values for the $MgO-SiO_2-AlO_{1.5}$ ternary

Mole fraction			H^e	
MgO	SiO_2	$AlO_{1.5}$	Toop-Muggianu	Final values
.5	.25	.25	-13451.336	-22124.990
.4	.4	.2	-7857.474	-17292.748
.4	.2	.4	-13019.940	-20210.219
1/3	1/3	1/3	-8193.079	-17319.420
.25	.5	.25	-4158.164	-10178.852
.25	.25	.5	-7260.797	-11241.445
.2	.4	.4	-4042.353	-52789.555

Table 31. Redlich-Kister terms through F from our computer file TI75 for the ternary system $AlO_{1.5}$-SiO_2-MgO.

6 7 4	log γ	H	Cp
B^a	16.274239	568481.33	-6.637291
C^a	-56.611459	-2158662.5	-15.02179
C^b	18.364036	764703.	23.56041
D^a	39.586942	1558140.	57.75104
D^b	-23.388194	-645556.5	-121.9810
D^c	16.585357	504529.5	58.41545
E^a	1.81443	164321.0	-90.23578
E^b	-5.075334	-556531.3	321.9720
E^c	2.160231	582914.3	-385.5388
E^d	5.831207	-52767.02	127.1332
F^a	-2.1809064	-100752.4	38.96796
F^b	10.9065889	503762.4	-194.8391
F^c	-21.814092	-100752.5	389.6780
F^d	22.321093	1007525	-389.6780
F^e	-10.9068664	-503762.4	194.8390

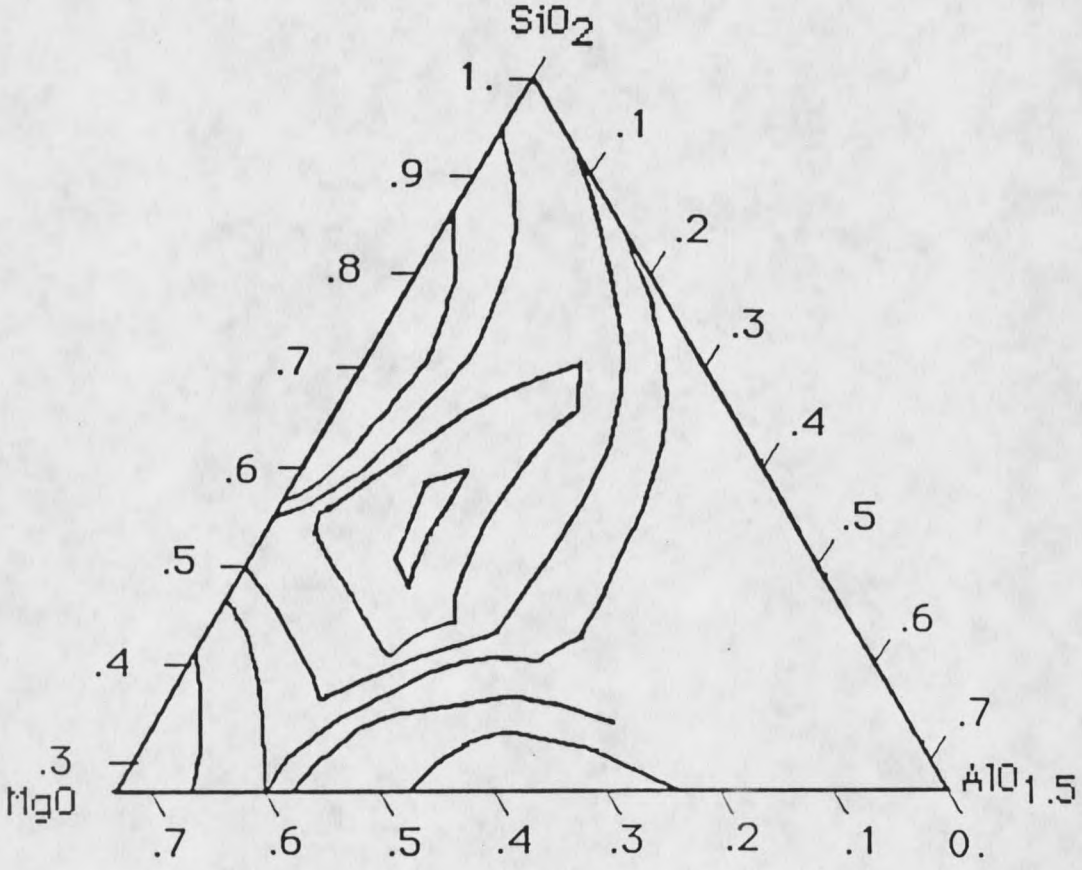

Figure 28. The calculated contour lines for the $MgO-SiO_2-AlO_{1.5}$ ternary system.

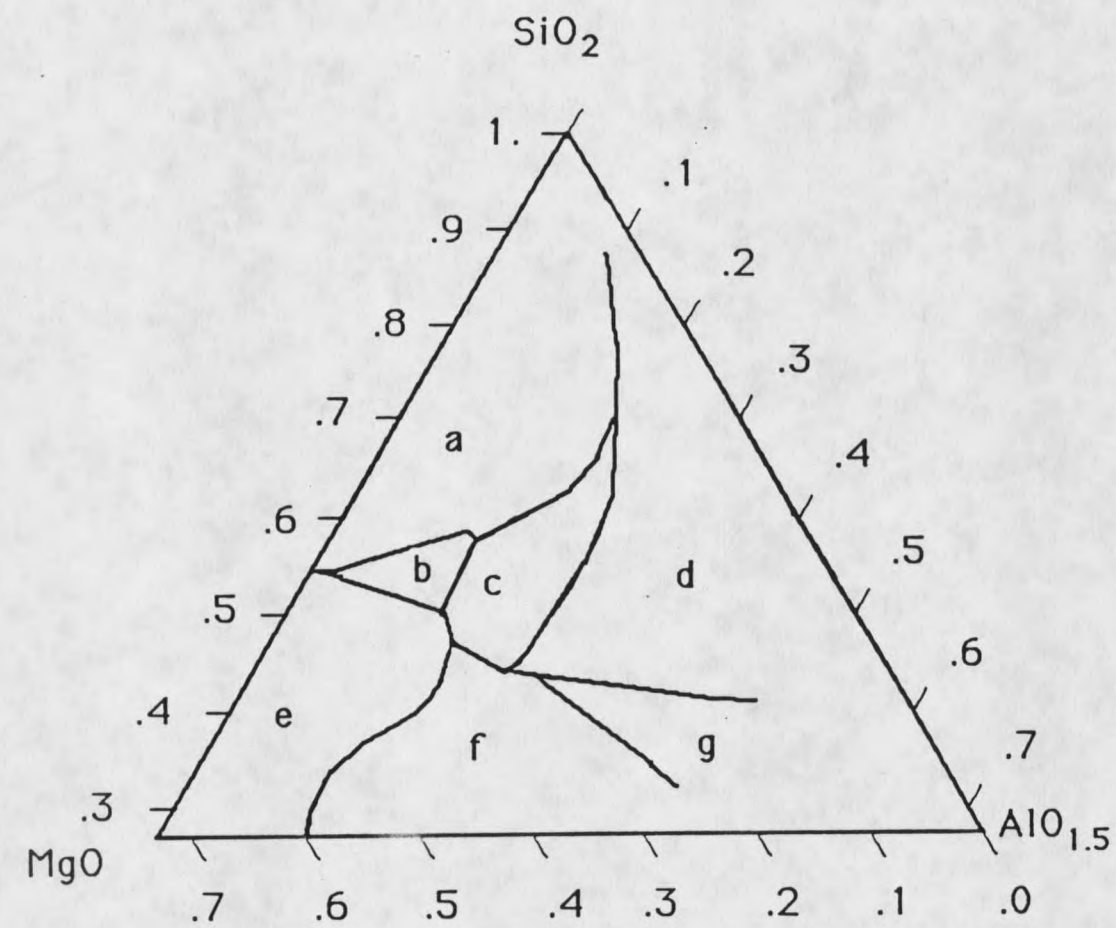

Figure 29. The calculated phase fields for the ternary system $MgO-SiO_2-AlO_{1.5}$.
a is the cristobalite field
b is the corderite field
c is the enstatite field
d is the mullite field
e is the forsterite field
f is the spinel field
g is the corundum field.

THE FeO-$FeO_{1.5}$-SiO_2-$Al_{1.5}$-CaO SYSTEM

Although not central to the main body of this work, it is worth while decribing the work that we did on the system FeO-$FeO_{1.5}$-SiO_2-$AlO_{1.5}$-CaO system. It is again necessary to describe the main components of the system and the stoichiometric compounds of interest. We have already obtained thermodynamic properties from SiO_2 and $AlO_{1.5}$ and many other of the stoichiometric oompounds involved. However, the iron oxides and calcium oxides must also be thermodynamically described along, with the stoichiometric compounds: hercynite, $FeAl_2O_4$; fayalite, Fe_2SiO_4 and anorthite, $CaAl_2Si_2O_8$. Several other compounds exist in this phase diagram, but they are outside the area in which we are interested.

The FeO-$FeO_{1.5}$ System

The first problem we had to solve in the five component system was obtaining thermodynamic properties for wustite, $FeO(c)$. This is a problem in that pure stoichiometric crystalline FeO does not exist in nature. Although, one can get close to the concentrations necessary, it is never quite reached. In order to solve this problem we had to calculate Redlich-Kister

coefficients for the FeO-$FeO_{1.5}$ system and then extrapolate back to pure FeO(c).

The existing phases present in the FeO-$FeO_{1.5}$ system are magnetite, Fe_3O_4(c); hematite, $FeO_{1.5}$; wustite, FeO(c); $FeO_{1.5}$(c,γ); $FeO_{1.5}$(l) and FeO(l). The thermodynamic properties of Fe_3O_4 listed in Table 32 were taken from the Geologic Survey Bulletin 1452[40] and the heat capacity equation and H_{298} are from NBS.[125] The heat capacity equation for Fe_3O_4 is valid from 850 K to 1870 K, the melting point of Fe_3O_4. The heat capacity and thermodynamic properties of $FeO_{1.5}$, hematite, in Table 32 are also from Bulletin 1452,[40] and the heat capacity is valid from 950 to 1805 K, the melting point of $FeO_{1.5}$. The heat capacity equation for $FeO_{1.5}$(c,γ) is estimated to be the same as that of $FeO_{1.5}$(c,hematite). The enthalpy and entropy of $FeO_{1.5}$(c,γ) were calculated from a lattice model for Fe_3O_4, assuming that the enthalpy of mixing of FeO and $FeO_{1.5}$(c,γ) is very small.

The heat capacity of FeO(l) is 68.2 J/mole-K at 1650 as measured by Coughlin et al.,[126] and is held constant up to 3000 K. The heat capacity of $FeO_{1.5}$(l) was assumed to be 10.% larger than that of the solid $FeO_{1.5}$(c). The enthalpies at 298.15 for both liquids were calculated from ΔH_{fus} data, and the Plank's function was adjusted to fit

Table 32. The heat capacity equations and thermodynamic properties of various stoichiometric compounds in the FeO-$FeO_{1.5}$-SiO_2-$AlO_{1.5}$-CaO system.

HEAT CAPACITY EQUATIONS

	A	B	C	D	E
$FeO_{1.5}$ (C, GAMMA)[a]	74.245	.136201		-51042186.	16953.56
Fe (C, GAMMA)	32.3431	.837930E-2	-.174110 E-7		
$FeO_{1.5}$ (C, HEMATITE)[a]	74.245	.136201		-51042186.	16953.56
FeO (C, WUSTITE)	56.709	.0251173	.377231E-4	.117640E-6	-.92509E-10
Fe_3O_4 (C, MAGNETITE)[a]	205.97	.052733		5.6413E+7	
Fe_2SiO_4 (C, FAYALITE)	188.14	.0414165	2.2411E-5	-3.6299E+6	
$FeO_{1.5}$ (LIQUID)[a]	74.245	.146200		-51042186.	16953.56
FeO (LIQUID)	68.2				
$FeAl_2O_4$ (C, HERCYNITE)	90.016	.037055	-.574449E-4	.352436E-7	
$CaAl_2Si_2O_8$ (ANORTHITE)	21.89929	.0527382	.141137E-4	-.457359E-7	.564705E-10

THERMODYNAMIC QUANTITIES	Y_{1000} J MOL^{-1}	H_{1000} -H_{298} J MOL^{-1}	H_{298} J MOL^{-1}	S_{298} J MOL^{-1} K^{-1}	V_{1000} CM^3
$FeO_{1.5}$ (C, GAMMA)	82.12558	50275.5	-401175.94	50.29333	10.0
Fe (C, GAMMA)	41.9488	28405.	0.0	9.41399	7.2118
$FeO_{1.5}$ (C, HEMATITE)	76.08	50275.5	-412320.	44.24774	10.0
FeO (C, WUSTITE)	87.292906	35875.90	-264522.47	45.75706	12.4874
Fe_3O_4 (C, MAGNETITE)	241.16403	147986.	-1118400.	146.14	45.83
Fe_2SiO_4 (C, FAYALITE)	228.4400	118426.	-1477896.	148.32	47.369
$FeO_{1.5}$ (LIQUID)	96.78606	50275.5	-371240.	61.77637	10.0
FeO (LIQUID)	93.50423	47866.17	-245660.	58.83758	
$FeAl_2O_4$ (C, HERCYNITE)	181.71161	115478.	-1983946.0	106.3	41.486
$CaAl_2Si_2O_8$ (ANORTHITE)	332.26016	201018.5	-4231800.	199.30	101.76

THE HEAT CAPACITY EQUATIONS ARE GIVEN BY $Cp=A+B(T-1000)+C(T-1000)^2+D(T-1000)^3 + E(T-1000)^4$. FOR THOSE COMPOUNDS MARK WITH (a), THE D AND E TERMS ARE $D(1/T^{-2} - 10^{-6})$ AND $E(T^{.5} - 1000^{.5})$. ANORTHITE ALSO HAS THE ADDITIONAL EINSTEIN TERM 38 E(T/700)

the known solid liquid equilibrium within the FeO-$FeO_{1.5}$ system.

There is heat capacity data available for the solids $FeO_{1.5}$, Fe_3O_4 and $FeO_{.947}$.[32,40] Using this data we were able to calculate Redlich-Kister coefficients for the heat capacity and the temperature dependence of the heat capacity for stoichiometric FeO shown in Table 33. With values for the heat capacity we were then able to proceed with calculating the Redlich-Kister coefficients for enthalpy. There is a substantial amount of enthalpy data for the iron oxide system.[126,127] L. S. Darken and R. W. Gurry[127] have measured the enthalpy of the solid solution at 1523 K with mole fractions of $FeO_{1.5}$ ranging from x = .111932 to x = 0.32. There is a substantial amount of good data for Fe_3O_4 and $FeO_{1.5}$ enthalpies[32,40], so we were able to calculate Redlich-Kister coefficients at 1523 K for the enthalpy and then convert these coefficients to 1000 K using the Redlich-Kister coefficients for heat capacity. These coefficients along with the log γ and C_p are listed in Table 33.

Darken and Gurry[127] have measured values of the partial pressures of CO_2 and CO over iron oxide solutions ranging from x_{FeO} = .8988 to x_{FeO} = .6406 at 1573 K. With values for the equilibrium constants for the reactions

$$Fe(c,\gamma) + CO_2 = FeO(wus) + CO \qquad (121)$$

Table 33. Redlich-Kister coefficients for the FeO-$FeO_{1.5}$ Solid Binary.

	A	B	C	D	E
log	-.535413	1.541358	-4.835708	7.388763	-3.670011
H^e	-10430.564	58374.976	-175289.548	256811.822	-129030.652
C_P	1.156545				
dC_P/dT	-.0226686				
d^2C_P/dT^2	-.746594E-5				

and

$$FeO(wus) + 1/2\ CO_2 = FeO_{1.5} + 1/2\ CO \qquad (122)$$

we can calculate activity coefficients at these mole fractions and this temperature. The equilibrium constants for reactions (121) and (122) are $K_{121} = 3.20143$ and $K_{122} = 1.33667$. Therefore

$$K_{122} = .133667 = a_{FeO}/a_{FeO_{1.5}}(CO/CO_2)^{1/2} \qquad (123)$$

and

$$K_{121} = 3.20143 = a_{FeO}/a_{Fe(c,\gamma)}(CO/CO_2) \qquad (124)$$

The activity of $Fe(c,\gamma)$ is 1 at the end of the range where $Fe(c,\gamma)$ is present. Knowledge of dependence of activities of the iron oxides as a function of mole fraction, is sufficient to calculate the Redlich-Kister coefficients for log γ for solid FeO_x shown in Table 33.

There is very little data on the enthalpy of the liquid in the $FeO-FeO_{1.5}$ system. There is data on the enthalpy of fusion of Fe_3O_4, ΔH_{fus} = 33000 cal/mole[128] and on the enthalpy of the liquid from x_{FeO} = .92 to .67.[129] We were able to use this data to calculate Redlich-Kister coefficients for the enthalpy of the liquid. We assumed an initial slope for the excess enthalpy at low concentrations for FeO of -12 kJ/mole of metal and -27 kJ/mole of metal at high concentrations with the excess enthalpy at x_{FeO} = 2/3 of -4.0017 kJ/mole of metal.

The Redlich-Kister coefficients in Table 34 for the log γ of the liquid were calculated from the equilibrium constants for the melting of the various solids at T = 1697, 1644 and 1870 K and from the activities of the solids calculated from the Redlich-Kister coefficients in Table 34.

Table 34. Redlich-Kister coefficients for the $FeO-FeO_{1.5}$ liquid binary.

	A	B	C
log γ	-.8557493	-.0237277	.1814582
H^e	-20633.607	-7500.000	1133.606

The Redlich-Kister coefficients for the other binaries present in this system were calculated from

enthalpy of fusion data and the known equilibria occurring within the various binaries. The ternary phase diagrams were calculated with Toop Muggianu interpolations, adjusting the activities to fit the equilibria. This sometimes required adjusting the binaries so that the enthalpy or log γ of the ternary phases did not become unrealistic when a Toop interpolation was done. The calculated phase diagrams for this system are shown as Figures 30 through 34. These figures are pseudoternary slices at 0% CaO up through 20% CaO. The iron oxide is reported in these diagrams as weight % $FeO_{1.5}$, however the computations correspond to substantial FeO present. In fact the average oxidation state of iron was picked to be that in equilibrium with water vapor and hydrogen with $(H_2O)/H_2) = 1.3$.

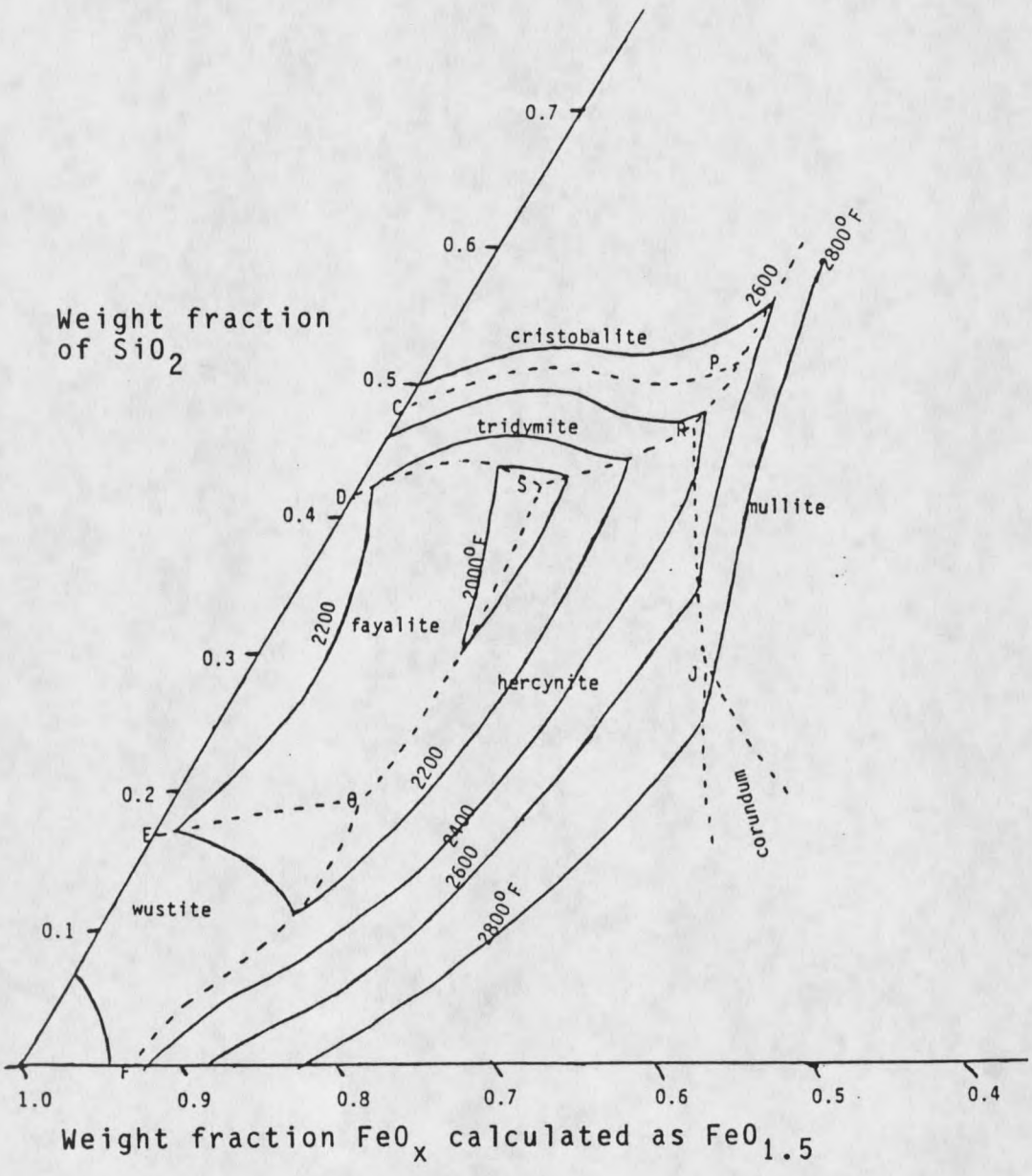

Figure 30. Contour lines in the $AlO_{1.5}$-SiO_2-FeO_x system versus weight fraction calculated as $FeO_{1.5}$ for H_2O/H_2 = 1.3. Temperatures are given in 200 degree Fahrenheit intervals.

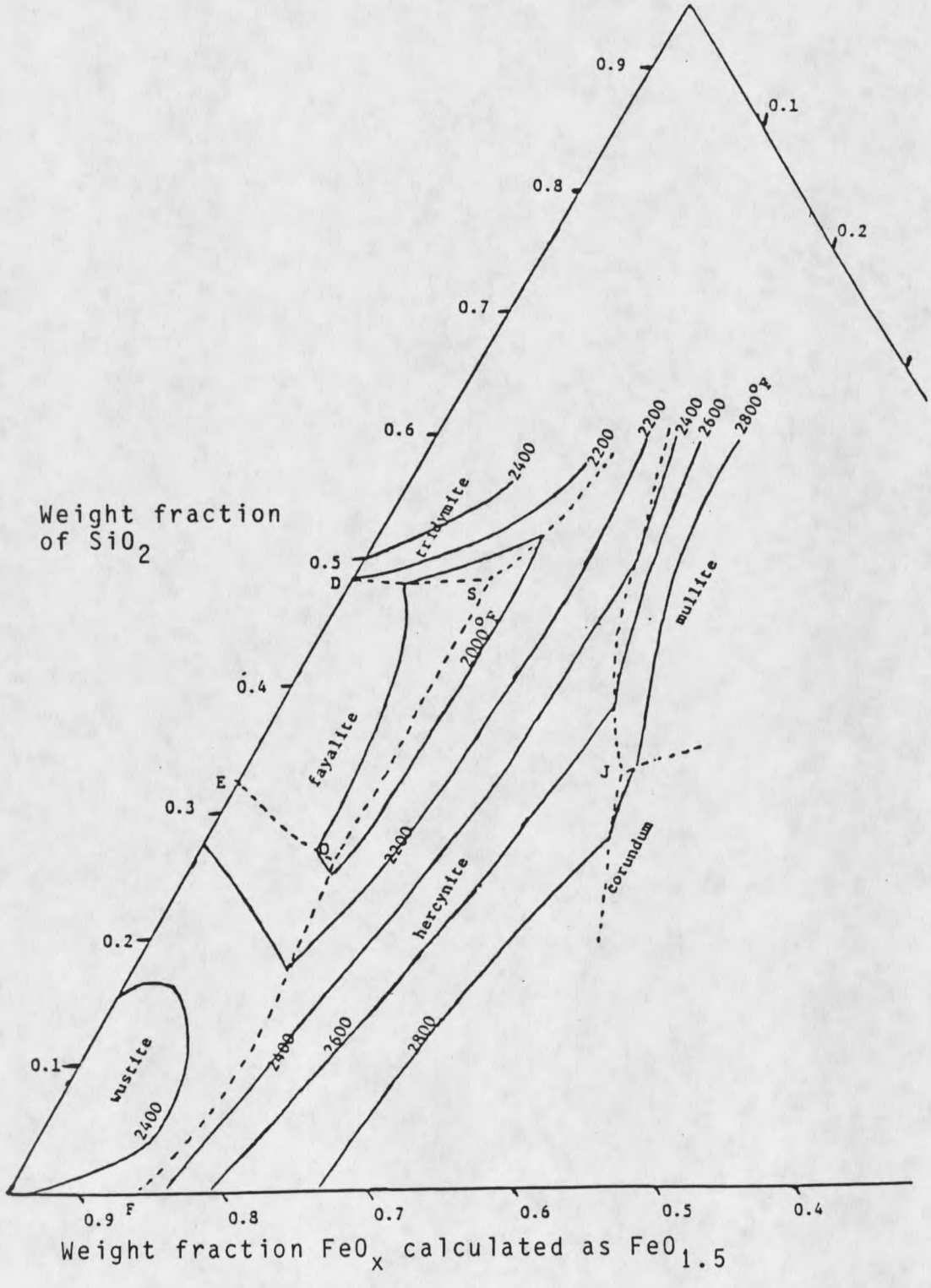

Figure 31. Contour lines in the $AlO_{1.5}$-SiO_2-FeO_x system at 5% CaO by weight and H_2O/H_2 = 1.3.

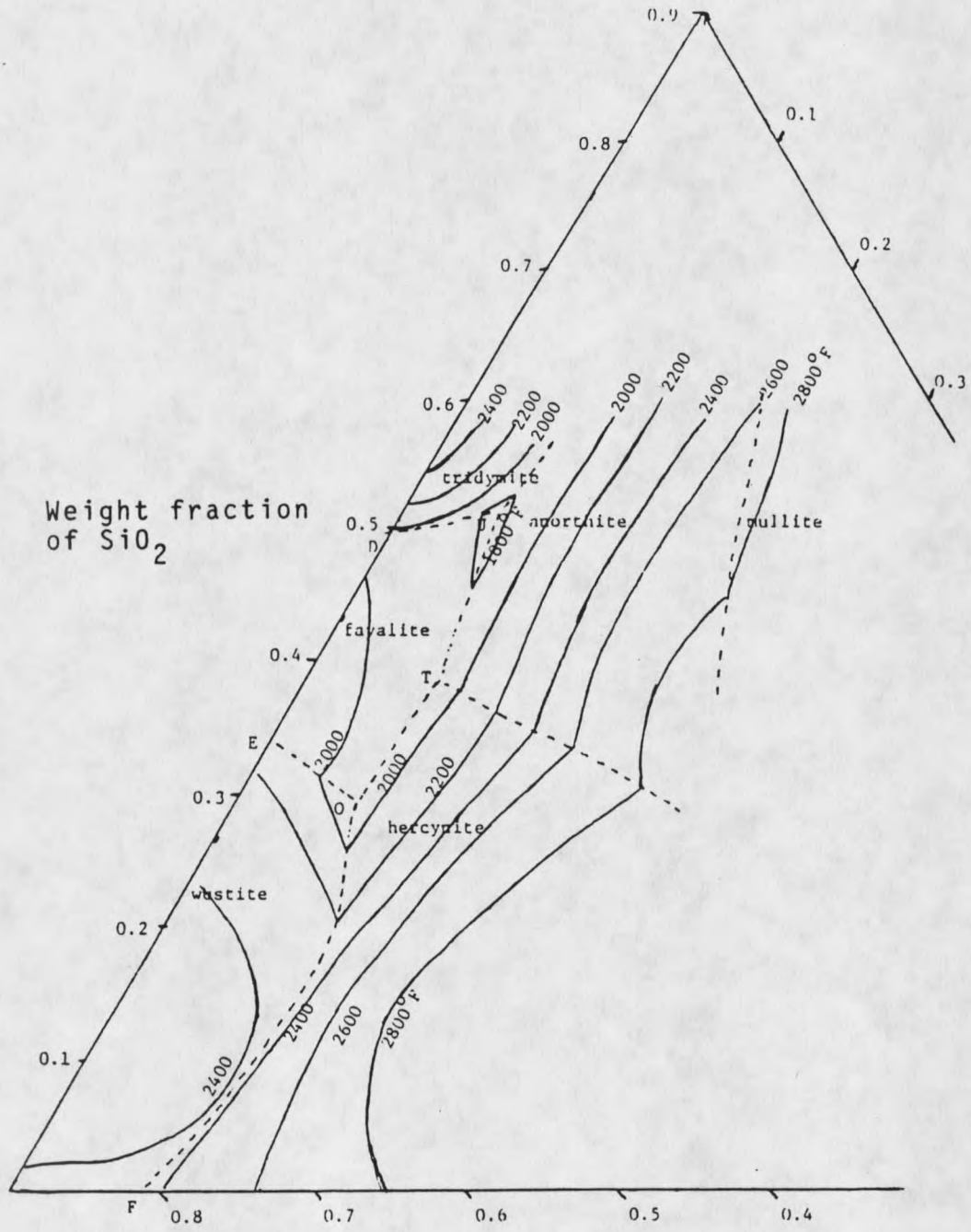

Figure 32. Contour lines in the $AlO_{1.5}$-SiO_2-FeO_x system at 10% CaO by weight and H_2O/H_2 = 1.3.

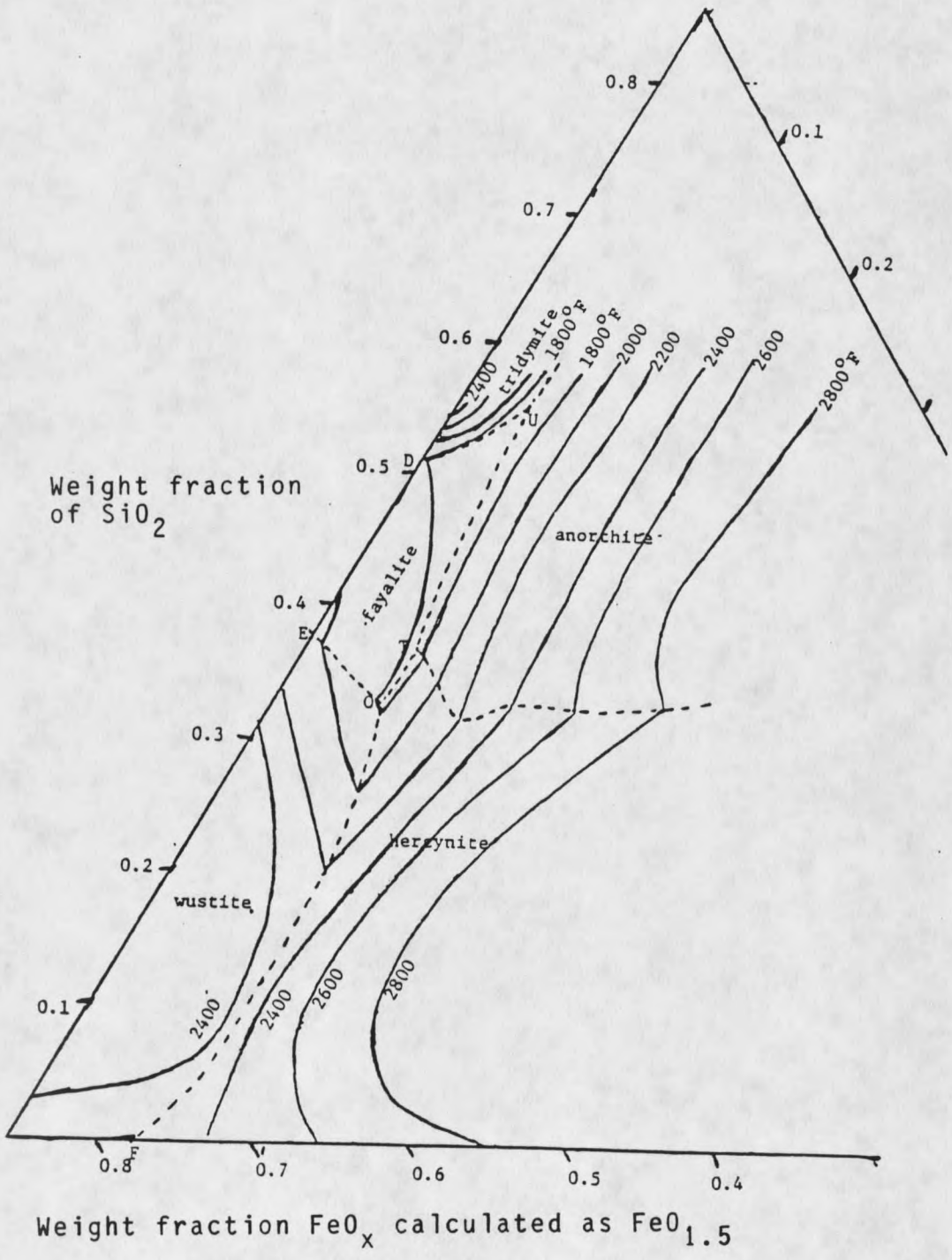

Figure 33. Contour lines in the $AlO_{1.5}$-SiO_2-FeO_x system at 15% CaO by weight and H_2O/H_2 = 1.3.

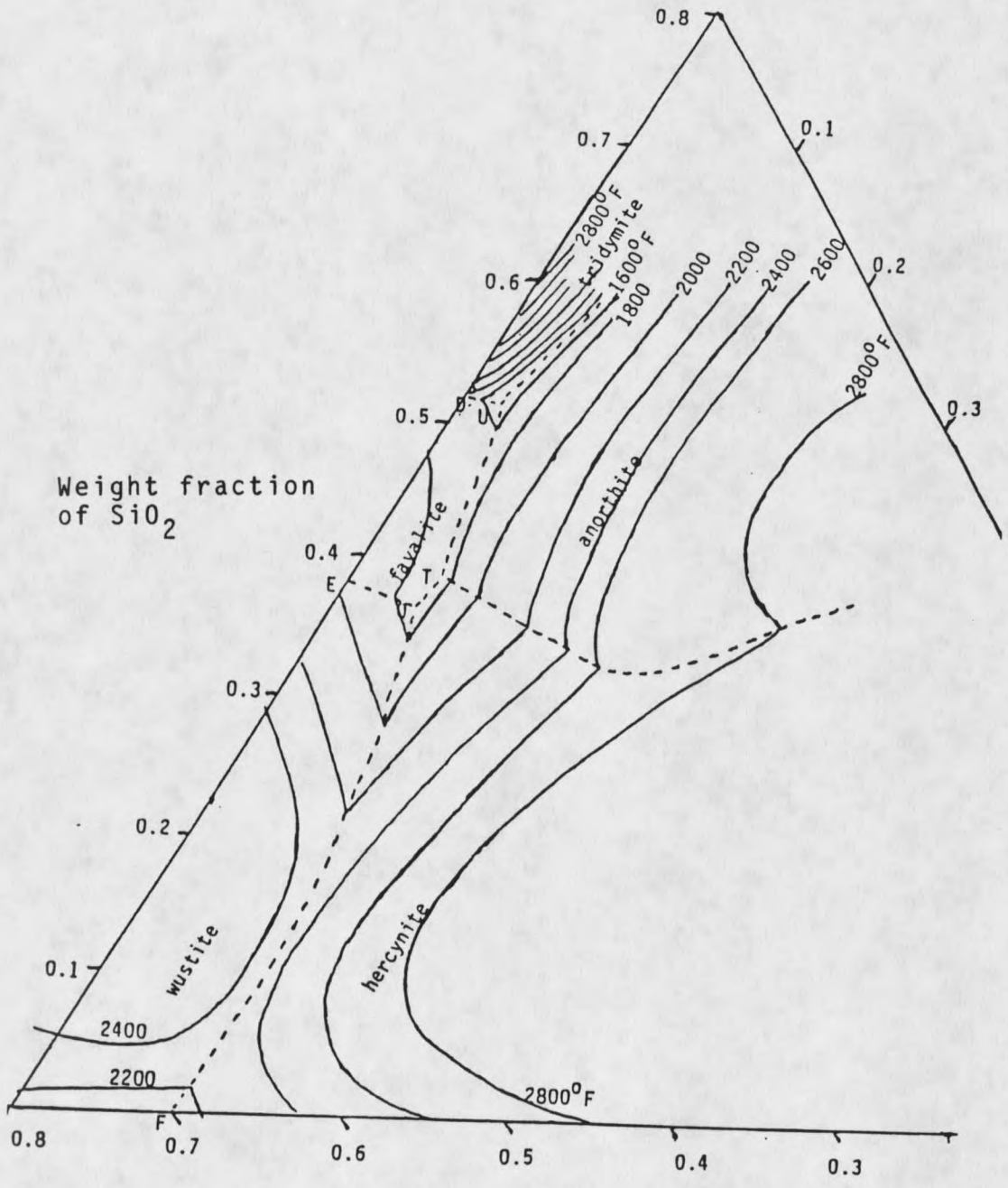

Figure 34. Contour lines in the $AlO_{1.5}$-SiO_2-FeO_x system at 15% CaO by weight and H_2O/H_2 = 1.3.

SUMMARY

Equations of state for the ternary system MgO-SiO_2-$AlO_{1.5}$ and its inherent stoichiometric compounds have been developed. In calculating equations of state for the various solids in this system we developed a useful relationship between the bulk modulus and the coefficient of thermal expansion. The equation is

$$K_{oT} = K_{oT_o}(V_{T_o}/V_T)^N.$$

We were able to show the reliability of this equation for the solids MgO and $AlO_{1.5}$. This equation is also used for many of the stoichiometric compounds in the ternary system with good results. However, this form is not accurate near the lambda transition in quartz.

The Pippard theory of second order phase transitions was used, along with X-ray measurements of the volume and measurements of the slope of the lambda transition versus pressure to resolve the 380 J/mole discrepancy between the standard compilations of Robie, et al.[40] and Stull, et al.[32] The JANAF value of 45354 ± 150 J/mole for $H_{1000} - H_{298}$ for quartz has been confirmed and refined to be 45452 ± 70 J/mole. Also, independent analysis by Richet, et al. based on drop calorimetry yields $H_{1000} - H_{298}$ = 45579 ± 150 J/mole for quartz.

From analysis of the phase equilibria and from the thermodynamic properties of magnesium oxide, silica, forsterite and enstatite along with a measured enthalpy of vitrification for enstatite, the enthalpies of fusion for $MgSiO_3$ and Mg_2SiO_4 were calculated to be 48.8 ± 3 kJ/mole and 92.9 ± 12 kJ/mole respectively. Also Redlich-Kister coefficients for this binary have been calculated for both the acidic and basic sides of the diagram, and the phase diagram has been calculated up to 1000 MPa.

Procedures for the calculation of three, four, and five component systems have been developed and refined here, along with methods of dealing with the silicate liquids. The development of lattice models for the solids also provides methods of dealing with equilibria over a wide range of temperatures and pressures. The development summarized in this thesis now makes it fairly easy to tackle most slag problems. We were able to calculate phase diagrams for the MgO-SiO_2-$AlO_{1.5}$ ternary and the five component system FeO-$FeO_{1.5}$-CaO-SiO_2-$AlO_{1.5}$ from analysis of the phase equilibria and from the thermodynamic measurements of the components of the phase diagrams.

REFERENCES CITED

1) G.W. Toop and C.S. Samis, Trans. Metal. Soc., AIME, 224, 878 (1962).

2) R. Flood and W. J. Knapp, J. Am. Ceram. Soc., 46, 60 (1963).

3) P.L. Lin and A.D. Pelton, Metal. Trans., 10b, 667 (1979).

4) T.J.B. Holland, A. Navrotsky and R.C. Newton, Contrib. Mineral. Petrol., 69, 337 (1979).

5) K.T. Jacob, Trans. Indian Inst. Mat., 32, 470 (1979).

6) A.D. Pelton, H. Schmalzried and J. Sticker, Ber. Bunsenges, Phys. Chem., 83, 241 (1979).

7) B. Sundman, Calphad VIII, Royal Inst. Mat. Tech., Stockholm, Sweden, 102 (1979)

8) M. Margules, Sitzungsber. Wien. Akad.,[2]. 104, 1243 (1895).

9) C.W. Bale and A.D. Pelton, Metal. Trans., 6A, 1963 (1975).

10) C.W. Bale and A.D. Pelton Metal. Trans., 5, 2323 (1974).

11) O. Redlich, A.T. Kister and C.E. Turnquist, Chem. Eng. Progress, Symposium Series, 48(2), 49 (1952).

12) O. Redlich and A.T. Kister, Ind. Eng. Chem., 40, 345 (1948).

13) I. Eliezer and R.A. Howald, Project Meeting Calphad VII, Max Planck Inst. Fur Metallforschung, Stuttgar V Schlosz Weitenberg, 221 (1978).

14) I. Eliezer, N. Eliezer, R.A. Howald and M.C. Verwolf, J. Phys. Chem., 82, 2688 (1978).

15) I. Eliezer, R.A. Howald, J. CHem. Soc., Farad. Trans., I, 74, 393 (1978).

16) Y.S. Touloukian, R.K. Kirby, R.E. Taylor and T.Y.R. Lee, "Thermophysical Properties of Matter", Vol.13 Plenum, New York, (1977).

17) G.K. White and O.L.Anderson, J. Appl. Phys., 37, 430 (1966).

18) H.F. Schaake, U.S. Air Force Report AFCRL-69-0538 [AD669579], (1969).

19) J.S. Browder and S.S. Ballard, Appl. Opt., 8, 793 (1969).

20) S. Ganeson, Phil. Mag., 7, 197 (1962).

21) F.D. Murnaghan, Proc. Natl. Acad. Sci. U.S.A., 30, 244 (1944).

22) O.L. Anderson J. Phys. Chem. Solids, 27, 547 (1966).

23) J.R. McDonald, Rev. Mod. Phys., 38, 669 (1966).

24) H. Spetzler, J. Geophys. Res., 75, 2073 (1970).

25) R.A. Howald, A.A. Moe and B.N. Roy, High Temp. Sci., 16, 111 (1983).

26) R.A. Swalin, "Thermodynamics of Solids", Wiley, New York, (1972).

27) Y.A. Chang, J. Phys. Chem. Solids, 28, 697 (1967).

28) O.L. Anderson, Phys. Rev., 144, 553 (1966).

29) N. Soga and O.L. Anderson, J. Am. Ceramic Soc., 49, 355 (1966); 50, 239 (1979).

30) O.L. Anderson, E. Schreiber, R.C. Liebermann, And N. Soga, Rev. Geophys., 6, 491 (1968).

31) W.J. Carter, S.P. Marsh, J.N. Fritz and R.G. McQueen, Natl. Bur. Stand. Spec. Publ., 326, 147 (1971).

32) D.R. Stull and H. Prophet, Natl. Stand. Ref. Data Ser., Natl. Bur. Stand., NO 37, (1971).

33) T.H.K. Barron, W.T. Berg and J.A. Morrison, Proc. R. Soc. London, Ser. A, 250, 70 (1959).

34) O.L. Anderson and P. Andreatch, J. Am. Ceramic Soc., 49, 404 (1966).

35) O.L. Anderson, Phys. Earth Planet Inter., 22, 173 (1980).

36) O.L. Anderson, Phys. Chem. Miner., 5, 33 (1979).

37) O.L. Anderson, Science, 213, 76 (1981).

38) O.L. Anderson and Y. Sumino, Geophys. Res. Lett., 8, 572 (1981).

39) O.L. Anderson, J. Geophys. Res., 84B, 3537 (1979).

40) A.W. Robie and D. Ter Haar, U.S. Geol. Survey Bull. 1452 (1978).

41) P. Richet, Y. Bottinga, L. Denielov, J.P. Petitet and C. Tequi, Geochim. Cosmochim. Acta, 46, 2639 (1982).

42) H. Le Chatelier, Comptes rendus Academie des Sciences, Paris, 108, 1046 (1889).

43) F. Liebau and H. Bohm, Acta Cristallographica, 38A, 252 (1982).

44) H. Grimm and B. Donner, J. Phys. Chem. Solids, 36, 407 (1975).

45) J.P. Bachheimer, J. Physique, Lett., 41, L59 (1980).

46) J.P. Bachheimer, P. Bastie, J. Barnarel and G.Dolino, Proc. International Conference on Solid Solid Transformations, 1533 (1981).

47) G. Dolino, J.P. Bachheimer and C.M.E. Zeyen, Solid State Comm., 45, 295 (1983).

48) G. Dolino, J.P. Bachheimer, B. Berge and C.M.E. Zeyen, J. de Phys., 45, 361 (1984).

49) G. Dolino, J.P. Bachheimer, F. Gervais and A.F. Wright, Bull. de Mineral., 106, 267 (1983).

50) T.A. Aslanyan and A.P. Levanyuk, Pis'ma v Zhurnal Eksperimental'noi i Teoreticheskoi Fiziki, 28, 76 (1978).

51) T.A. Aslanyan and A.P. Levanyuk, Solid State Comm., 31, 547 (1979).

52) T.A. Aslanyan and A.P. Levanyuk, Ferroelectrics, 53, 231 (1984).

53) A.B. Pippard, Phil. Mag., 1, 473 (1956).

54) L.H. Cohen, W. Klement and H.G. Adams, Am. Mineral., 59, 1099 (1974).

55) A.J. Hughes and A.W. Lawson, J. Chem. Phys., 36, 2098 (1962).

56) W. Klement, J. Geophy. Res., 73, 4711 (1968).

57) W. Klement and L.H. Cohen, J. Geophy. Res., 73, 2249 (1968).

58) N.N. Sinel'nikov, Doklady Akademie Nahk SSSR., 92, 369 (1953).

59) H. Moser, Physikalische Zeitschrift, 37, 737 (1936).

60) R.J. Ackerman and C.A. Sorrell, J. Appl. Cryst., 1, 461 (1974).

61) W.L. Bragg and E.J. Williams, Proc. R. Soc. London Series A, 145A, 699 (1934).

62) A.W. Ross and D. Ter Harr, Physica, 25, 343 (1959).

63) L.D. Landau and E.M. Liftshiftz, Statistical Physics, Pergamon Press Ltd., London, Chapter 14, 453 (1958).

64) L.P. Kandanoff, W. Gotz, D. Hamblen, R. Hecht, E.A.S. Lewis, V.V. Pankianskas, M. Royle, J. Swift, D. Aspens and J. Kane, Rev. of Modern Physics, 39, 395 (1967).

65) M. Levy, J.C. Le Guillou and J. Zimm-Justin, Phase Transitions, Cargest, Plenum Press, New York, (1980).

66) M.S. Ghiorso, I.S.E. Carmichael and L.K. Moret, Cont. Mineral. Petrol., 68, 307 (1979).

67) S.K. Filatov, I.G. Polyakova, A.G. Gailkovoi and I.E. Kamentsev, Soviet Phys. Cryst., 27, 624 (1982).

68) CODATA Task Group, J. Chem. Therm., 8, 603 (1975).

69) F.C. Kracek, K. Neuvonen, G. Burley and R.J. Gordon, Carnegie Institution of Washington Yearbook, 52, 69 (1953).

70) A. Navrotsky, R. Hon, D.F. Weill and D.J. Henry, Geochim. Cosmochim. Acta, 44, 1409 (1980).

71) E.W. Kammer, T.E. Pardue and H.F. Frissel, J. App. Phys., 19, 265 (1948).

72) P.W. Mirwald and H.J. Massone, J. Geophys. Res., 85B, 6983 (1980).

73) J.S. Weaver, D.W. Chipman and T. Takahashi, Am. Mineral., 64, 604 (1979).

74) N. Soga, J. Geophy. Res., 73, 827 (1968).

75) H.J. McSkimmin, P. Andreatch and R.N. Thurston, J App. Phys., 35, 1624 (1965).

76) R. Boehler, J. Geophys. Res., 87, 5501 (1982).

77) Levin, Louise and C.T. Prewitt, Am. Mineral., 66, 324 (1981).

78) J.L. Holm, O.J. Kleppa and E.F. Westrum, Geochem. Cosmochima. Acta, 31, 2289 (1967).

79) F.R. Boyd and J.L. England J. Geophys. Res., 65, 749 (1960).

80) N. Eliezer, R.A. Howald, M. Marinkovic and I. Eliezer, J. Phys. Chem., 82, 1021 (1978).

81) M.A. Moseman and K.S. Pitzer, Am. Chem. Soc., 63, 2348 (1941).

82) L.H. Cohen and W. Klement, Phil. Mag.,A, 39A, 399 (1979).

83) W. Johnson and A.W. Andrews, Trans. British Ceram. Soc., 55, 227 (1956).

84) B.J. Skinner, In S.P. Clark,Jr., Ed., Handbook of Physical Constants. Memoir-Geological Society of America Memoir,97, (1966).

85) A.J. Leadbetter and A.F.Wright, Phil. Mag., 33, 105 (1976).

86) J.F. Bacon, A.A. Hasapis and J.W.,Jr Wholley, Phy. Chem. Glasses, 1, 90 (1960).

87) W. J. Cambell and C. Grain, U.S. Bur. Mines Rept. of Invest.,5757, (1961).

88) C.J. Enberg and E.H. Zehms, J Am. Ceram. Soc., 42, 300 (1959).

89) G. Simmons and H. Wang "Single Crystal Elastic Constants and Calculated Aggregate Properties" MIT Press Cambridge,MA, (1971).

90) W.E. Tefft, J. Res. Natl. Bur. Stand., Sect., A70, 277 (1966).

91) E.E. Shpil'rain, D.N. Kagan and L.S. Barkhatov, High Temperatures High Pressures, 4, 605 (1972).

92) R. Orr, J. Am. Chem. Soc., 75, 528 (1953).

93) K.K. Kelly, J. Am. Chem. Soc., 65, 339 (1943).

94) E.G. King, R. Barany, W.W. Weller and L.B. Pankratz, U.S. Dept. Interior Bur. of Mines. Rept. of Invest.,6962, (1972).

95) E.K. Graham Jr., and G.R. Barsch, J. Geophy. Res., 74, 5949 (1969).

96) S. P. Clark Jr., Ed., "Handbook of Physical Constants" Memoir-Geological Society of America, Memoir 97.

97) K.K. Kelly, U.S. Bur. of Mines Bull.,584, 232 (1937).

98) J.E. Grover, Trans. Am. Geophys. Union, 53, 539 (1972).

99) F.R. Boyd and J.L. England, Year Book Carnegie Inst. Washington, 64, 117 (1965).

100) G.R. Rigby, G.H.B. Lovell and A.T. Green, Trans. British Ceramic Soc., 45, 137 (1946).

101) E. Schreiber, J Appl. Phys., 38, 2508 (1967).

102) Z.P. Chang and G.R. Barsch, J. Geophys. Res., 78, 2418 (1973).

103) L. Anderson, E. Schreiber and R.C. Lieberman, Rev. Geophys., 6, 491 (1968).

104) D.R. Chang and R.A. Howald, High Temperature Science, 15, 209 (1982).

105) O. Kubachewski and C. B. Alcock, Metallurgical Thermochemistry fifth edition. pg. 330 (1979).

106) K.K.Kelly, U.S. Bur. Mines Bull.,393, (1936).

107) L. Kaufman, Calphad, 3, 27 (1979).

108) I. D. MacGregor, Annual Report Director of the Geophysical Laboratory,1455, 135 (1965).

109) N.L. Bowen and J.F. Schairer, Am. J. Sci., 39, 151 (1935).

110) R.L. Hervig, D. Scott and A. Navrotsky, Geochima et Cosmochmica Acta, 49, 1497 (1985).

111) M. Hoch, Private Communication.

112) M. A. Michels and E. Wesker, Solid State Ionics 16 , 33 (1985).

113) W.P. White, Am. J. Sci., 47, 1 (1919).

114) S. Kambayashi and E. Kato, J Chem. Thermodynamics, 15 , 701 (1983)

115) I.F. Reibling, Can. J. Chem., 43, 2811 (1964)

116) R.A. Howald and I. Eliezer, J. Phys. Chem., 82, 2199 (1978)

117) Do R. Chang, R.A. Howald and B.N. Roy, Calphad, 6, 83 (1982)